Progress in Aerospace Sciences xxx (xxxx) xxx

Contents lists available at ScienceDirect

Progress in Aerospace Sciences

journal homepage: www.elsevier.com/locate/paerosci

Technology exploration of zero-emission regional aircraft: Why, what, when and how?☆

Evangelia Pontika [a,*], Panagiotis Laskaridis [a], Phillip J. Ansell [b], Kiruba Haran [c], Rukshan Navaratne [d], Timoleon Kipouros [a]

[a] Centre for Propulsion and Thermal Power Engineering, Cranfield University, College Road, Cranfield, Bedford, MK43 0AL, England, United Kingdom
[b] Department of Aerospace Engineering, University of Illinois Urbana-Champaign, 104 S. Wright St, Urbana, 61801, IL, USA
[c] Department of Electrical and Computer Engineering, University of Illinois Urbana-Champaign, 306 N. Wright St, Urbana, 61801, IL, USA
[d] School of Engineering, Cardiff University, The Parade, Cardiff, CF24 3AA, Wales, United Kingdom

ARTICLE INFO

Dataset link: https://doi.org/10.57996/cran.ceres-2809

Keywords:
Fuel cells
Batteries
Hydrogen
Aviation
Roadmaps

ABSTRACT

The paper focuses on the exploration and comparison of zero-emission technology strategies for regional aircraft. While significant progress is made on the development of technologies, systems and aircraft configurations, major challenges and uncertainties mean that various strategies are considered but are difficult to compare as they rely on different technologies, metrics, requirements, maturity levels and sustainability targets. A novel, holistic approach that captures inter-dependencies, synergies and combined impact of technologies is developed to evaluate the feasibility of such aircraft over 2 horizons, quantify performance and emissions through various phases of the life cycle, establish technology bottlenecks and required step changes and classify developments in terms of impact and risk. For at least 30 passengers at 300 nmi, significant advances are required for fuel cells (2 kW/kg), electric machines (13 kW/kg), power distribution (>1.5 kVolts), and thermal management systems (3.5 kW/kg and 3.5 kW/kW). These will lead to major mission level (+90%) and lifecycle energy penalties (up to +177%) with a carbon intensity level of 6.5 kg_{CO2}/kg_{H2} (ex. blue, turquoise, green hydrogen) required to breakeven current CO_2 levels. Step changes including superconductivity and high temperature fuel cells, along with aircraft mass and drag reductions are required to increase capacity to pax > 40 and 800 nmi, and achieve energy reductions against existing designs. The energy density of batteries and the need of gas turbines to meet diversion and hold requirements limit full electric variants to 30 passengers at 200 nmi with 480 Wh/kg battery energy density but they can offer an exceptional energy per passenger benefit (~40% reduction) against current aircraft.

Contents

☆ This article is part of a Special issue entitled: 'Green Aviation' published in Progress in Aerospace Sciences.

* Corresponding author.
E-mail address: Evangelia.Pontika@cranfield.ac.uk (E. Pontika).

https://doi.org/10.1016/j.paerosci.2025.101171
Received 7 January 2025; Received in revised form 14 September 2025; Accepted 8 December 2025

1. Introduction

1.1. Motivation

Aviation has an essential social and economic role and while significant progress has already been made in terms of efficiency and emission improvements the need to urgently address climate change calls for the decarbonisation of the sector. The development of a zero tailpipe emissions regional aircraft with the ability to carry 20–50 passengers over 200–800 nmi will be a major technological and sustainability breakthrough as well as a vital milestone in the decarbonisation of aviation.

Decarbonisation strategies and technology development programmes such as Clean Aviation in Europe [1], ATI's Destination Zero in the UK [2] and NASA's Sustainable Flight National Partnership in the US [3] focus on cross sector collaborations for the development of innovative technologies required to decarbonise aviation by 2050. While significant progress is made across various fields the technological challenges and uncertainties that need to be addressed mean that several options are examined and alternative technology roadmaps are under consideration making comparison difficult due to the different levels of technological maturity and risk as well as the use of diverse metrics, requirements and sustainability targets. These challenges are reflected in the findings reported in the open literature that are mainly based on three areas:

Nomenclature

α	Speed of Sound
D	Drag [N]
η	Efficiency
$\eta_{grid,trans}$	Electrical Grid Transport Efficiency
η_{grid}	Electrical Grid Overall Efficiency (production and transport)
η_{tank}	Tank Gravimetric Efficiency
BED	Battery Energy Density [Wh/kg]
CI	Carbon Intensity - gCO2/kWh for electricity production and gCO2/kgH2 for hydrogen production
CML	Cable Mass per Length [kg/m]
EED	Effective Energy Density [Wh/kg]
EER	Energy Efficiency Ratio: Heat Dissipated/TMS Parasitic Power Consumption [kW/kW]
EFC	Engine Flight Cycles
f_{PLT}	Energy Demand for Hydrogen Production, Liquefaction and Transport [MJ_{el}/MJ_{LH2}]
$faero$	Aerodynamic Efficiency Improvement (drag reduction factor)
$FCPD$	Fuel Cell Power Density [kW/kg]
FE	Flight Energy [MJ]
γ	Specific Heat Capacity Ratio
LC	Liquid Cooling
LCE	Lifecycle Energy [MJ]
M	Mass [kg] or Mach Number [-]
M_f	Fuel Mass [kg]
MPD	Motor and Power Electronics Power Density [kW/kg]
$NPPC$	Net Power Performance Coefficient: Heat Dissipated/Additional Consumed Power due to the TMS [kW/kW]
$OEW/MTOW$	Operating Empty Weight to Maximum Takeoff Weight Ratio
P	Power [W] or Pressure [Pa]
RP	Relative Power
SoH	State of Health
T	Temperature [K]
THS	High-Temperature Superconducting
$TMSMF$	TMS Mass Factor: Heat Dissipated/TMS Mass [kW/kg]
TMS	Thermal Management System
V	Velocity [m/s]
VCC	Vapour Cycle Cooling
SC	Superconductivity

i. Development and assessment of individual enabling technologies
ii. Optimisation studies focusing on aircraft or system level architectures assuming a limited range of technology levels
iii. Detailed design of components and systems based on set inputs and technology levels. Some limited studies on the life cycle impact of these novel solutions exist but they are usually focusing on specific aircraft or energy solutions.

The present study introduces a novel and holistic approach that focuses on the overall assessment of a zero tail-pipe emissions regional aircraft while capturing the impact of different technologies along with their synergies, interactions and interdependencies on the overall performance, operations and life cycle emissions of the aircraft. Three Zero Emission Electrification Strategies are considered: a hydrogen electric with the use of PEM fuel cells, a full electric with the use of batteries and a hybrid electric combining batteries and fuel cells. The main contribution of the work is the analysis of the overall performance and operation of the aircraft along with the interdependencies and impact of the different technologies. The findings are then analysed to:

i. quantify, compare and contrast the impact of the different electrification strategies during different phases of the life cycle of the aircraft and over two horizons (2035 and 2050)
ii. establish technology bottlenecks along with aircraft operational and performance limitations
iii. develop combined, synergistic and interdependent technology roadmaps and trajectories required to achieve set targets in terms of passengers, range, energy consumption and emissions impact
iv. provide a classification of zero-emission technologies and aircraft technologies in terms of impact/benefits and risk.

In this context, the paper addresses the following aspects:

a. Why a life cycle analysis that extends beyond the emissions produced during the mission profile is important and why the development of a zero-emission regional aircraft is a major milestone for the decarbonisation of aviation
b. What are the technology bottlenecks, performance and operational limitations and appropriate targets
c. When these targets can be met
d. How technologies need to be developed and combined to achieve these targets.

1.2. Contribution

The novelty of this technology exploration is based on the selection and parameterisation of performance characteristics, attributes and figures of merit covering a wide range of key zero-emission and enabling technologies. The approach enables the combined effects of the technologies, including improvements in aerodynamic and structural efficiency at aircraft level, along with their synergies, interactions and interdependencies to be captured and evaluate the prospects and overall performance of zero-emission regional aircraft at three different levels including impact on payload and range, energy efficiency at mission level, emissions and energy efficiency accounting for life cycle aspects. In terms of contribution the paper clearly identifies and establishes technology limits and bottlenecks. It also gives emphasis in establishing thresholds and identifying regions of diminishing returns related to the advancement of individual technologies along with the impact of step changes in the technology development trajectories over different horizons while also considering risk and scalability aspects. Findings highlight that the overall performance of the different zero-emission regional aircraft variants and the impact of the selected technologies depend heavily on the criteria and figures of merit as well as the region that the aircraft will operate and the available energy infrastructure. Full electric variants offer significant benefits in terms of energy efficiency and environmental impact at mission and life cycle levels but underperform in terms of payload, range and scalability aspects. Although major developments are required to realise benefits there are no step changes in technologies and overall aircraft design that could address the limitations in terms of range and payload. Fuel cell variants on the other hand can offer improved payload and range compared to full electric variants while step changes in technology development including the adoption of high temperature PEM fuel cells and hyper/superconductive electrical distribution systems along with aerodynamic and structural improvements at aircraft level can offer payload and energy efficiency figures comparable to and in some cases even better than existing aircraft. In terms of impact, the overall approach and findings inform the selection, prioritisation and development of required technologies and assessment criteria of future zero-emission aircraft.

1.3. Review of technological explorations and technology targets

1.3.1. On-board technologies

Since 2016, Wheeler [4] discussed electric technology needs for more electric and all electric aviation, and suggested that the electric machine industry will need to achieve the power density targets of 10 kW/kg, 20 kW/kg and 50 kW/kg in the next 10, 15 and 25 years. In 2019, a NASA report [5] identified battery energy density thresholds focusing on how improvements in the aerodynamic efficiency through advanced aircraft concepts such as Boundary Layer Ingestion can reduce the energy requirements of the mission and facilitate the application of electric technologies. It was found that thin haul aircraft (300 nmi, 20 pax) require a battery energy density (BED) of 1460 Wh/kg and regional aircraft (700 nmi, 80 pax) a BED of 1870 Wh/kg.

In 2021, following a workshop, the Argonne laboratory produced a white paper [6] proposing technology thresholds for enabling electric flight for different aircraft classes. They proposed that eVTOL for urban air mobility and 20-pax commuter with limited range capability can be enabled at 300 Wh/kg but the sweet spot for the desired capability for commuter and urban air mobility was predicted at 400 Wh/kg. Moving to larger applications, they suggest that hybrid electric flight for regional aircraft and short-range single aisle with 150 pax can be achieved from 500 Wh/kg and electric flight for 150 pax single aisle and longer range require a battery energy density higher than 700 Wh/kg. Details of the underlying assumptions such as ranges, technology levels for the rest of the system and overall methodology followed to extract the values are not included in the white paper. In 2021, Byahat et al. [7] calculated well to wake and lifecycle emissions for a battery-powered 19-pax commuter aircraft performing a 100 nmi mission. The lifecycle analysis considered battery charging under electricity grid scenarios in the USA and the effect of material manufacturing and end-of-life processes for the aircraft. The grid scenarios included a 2035 advanced grid which is close to today's grid with slight improvements, a transition to 50% renewable sources of energy and 100% renewable sources. The mass estimations and materials emissions estimations were performed for three cases: an advanced conventional aircraft, an electric aircraft with optimistic electrical technology level in 2035 and an electric aircraft with intermediate electrical technologies in 2035. The considered electrical technologies were the battery energy density, the motor power density and the converter power density. They predicted that the advanced conventional aircraft and the electric aircraft will always result in an increase in emissions associated with materials but even the most conservative grid scenario still offers substantial well to wake emissions reductions of 88%. However, the materials emissions are a small fraction of the lifecycle emissions, therefore, the total emissions reduction offered by the electric aircraft range between 79% and 94% for the most pessimistic and most optimistic electric technology-grid scenarios respectively. In 2021, Karpuk and Elham [8] investigated the effect of aircraft technologies on the feasibility, mass and direct operating cost of electric regional aircraft for a fixed set of future technology factors for the electric powertrain and variable battery energy density. The aircraft improvements included the airframe structural weight, laminar flow ratio and load factor. They observed that the same Maximum Take-off Mass can be achieved with 900 Wh/kg and no aircraft improvements or with 600 Wh/kg and aircraft improvements.

In 2022, Viswanathan et al. [9] discussed the requirements for battery-powered flights in terms of total energy requirement, power requirement, battery energy density but also battery safety and certification. In 2022, Mukhopadhaya and Graver [10] reviewed missions in the turboprop market in terms of passenger (pax) capability and range, and evaluated the fraction of the market that can be replaced by electric aircraft if the BED is improved from 250 Wh/kg to 500 Wh/kg under two scenarios of empty mass fraction reductions. They proposed that an advanced BED = 500 Wh/kg can help replace 2/3 of the commuter market and 1/4 of the turboprop regional market. In 2022, the Aviation Impact Accelerator report [11] proposed that a 1500 km flight with 50 pax using a fuel cell system power density of around 1.8 kW/kg combined with 2021 aircraft design is impossible, while the same fuel cell system power density combined with a 2035 aircraft design is possible with a 20% energy pernalty relative to a kerosene aircraft. They also estimated the operating range of battery-powered aircraft for a range of battery pack energy densities from 250 Wh/kg to 550 Wh/kg. At 250 Wh/kg, an operating range of 150 km is projected and at 550 Wh/kg a operating range of 700 km is projected, however, the number of passengers was not stated. The underlying assumptions at the other subsystems and synergies with other subsystems were not analysed.

In 2023, Misley et al. [12] investigated potential fuel savings in three mission ranges by using six different battery cell products in a hybrid electric aircraft with distributed propulsion. In the aircraft modelling the maximum take-off weight was constrained. Three cell types were state of the art and three were future technologies, and the battery discharge profile during each mission profile was calculated based on the cell discharge characteristics. The optimum energy management strategy in terms of fuel savings, for the shorter-range mission (500 km) favoured the cells with high power density and high C rate even if the battery energy density was as low as 250 Wh/kg. For the 1100 km range mission, the optimum energy management strategy favoured the three cells with low power density, low C rate and high energy density (299–405 Wh/kg) which corresponded to future technology cells. However, even with the three future cells the fuel savings were in the range of 0.5% up to 2.5% for the best among the considered cells. In 2023, Palaia et al. [13] investigated the impact of variable battery energy density on the fuel consumption of a hybrid electric regional aircraft, while the rest of the electric components were fixed at future optimistic power densities. They concluded that fuel burn savings begin at 500 Wh/kg, only for design ranges up to 600 nmi, and at the expense of higher Maximum Takeoff Weight (MTOW) and penalties at the aircraft capabilities. It was also observed that further increasing the MTOW does not bring a benefit on the fuel burn. In 2023, Staggat et al. [14] analysed a battery-supported fuel cell regional aircraft and parameterically explored the combined impact of BED and hybridisation factor (HF) on the maximum take-off mass of the aircraft. An improvement in BED from 405 Wh/kg to 825 Wh/kg for HF = 0.38 reduced the Maximum Takeoff Mass (MTOM) by a factor of two, but even the optimum factors used in their study (BED = 1000 Wh/kg and HF = 0.5) still resulted in a 5% heavier MTOM than the conventional. In 2023, Kirk et al. [15] performed a BED and motor size parametric analysis for three classes of hybrid electric aircraft (18-pax at 250 nmi, 48-pax at 460 nmi, and 78 pax at 1250 nmi). They calculated that a 18-pax hybrid electric aircraft with 250 nmi range can have a 12.8% reduction in CO_2e with a 153 kW motor and BED = 500 Wh/kg, while the 48-pax and 78-pax hybrid electric aircraft demonstrated CO_2e penalties for 500 Wh/kg at their design ranges. The 78-pax hybrid electric aircraft started offering minimal CO_2e reductions at 750 Wh/kg and for the reduced range of 500 nnmi. In 2023, Hales et al. [16] evaluated fuel cell (FC) development needs in the H2GEAR project and highlighted the need for transitioning to Intermediate-Temperature Polymer Electrolyte Membrane Fuel Cell (IT-PEMFC) and High-Temperature Polymer Electrolyte Membrane Fuel Cell (HT-PEMFC) to reduce thermal management challenges. They set targets for TRL6 with specific power density of the combined stack, Balance of Plant (BoP) and Thermal Management System (TMS) at 1.3 kW/kg, >2.1 kW/kg and >2.8 kW/kg by 2030, 2035 and 2040 respectively. The targeted platforms are 48 pax and 96 pax with propeller or ducted fan, and the electrical system will be cryogenic, superconducting improving the powertrain efficiency from 84.4% to 93.6% [16]. In 2024, Wood et al. [17] performed mass and performance estimations for the 48 pax and 96 pax aircraft, and they target 800–900 nmi for the 48-pax aircraft and 1600 nmi for the 96 pax aircraft.

In 2024, Jagtap et al. [18] evaluated the impact of aircraft technology advancements in combination with variable liquid hydrogen (LH2)

tank gravimetric index on the energy consumption, fuselage length and take-off weight of a hydrogen gas turbine (GT), long-haul, wing and tube aircraft using the Breguet equation. They included the skin friction coefficient, the gas turbine overall efficiency and a structural mass reduction factor. It was found that the aircraft's specific energy consumption ranged from +29% to −33% relative to today's baseline Jet A aircraft. A modest tank gravimetric index of 35% combined with the optimum values of the remaining factors can still offer an energy saving of approximately -15%. In 2024, Tiwari et al. [19] reviewed and summarised the progress in liquid hydrogen propulsion projects with a focus on fuel cells, hydrogen gas turbines, storage and motors. They plotted the evolution of PEMFC system power density since 2000 as well as the projected specific power in future planned projects, and the highest fuel cell system power density in 2035 is projected at nearly 5 kW/kg. In 2024, ZeroAvia's white report [20] discussed the feasibility of fuel cells for regional and narrow body aircraft. Their current fuel cell for 20-seat commuter aims to achieve a 1.5 kW/kg power density at system level. For the 20-seater they are developing 20 kW/kg inverters and 5 kW/kg motors with 660 kW max power. To replace regional turboprop aircraft, they foresee a need for 3.5 kW/kg stack power density and system power density just above 2 kW/kg, while the regional jet class would require a system power density of 2.4 kW/kg. Regarding the hydrogen storage, they comment that aluminium tanks can achieve a gravimetric index of 0.35, glass fibre tanks could offer a gravimetric index of 0.45 but have low maturity, while carbon-fibre composite could reach 0.65. It is suggested that a 10 kW/kg FC power density is needed for a fully electric narrowbody, while a 3–4 kW/kg FC power density would be sufficient for a hybrid fuel cell system for narrowbody aircraft.

In 2025, Adler and Martins [21] reviewed and compared different solutions for carbon-neutral flight using aircraft-sizing methods. First, the different loss mechanisms during production and the input energy required to produce 1 MJ of electricity for battery charging, 1 MJ of LH2 and 1 MJ of e-SAF were compared. E-SAF was found the most energy-demanding, and battery charging was the least energy-demanding. Then, they mapped out which solution becomes more efficient at different cruise speed-range combinations, with battery systems (either propeller or fan) winning over the low range regions below 100 nmi, fuel cell powered propellers winning over the longer ranges over 100 nmi, but at cruise speeds below 300 knots, and hydrogen combustion jet taking over the longer ranges and higher speed regions. A sensitivity analysis showed how much these "optimum" regions can shift with improvements in battery energy density, fuel cell efficiency and fuel cell power density. They estimate that batteries with 1000 Wh/kg can serve ranges up to 800 nmi, and fuel cells with efficiencies >70% and >5 kW/kg combined with fans can power long-range flight at cruise speeds over 350 knots more efficiently than combustion options.

1.3.2. Emphasis on lifecycle

Another portion of the literature focuses on lifecycle aspects using economic metrics and total CO_2 under distinct technological scenarios characterised with a combined measure of benefit. In such studies, there is usually insight into global climate impact effects, but the granularity of the individual technologies within the scenarios is often limited. In 2023, Delbecq et al. [22] performed a review of sustainable aviation scenarios and technological levers in this direction. They discussed technological aspects in the context of six global fleet scenarios with different energy efficiency gains due to the different combinations of introduced aircraft types and time of introduction. The focus of this review was more on global aviation climate impact at a higher level and discussed budgeting aspects and lifecyle energy and emissions for different fuel types, fuel sources, BED and hydrogen tank gravimetric efficiency, with less granularity on individual "on-board" technologies. They referred to the all-electric 180-pax aircraft from [23] and presented the lifecycle CO_2 breakeven years for different battery energy density scenarios and based on the projection for the grid carbon intensity evolution. For a BED = 800 Wh/kg and a grid scenario with use of renewables, a 500 nmi all-electric short range aircraft was not expected to breakeven the lifecycle CO_2e emissions of conventional before year 2042. Another technological remark was that an energy penalty relative to the conventional kerosene aircraft should be expected for hydrogen aircraft with tank gravimetric efficiencies below 55%. In 2019, Gnadt et all [23] compared the potential of Li-on, Li-air and Li-S batteries and, using the Breguet equation, they estimated the maximum range for battery energy densities from 0 to 2000 Wh/kg combined with three scenarios of aircraft technology parameters. Among their findings, Li-S battery with 1000 Wh/kg combined with aircraft technology of L/D = 25, overall aircraft efficiency of 0.8, battery mass fraction of 0.5 and active to total battery mass ratio 0.6 was projected to achieve a 180-pax aircraft of 2000 nmi. The also discussed energy consumption implications based on the grid and battery technology.

In 2023, Barros Pintos et al. [24] compared the CO_2 per revenue passenger and kilometers (RPK) of three propulsion technologies against the conventional Jet A case (50% SAF Blend, Li-S batteries and blue LH2), while the technology factors were fixed. In [25,26] in 2018, the analysis focused on economic performance metrics and global aviation environmental impact under different aircraft advancement scenarios and operational measures. In 2022, Mukhopadhaya and Rutherford [10] compared the fuel cost per RPK, RPK coverage, energy per RPK and CO_2e per RPK of future hydrogen aircraft in 2050 under two hydrogen tank gravimetric efficiency scenarios (0.2 and 0.35) and two aircraft classes (regional and narrow-body)

In 2024, Smith and Mastorakos [27] produced payload-range design envelopes for large commercial aircraft in 2050, and compared four fuel types (Jet A, LNG, LH2 GT, LH2 FC) as well as dual fuel combination. The technology levels for the electric engine specific power, FC power density, FC efficiency and electrolyser efficiency were projected by fitting historical data and future projections in the literature. The LH2 aircraft had passenger and payload reductions, and to meet the IATA emission targets under the average European grid, the well-to-wing energy relative to the conventional aircraft design point should not be higher than 2.

In 2024, Cybulsky et al. [28] used a FC system retrofit approach on the regional aircraft De−Havilland Dash 8−400 using an energy-based version of the Breguet equation assuming that the fuel cell version has the same energy requirement per mile as the conventional. The motors were fixed at 12 kW/kg while the technology variables were the fuel cell system power density and the hydrogen tank gravimetric index to determine payload reduction. They identified that a fuel cell system power density increase to 2 kW/kg followed by the tank gravimetric efficiency at 0.5 will be the most impactful factors in limiting the payload reduction. If the tank gravimetric efficiency is at 0.35, a 800 nmi mission with no payload reduction (i.e. 78 pax) was foreseen with a fuel cell system power density at 2 kW/kg, and a 1000 nmi with no payload reduction was foreseen with a fuel cell system power density at 2.4 kW/kg. The baseline technology scenario for the lifecycle analysis assumed a fuel cell efficiency at 60%, tank gravimetric efficiency at 0.35 and fuel cell system power density at 1 kW/kg, which involved a payload reduction. Then, they analysed the energy demand of flights up to 1000 nmi that can be decarbonised with a fuel cell regional aircraft within a network in Europe, and how this demand for aviation will impact the required hydrogen production capacity under different infrastructure policy scenarios. They project that, depending on the technology mix, the CO_2 could be reduced by 90% for the aviation segment converted to hydrogen.

1.4. Existing targets and roadmaps

Several organisations and programmes have published technology roadmaps for aviation (Figs. 1 and 2). However, further discussion is needed on the technology gaps to be addressed in order to achieve

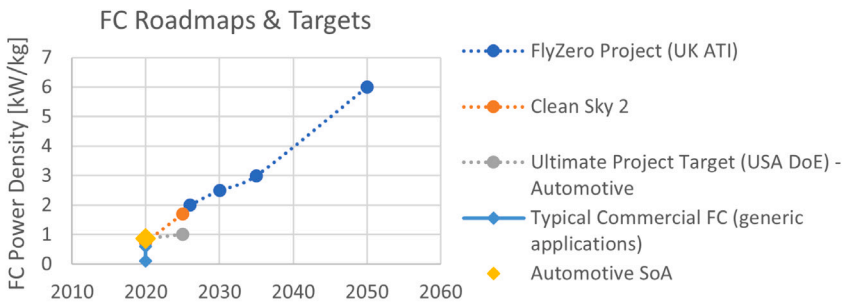

Fig. 1. Targets for FC power density [29–31].

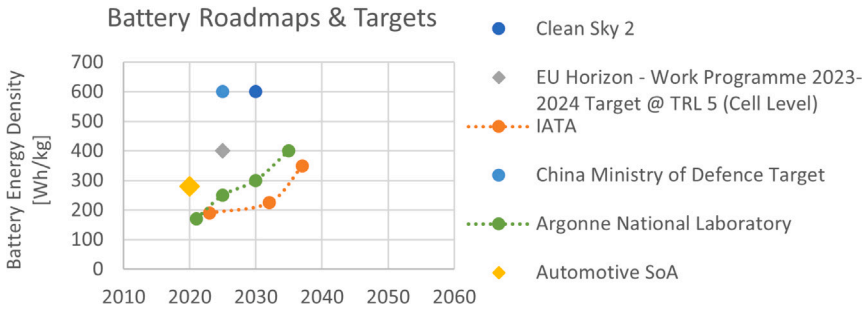

Fig. 2. Battery energy density targets [6,32,33].

each technology level and which are the critical technology values. In addition, on-board technology and infrastructure roadmaps are usually separate or the latter usually have limited granularity and detail in the technology aspects. The synergy between energy production technologies and on-board technologies on achieving lifecycle targets has not been fully explored.

2. Methodology

2.1. Overall methodology

A systematic technological design space exploration is synthesised to combine in-flight performance calculations, step changes in a comprehensive set of technology values that cover the most critical enabling systems, lifecycle calculations and finally degradation and time-on-wing. The steps of the methodology are:

1. Selection of technology factors that represent enabling systems and their range considering today's values to future projections.
2. Flight mission analysis using aircraft performance and propulsion system simulations at MTOW. At this stage, the flight mission analysis is considered "agnostic" to technology factors and the propulsion system only understands a power requirement that comes from the combined aircraft mass.
3. Performing system mass estimations using the technology factors from step 1 and the mission energy/fuel to define the pax capability.
4. From step 2 and 3, estimating the in-flight energy (FE) per passenger. This is the in-flight figure of merit and an input to the lifecycle emissions and energy estimation.
5. The technology values stop being "agnostic" and they are mapped out to the technology gaps that need to be addressed.

A representative 70-pax regional aircraft platform with MTOW = 23000 kg is used as the basis for the mission analysis and aircraft energy requirements. The purpose is to use an aircraft design that is representative enough of this aircraft class while avoiding to engage in an infinite loop of aircraft design iterations every time the technology values and the MTOW would change. Existing studies such as Palaia et al. [13] (for a hybrid system though) have indicated that an increase in the MTOW just to carry additional system mass does not bring particular benefit and the technology factor is the critical parameter. For this reason, in this paper the MTOW and available volume in the fuselage are maintained as constraints and for each combination of technology factors the trade-off between system mass and passenger capability is varied. However, to consider future aircraft designs, two technology factors associated with aircraft technologies are imposed, such as the aircraft structural efficiency and the aerodynamic efficiency improvement. Nevertheless, even if the technology becomes available retrofit systems for existing aircraft are expected to be the first step in a gradual conversion of fleets over time until all aircraft fleets are fully replaced with the future generation. Certification of electric propulsion systems on existing airframes is also expected to be faster than on clean sheet aircraft designs.

The investigated technology factors are distinguished in two groups and each group is divided into types of technologies:

1. The "on-board" technology factors that affect the in-flight energy consumption per passenger. The in-flight CO_2 emissions are zero since only fuel cells and batteries as considered. This group includes the:
   - Electrical technologies and power sources: motor and power electronics power density (MPD), cable mass per length (CML), fuel cell power density (FCPD) and battery energy density (BED)
   - Other enabling technologies: the thermal management system mass factor (TMS MF) and the net power performance coefficient (NPPC), and the hydrogen tank gravimentric efficiency (η_{tank})
   - Aircraft technologies: the operating empty weight to the maximum takeoff weight (OEW/MTOW) and the aerodynamic efficiency improvement (f_{aero})
2. The lifecycle technology factors that represent energy production methods, grid infrastructure and degradation. This group includes:

Table 1
Default values of parameters in parametric analyses and trade-off maps unless mentioned otherwise.

Parameter	FC A/C	Battery A/C
BED [Wh/kg]	–	500
FCPD [kW/kg]	2	–
MPD [kW/kg]	13	13
CML [kg/m]	15	15
TMS MF [kW/kg]	3.5	3.5
NPPC [kW/kW]	3	3
η_{tank}	0.35	–
OEW/MTOW	0.5848	0.5848
f_{aero}	0	0

- Energy production methods & infrastructure: carbon intensity (CI) of the electrical grid and hydrogen production, and the energy demand to produce, liquify and transport the hydrogen (f_{PLT})
- Degradation: Degradation Rate and End of Life State of Health.

In the subsequent gradient analysis and 2D technology factor maps, unless mentioned otherwise, the rest of the on board technology factors are fixed at the values in Table 1.

More details on the calculations and used equations are included in Appendix.

3. Technology factor exploration - impact on aircraft

3.1. Fuel cell aircraft

3.1.1. Gradient analysis

The gradient analysis reveals the rate of return of one unit step-change in technology. However, there are two aspects to be considered:

1. From a clearly numerical perspective, threshold technology factor values can be identified above which the rate of return becomes diminishing. However, this does not mean that these thresholds coincide with the values that correspond to technology breakthroughs.
2. There are technology breakthroughs that if achieved will make easier to move by more technology factor value steps. Step changes by technology breakthroughs have uncertainty and are harder to predict.

The gradient analysis identifies the threshold values at level 1. For example, a 1 kW/kg step change in FCPD is more impactful from 1 kW/kg to 2 kW/kg than from 2 kW/kg to 3 kW/kg (Fig. 3a,b). Similar observations of diminishing rate of return can be deduced for all technologies, except for the aircraft technologies. An improvement in OEW/MTOW and f_{aero} offers linearly increasing pax capability. Despite the diminishing rate of return for most factors, if a technology breakthrough is achieved, accumulated steps can still offer a considerable accumulated benefit.

The small offset between the range curves is a result of the small change in fuel and tank mass. However, for lower η_{tank} the distance between the range curves becomes greater (Fig. 3k). The TMS NPPC is associated with the operating temperature of the FC and induces a great energy and pax penalty. A value of 3 kW/kW corresponds to Low-Temperature Polymer Electrolyte Membrane (LT-PEMFC) and reaching a value of 5 kW/kW with HT-PEMFC brings great benefit (+12 pax at 300 nmi).

3.1.2. Technology target scenarios

The design space of the technology variable combinations is a multi-dimensional problem (Fig. 4). The figures of merit for each technology combination are the passenger capability and in-flight energy per pax relative to the conventional. The number of passengers is important for the business case of implementing these technologies on this aircraft size while the in-flight energy per pax is associated with lifecycle impacts, infrastructure requirements and costs.

Milestone 1: 30 pax

A minimum 30-pax capability is important for creating a business case. There are many combinations of technology factors that can lead to the same pax or FE/pax. For example, 30 pax can be achieved with HT-PEMFC (NPPC = 5 kW/kW), high hydrogen storage efficiency (0.5) and medium level in electrical technologies, or with NPPC = 3.5 kW/kW, conservative hydrogen storage (0.35) and advanced motors with 13 kW/kg and cables at 15 kg/m. The question is which technology combination can be achieved first?

Milestone 2: In-Flight Energy Breakeven

To breakeven the FE/pax of the conventional, a further improvement of motor power density and cable mass combined with a medium improvement in aircraft technologies is needed. Improvements in aircraft technology can compensate for the energy penalty caused by the adoption of electrical technologies. These improved technology factors result in a 49-pax capability at 300 nmi (Table 2).

Milestone 3: Energy Efficient Aircraft and Upscaling

In the longer term, improved energy performance and pax capability at the maximum allowed by the hydrogen volume constraint could be achieved under two technology pathways:

- emphasis on aircraft technologies and medium improvement in electrical technologies

- emphasis on electrical and FC technologies and medium improvement in aircraft technologies

Focus on Superconductivity

Superconductivity can offer a 30 pax capability at 300 nmi, but on its own cannot breakeven the FE/pax of the conventional without IT/HT PEM with high power density and improved TMS performance, or without aircraft improvement.

What if HT-PEMFC technology does not mature?

If IT/HT-PEMFC technology does not mature, the TMS NPPC would remain at 3 kW/kW due to the low-grade heat of LT-PEMFC (Fig. 33), and only a small improvement in the FCPD and the TMS MF could be expected through design, manufacturing and material improvements. To compensate for the lack of the anticipated breakthrough in PEMFC technology, both the electrical technology and aircraft technology are boosted to the advanced values, but the achieved pax capability would only be 25 with an energy penalty of +118% relative to the conventional aircraft.

3.1.3. Technology levels trade-offs and upscaling benefits

The 2D trade-off maps examine combinations of two parameters in a continuous space, while a third parameter represents a step change in another technology, and serve two purposes:

- From the set values (Table 1) the maps can be used to identify the required upscaling in an individual parameter or combination of two parameters to meet any pax or flight energy target.
- They serve as an uncertainty quantification for deviation from targets

Keeping the same aircraft technology, if the MPD is limited to 8 kW/kg (Fig. 5a,b), the FE/pax of the conventional cannot be breakeven, and an improved FCPD at 2 kW/kg from today's 0.9 kW/kg cannot offer a 30-pax capability with NPPC = 3 kW/kW (LT-PEMFC), but is restricted to 15 pax. An MPD = 8 kW/kg would result in a 30-pax capability if combined with FCPD = 2 kW/kg and NPPC = 5 kW/kW. On the other side, MPD upscaling to 13 kW/kg enables 30 pax if combined with FCPD = 2 kW/kg and NPPC = 3.5 kW/kW, which could correspond to a small increase in the operating temperature of the FC stack and improved materials. Therefore, if 30 pax is targeted, it becomes a question of whether it is easier for the technology development to achieve an advanced motor with MPD = 13 kW/kg combined with an incremental improvement in LT-PEMFC, or to achieve MPD 8 kW/kg

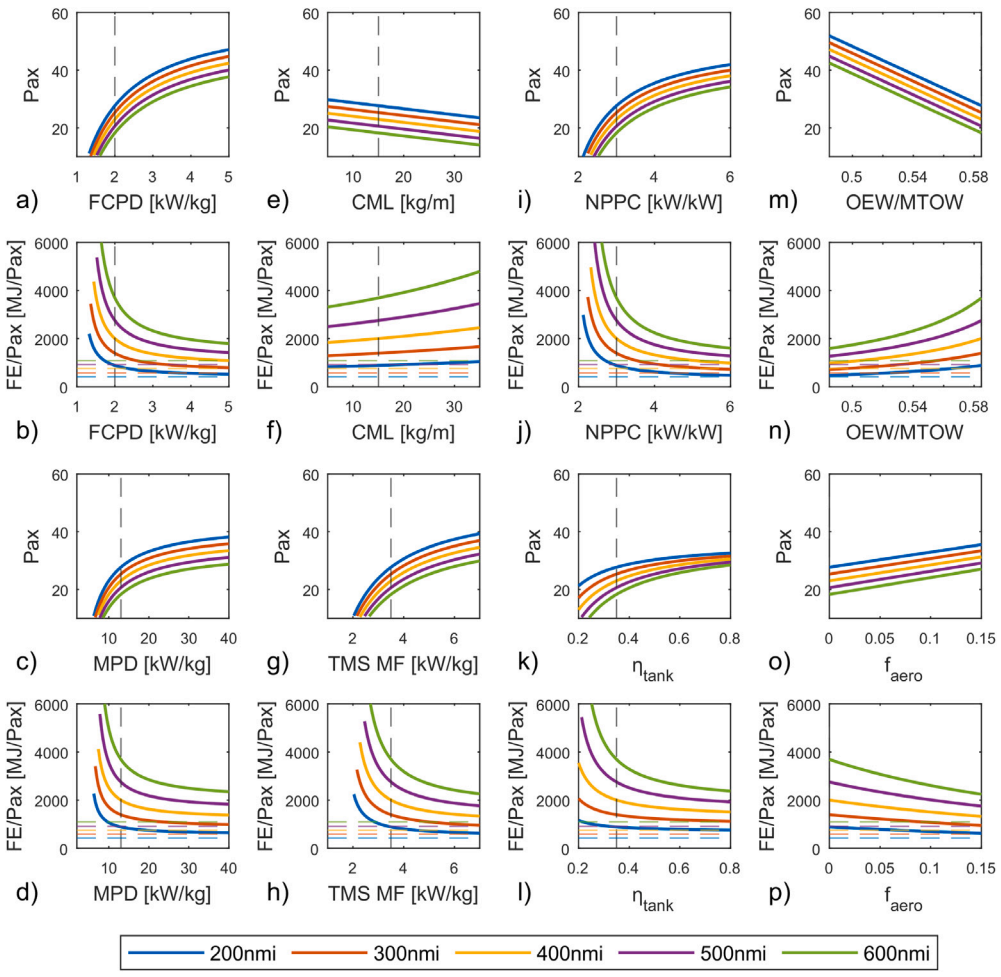

Fig. 3. Gradient analysis for the FC aircraft. The horizontal dashed lines correspond to the conventional aircraft for the range with the same colour.

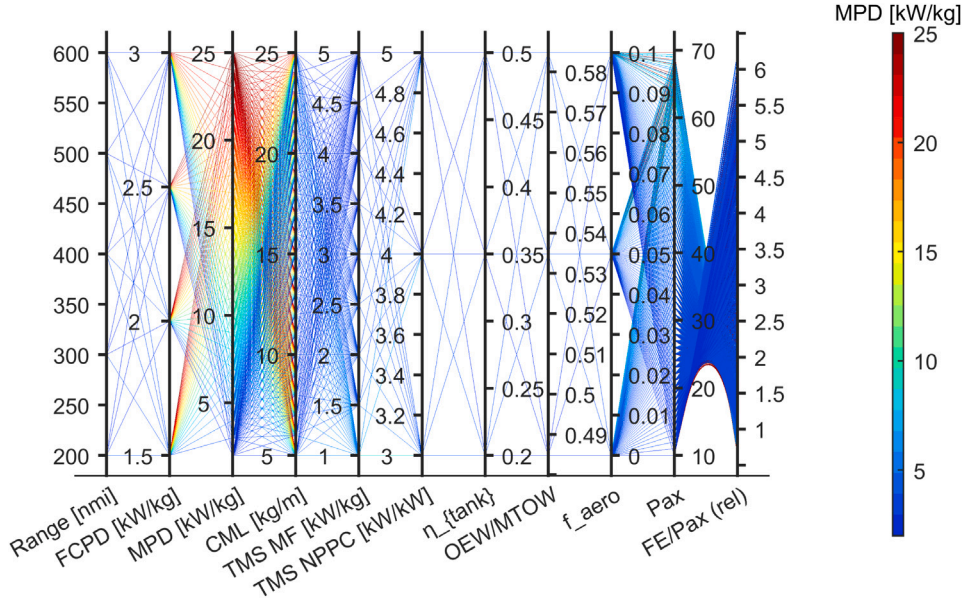

Fig. 4. Combinations of technology targets for FC aircraft.

combined with a breakthrough in HT-PEMFC technology with NPPC = 5 kW/kW.

The NPPC has a domino effect from the point of view that it influences the mission energy, the tank mass and all the power-depended component masses (FC, motor, TMS). Any NPPC increase, thus, decrease in TMS drag and/or parasitic power consumption will decrease all the components' power requirement and heat generation, while the TMS mass factor only has a direct impact on mass (Fig. 6). In reality,

Table 2
Indicative combinations of technology targets for the FC aircraft under different criteria for 300 nmi.

Criteria	FCPD [kW/kg]	MPD [kW/kg]	CML [kg/m]	TMS MF [kW/kg]	TMS NPPC [kW/kW]	η_{tank}	OEW/ MTOW	f_{aero}	Pax	FE/pax [MJ/pax]	FE/pax (rel)
set values	2	13	15	3.5	3	0.35	0.5848	0	25	1413	2.43
30 pax, energy penalty (v1)	2	8	25	3.5	5	0.5	0.5848	0	30	995	1.7
30 pax, energy penalty (v2)	2	13	15	3.5	3.5	0.35	0.5848	0	30	1105	1.9
in-flight energy breakeven	2	9	15	3.5	5	0.5	0.5348	0.05	49	584	1.004
max pax allowed by volume, emphasis on aircraft technologies	2	10	15	4	5	0.5	0.4848	0.1	68	403.5	0.69
max pax allowed by volume, emphasis on electrical technologies	2.5	13	8	5	5	0.6	0.5348	0.05	68	421	0.72
Emphasis on SC (with $\eta_{motor} = 99\%$)	1.5	25	5	3	5	0.4	0.5848	0	30	962	1.65
What if HT-PEMFC is not achieved? Emphasis on other technologies	1.5	13	8	1.5	3	0.6	0.4848	0.15	25	1268	2.18

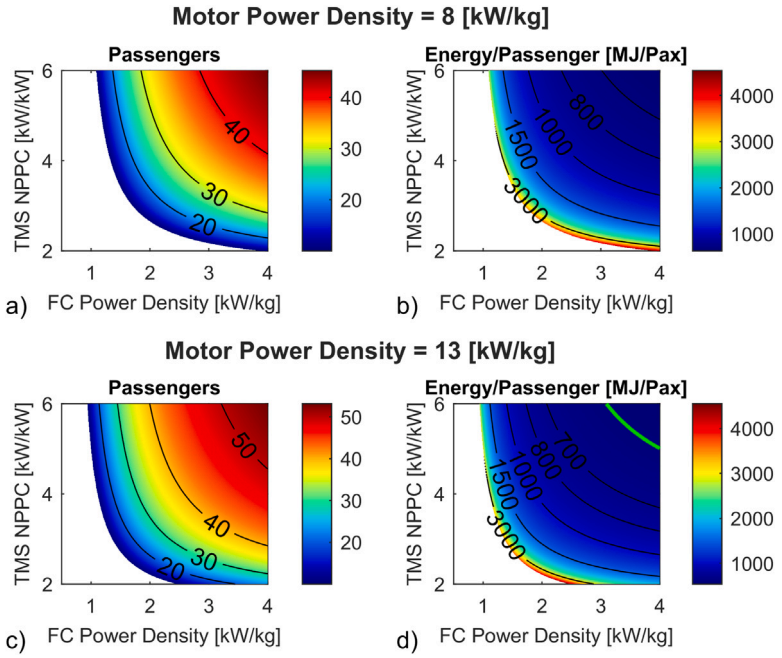

Fig. 5. Trade-off in FC power density and TMS NPPC along with benefits from motor technology upscaling for FC aircraft.

an interrelationship between TMS MF and TMS NPPC improvement is expected, but it depends on the type of TMS and where the TMS improvement comes from.

The NPPC affects fuel consumption, therefore, it influences the impact of the tank gravimetric efficiency changes across each NPPC constant line. From the default values (Table 1), the pax capability can improve from 25 to 30 (Fig. 7c), if the NPPC increases from 3 kW/kW to 3.5 kW/kW, or the tank gravimetric efficiency from 0.35 to 0.6. If the MPD reaches only 8 kW/kg (Fig. 7a), an NPPC = 5 kW/kW, or a combination of NPPC = 4.2 kW/kW and $\eta_{tank} = 0.6$ is needed to have a 30-pax capability.

For today's aircraft technology (OEW/MTOW = 0.5848), the in-flight energy per pax of the conventional 50-pax aircraft cannot be breakeven even if the TMS mass factor is maximised, along with FCPD = 2 kW/kg (Fig. 8f). A reduction in the aircraft structural mass up to 17.1% can be a catalytic factor in breaking even the energy/pax of the conventional 50 pax and 70 pax regional aircraft (Fig. 8b), and overall it can alleviate the constraints and penalties of the electrical technologies.

The last trade-off map that is examined for the FC aircraft is the MPD vs. Cable Mass/Length (CML) in Fig. 9. For the cable length of 20 m which was assumed for this aircraft class, the rate of change across the MPD value is more significant than across the CML values (y axis). For higher cable lengths the impact of CML would increase, so the y axis could be scaled accordingly to achieve the same trade-off map. In reality, the evolution of these two parameters is expected to be linked as they are both dependent on electrical technology improvements and system voltage. Finally, it is observed that at lower NPPC, where there is a higher power penalty due to the TMS, the same isolines for pax and energy/pax are shifted to the right of the map, while each incremental step of MPD has a higher relative impact due to the higher system power.

Starting from the baseline technology values that are the minimum to start considering the potential of regional aircraft, it seems

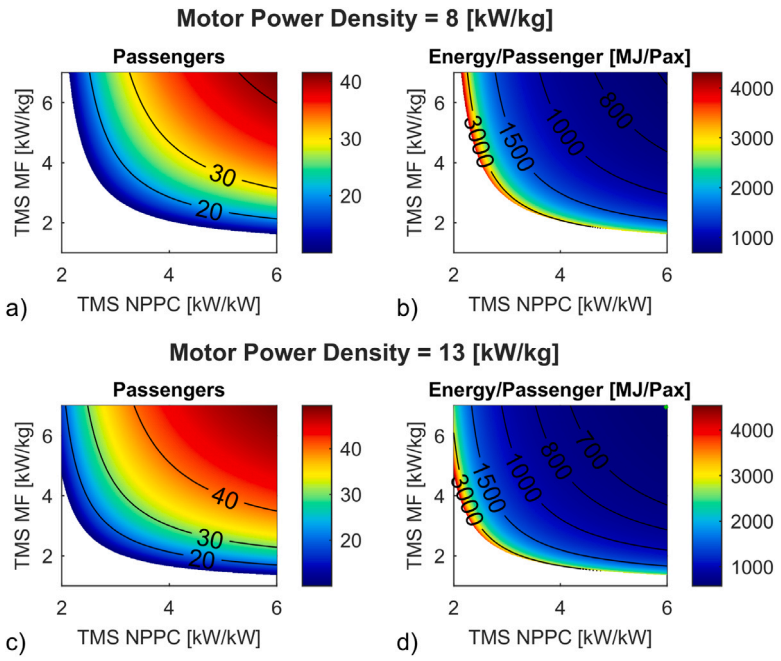

Fig. 6. Trade-off in TMS NPPC and TMS mass factor along with benefits from motor technology upscaling for FC aircraft. The green line represents the energy/pax of today's 50-pax regional aircraft.

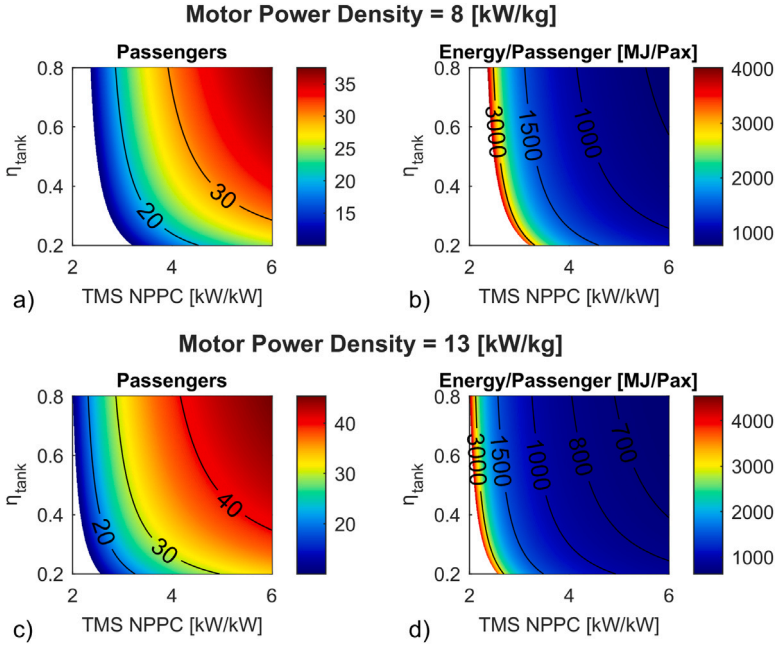

Fig. 7. Trade-off in TMS NPPC and tank gravimetric efficiency along with benefits from motor technology upscaling for FC aircraft.

extremely difficult for the FC aircraft to crossover the breakeven line with upscaling only in 1 or 2 technologies.

3.2. Battery aircraft

3.2.1. Reserve mission approach for battery aircraft

The provision for the energy source to cover the diversion mission and holding time is a critical factor in the feasibility of a battery aircraft. Typical specifications for the diversion mission and holding time of a regional aircraft are presented in Table 3.

For a 200 nmi fully electric mission, the reserve battery mass can be ~45% of the total usable battery energy (up to SoC = 20%). This entails a significant mass penalty, which is 3846 kg for 500 Wh/kg, while maintaining one gas turbine in case of a diversion requires only 948 kg additional mass (Table 4). For this reason, all the subsequent battery aircraft analysis will consider a gas turbine for the diversion mission and reserve fuel.

Table 3
Reserve mission specifications.

Diversion range	100 nmi
Diversion altitude	10 000 ft
Diversion mach	0.39
Hold time	30 min
Hold altitude	1500 ft

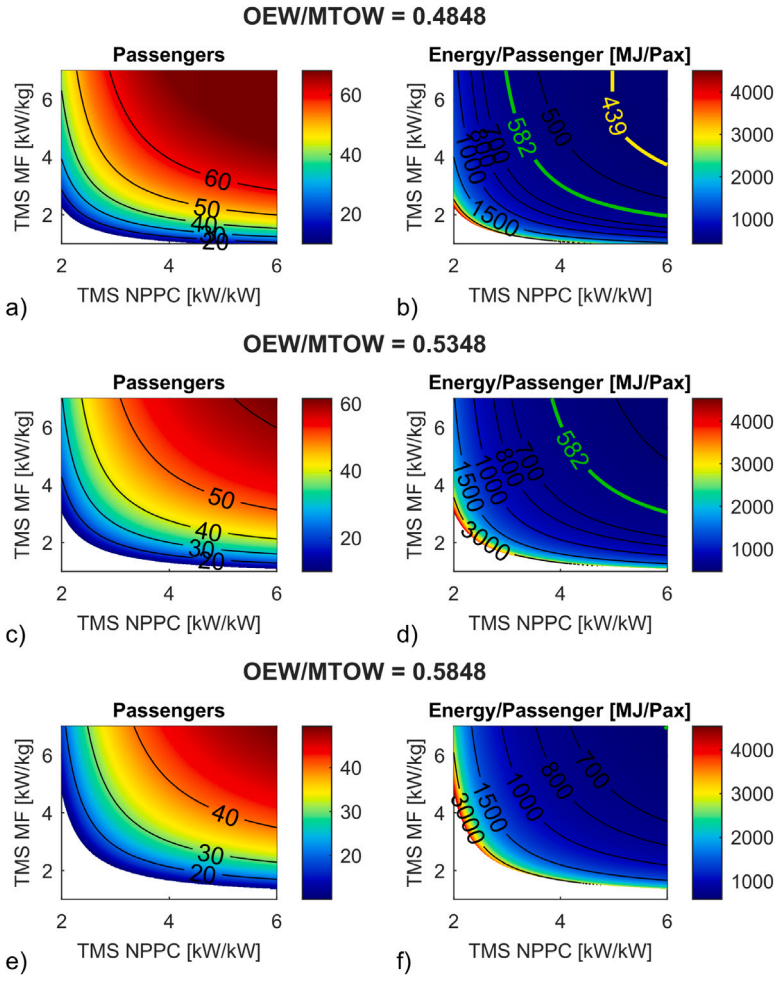

Fig. 8. Trade-off in TMS NPPC and TMS mass factor along with benefits from aircraft structural efficiency improvement for FC aircraft. The green line represents the energy/pax of today's 50-pax regional aircraft and the yellow line represents the energy/pax of today's 70-pax regional aircraft.

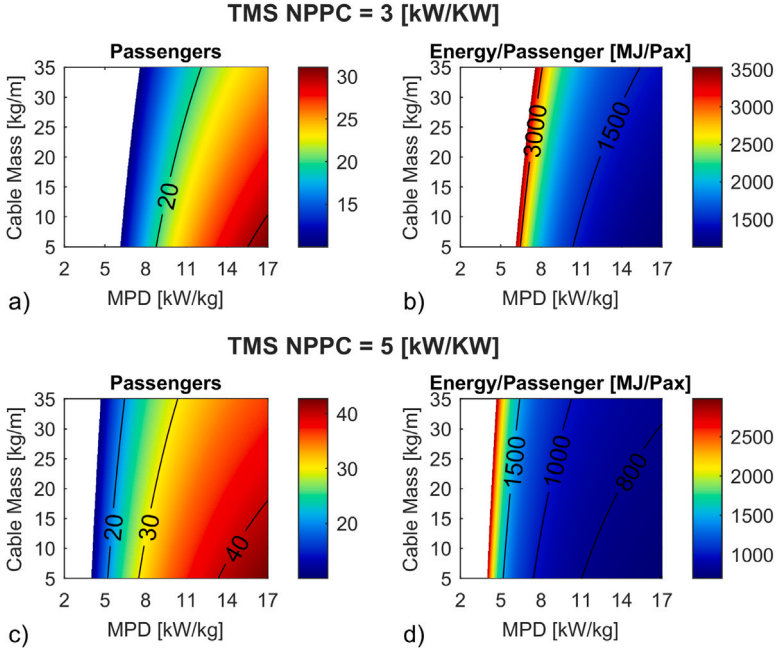

Fig. 9. Trade-off in motor and power electronic power density and cables mass/length along with benefits from improving the TMS NPPC for FC aircraft.

Table 4
Mass penalty of reserve battery energy and mass penalty of gas turbine reserve.

Diversion and hold with battery	Diversion and hold with GT and fuel
Reserve battery energy = 1923 kWh	GT mass = 481 kg
(Reserve battery energy)/(total usable battery energy) = ~45%	Reserve fuel mass = 467 kg
Reserve battery mass @ 500 Wh/kg = 3846 kg	Reserve total mass = 948 kg
Reserve battery mass @ 750 Wh/kg = 2564 kg	(includes 5% contingency)

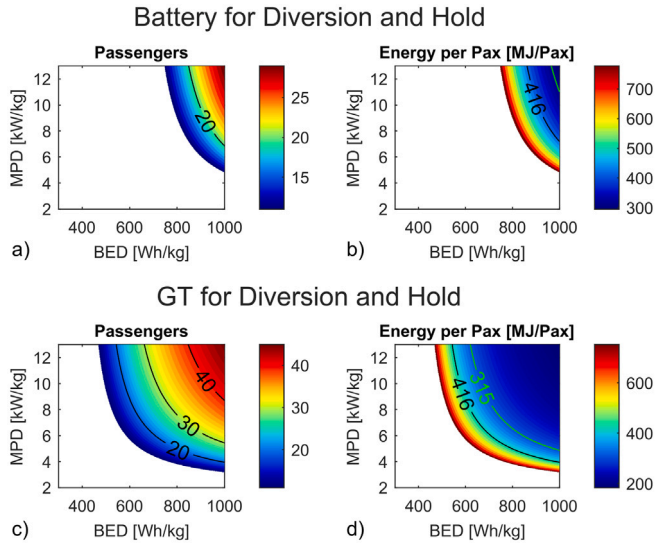

Fig. 10. Battery energy density and motor power density pax capability and energy performance trade-off for a 200 nmi mission using battery reserve energy and a GT for the diversion.

Without the use of a gas turbine for reserves, a 200 nmi battery mission with more than 10 pax becomes feasible if the battery technology reaches a BED > 850 Wh/kg and the MPD > 7 Wh/kg. However, if a gas turbine is used for reserves, a 200 nmi battery mission becomes feasible for BED > 500 Wh/kg and MPD > 7 kW/kg. Different enabling combinations can be extracted from Fig. 10.

Maintaining one gas turbine and reserve fuel becomes an enabling solution for battery aircraft. A similar approach is also considered for the electric aircraft of Heart Aerospace [34]. The fully electric range of the first version will be up to 200 km (108 nmi), the diversion mission will be with a gas turbine and longer ranges will be hybrid until the battery technology further improves.

3.2.2. Technology target scenarios

The pax capability and the in-flight energy per passenger of a battery aircraft for combinations of technology factors have been analysed using parallel coordinates plot due to the multidimensional nature of the problem (Fig. 11). The technology factor combinations that lead to a passenger capability below 10 pax have been filtered out.

After the design space (Fig. 11) was analysed and reviewed, some distinct technology development scenarios are summarised in Table 5. Due to the low operating temperatures of batteries, the NPPC has been kept constant at 3 kW/kW as it will be explained in Section 5.2.

BED targets under set levels for the other technologies

First, BED targets are identified to achieve a minimum 30 pax capability (Table 5, No 1–3) under set targets for the electrical technologies and advanced aircraft. If the aircraft technologies reach OEW/MTOW = 0.5358 and f_{aero} = 0.05 respectively, combined with an advanced MPD = 13 kW/kg, the minimum BED targets to achieve 30 pax drop at 480 Wh/kg for 200 nmi, 690 Wh/kg for 300 nmi and 900 Wh/kg for 400 nmi (Table 5).

What if BED does not go beyond 350 Wh/kg?

The next scenario (Table 5, No 4) examines a pessimistic case where novel battery chemistries do not mature for aircraft applications and BED does not go beyond 350 Wh/kg (potentially with improving the pack/cell ratio of existing chemistries and small chemistry improvements of current battery technology). In this case, it becomes crucial that both electrical and aircraft technologies are pushed to advanced levels to compensate for the barrier in battery development. A 200 nmi fully electric flight will still be possible with 30 pax and energy saving, but longer ranges will not be feasible in fully electric mode.

Optimistic levels across all technologies

Considering that it will be very challenging for batteries to exceed 600 Wh/kg the last scenario investigates the energy performance using advanced electrical technologies and aircraft technologies (OEW/MTOW improvement by 17% and aerodynamic improvement by 15%) combined with BED at 600 Wh/kg. In this optimistic scenario, 200 nmi is feasible with 62 pax, 300 nmi with 43 pax and 400 mi with 24 pax, and all three ranges will be performed with energy/pax saving compared to the conventional aircraft.

3.2.3. Gradient analysis

In the battery aircraft gradient analysis (Fig. 12), the x value at which the line starts existing signifies at which value this technology factor starts enabling a regional aircraft with at least 10 pax. At values shortly beyond the enabling thresholds, the energy/pax drops below the conventional due to the high battery efficiency. There is a significant offset between the curves of different range, while for the FC aircraft the curves nearly coincided due to the low mass change between the ranges. The gradient of the pax and FE/pax is still far from becoming flat even at the BED upper limit (Fig. 12a,b). Significant benefits would continue to be found at BED beyond the presented range. Improvements in the two factors associated with the TMS offer low pax capability benefits in the order of 2–3 pax because of the low heat generation of a battery system. Even at extremely low NPPC in the order of 2 kW/kW, the TMS power penalty is around 6% as will be analysed in Section 5.2. Further reducing this 6% power penalty is welcome as it would reduce the battery energy but TMS is not a major bottleneck for battery aircraft.

3.2.4. Technology levels trade-off and upscaling benefits

The primary enablers of the battery aircraft are the BED, the MPD and the OEW/MTOW and their trade-offs in the battery aircraft performance are presented in Fig. 13. The aerodynamic efficiency improvement also has a beneficial effect in reducing the energy consumption and battery mass, but with improvements up to 10% it is not considered as critical as the BED, rather than a welcome boost to reduce the minimum required BED or MPD.

3.3. Effective energy comparison of fuel cell and battery aircraft

The performance of a fuel cell aircraft and a battery aircraft will be compared on the basis of the effective energy density (EED) of the systems. The EED is defined as the ratio of the propulsion energy for the mission to the total mass of the system. The deviation of the real BED of the battery from the EED considers the 20% unused battery energy, the mass of the electric system and the TMS (Eq. (1)), while the EED of the FC system includes the mass of the FC, the electric system, the TMS, the tank as well as the mass of the hydrogen that needs to be stored to provide the propulsion energy (Eq. (2)).

$$EED_{Bat,system} = \frac{Propulsion\ Energy}{M_{Bat} + M_{motor} + M_{PE} + M_{cables} + M_{TMS}} \quad (1)$$

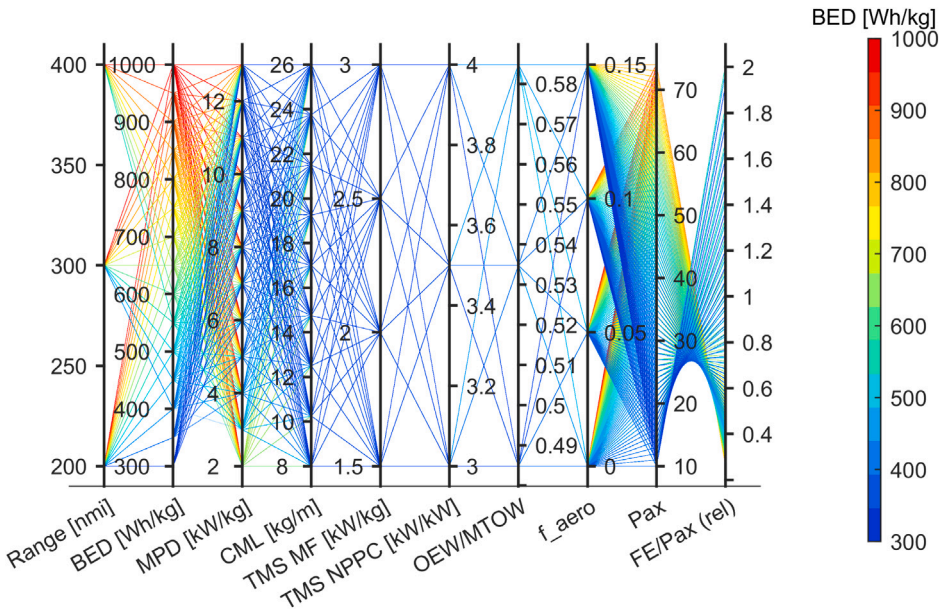

Fig. 11. Technology factor combinations for battery aircraft with range between 200–400 nmi.

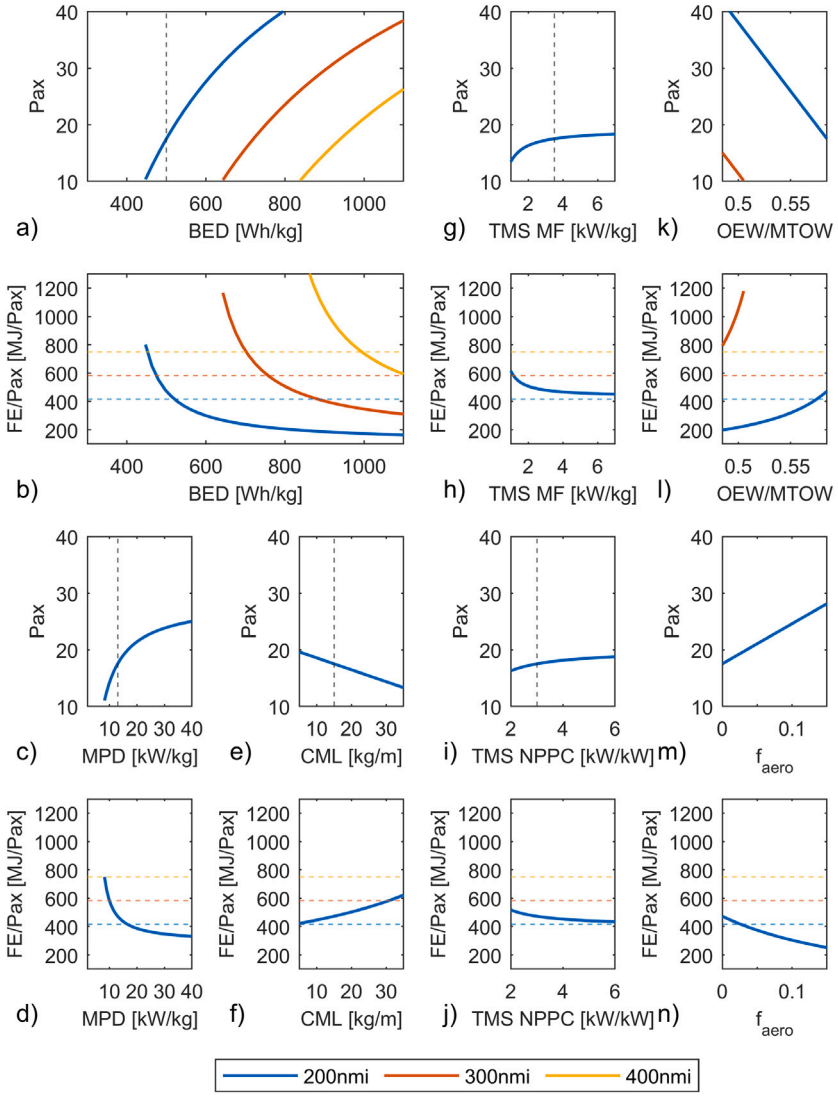

Fig. 12. Gradient analysis for the battery aircraft. The horizontal dashed lines correspond to the conventional aircraft for the range with the same colour.

Table 5
Combinations of technology factors for battery aircraft.

No	Range	Criteria	BED [Wh/kg]	MPD [kW/kg]	CML [kg/m]	TMS MF [kW/kg]	NPPC [kW/kW]	OEW/ MTOW	f_{aero}	Pax	FE/pax (rel)	FE/pax [MJ/pax]
1	200	At least 30 pax	480	13	15	3.5	3	0.5348	0.05	30	0.63	263
2	300	At least 30 pax	690	13	15	3.5	3	0.5348	0.05	30	0.65	378
3	400	At least 30 pax	900	13	15	3.5	3	0.5348	0.05	30	0.66	494
4	200	What if the battery does not exceed 350 Wh/kg?	350	13	15	3.5	3	0.4848	0.15	30	0.57	236
5	200	Optimistic targets	600	13	8	3.5	3	0.4848	0.15	62	0.27	114
6	300	Optimistic targets	600	13	8	3.5	3	0.4848	0.15	43	0.41	237
7	400	Optimistic targets	600	13	8	3.5	3	0.4848	0.15	24	0.74	555

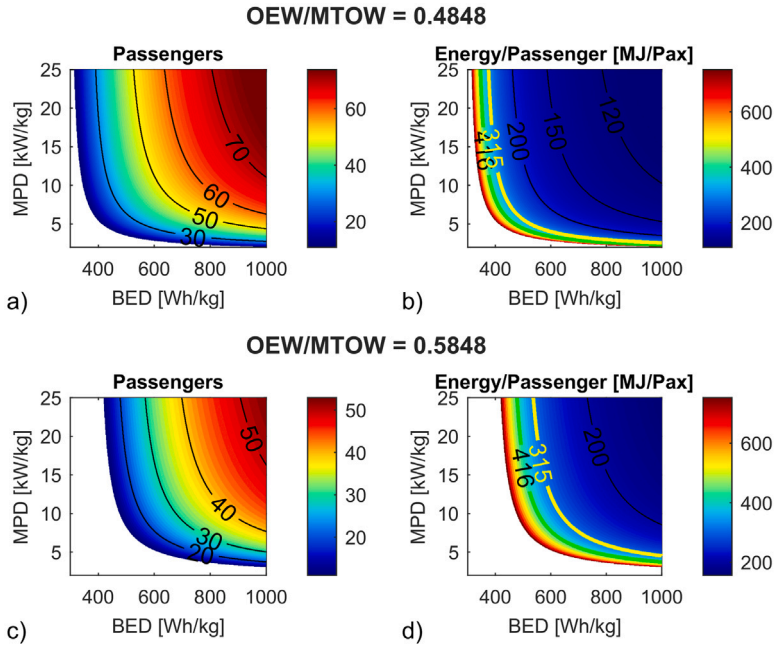

Fig. 13. Battery energy density and motor power density trade-off for different aircraft structural efficiency at 200 nmi. The green line indicates the levels of today's 50-pax regional aircraft, and the yellow line the levels of today's 70-pax regional aircraft.

$$EED_{FC,system} = \frac{Propulsion\ Energy}{M_{FC} + M_{motor} + M_{PE} + M_{cables} + M_{TMS} + M_{tank} + M_{H2}} \quad (2)$$

The propulsion energy was defined as the energy provided by the motor to the propeller. It was preferred over the consumed energy so that there is a fairer comparison between the highly efficient battery and the less efficient FC system that needs to store more hydrogen energy.

The EED of the battery system improves slightly with increasing range (Fig. 14a,c,e). The battery mass, which has the most impact, scales up with range, while the rest of the components are sized for power and have constant mass. The EED of the FC system improves significantly at higher range, because most of the components are sized for power and a small amount of hydrogen and tank mass is added for higher ranges (Fig. 14b, d, f). Also, the battery aircraft is less sensitive to the TMS variations, while the FC system EED is constained at low TMS MF.

Ultimately, the breakeven surface where the $EED_{Bat,system}$ equals the $EED_{FC,system}$ is presented for combinations of TMS MF, FCPD and BED, and three mission ranges in Fig. 15. For combinations on the left of the surfaces, the FC system has higher EED, and on the right the EED of a battery system is higher. At lower TMS MF and lower range, the battery system EED breakevens with the FC system TMS at lower BED. Despite the NPPC at 3 kW/kW, which penalises the FC system significantly, if FCPD>2 kW/kg and TMS MF>3 kW/kg, the battery system cannot breakeven the FC system EED without BED>750 Wh/kg at any range. At ranges over 400 nmi, even with the most pessimistic FC factors (TMS MF = 1 kW/kg and FCPD = 1 kW/kg), the FC system EED cannot be matched without BED>600 Wh/kg.

3.4. Hybrid FC - battery aircraft

The FC system sizing is driven by the maximum power and heat, while the battery system mass is driven by the energy. Hybrid combinations of FC-Bat can improve the energy performance and pax (Fig. 16) by exchanging TMS and FC mass with battery mass (Fig. 17).

The triangular regions in Fig. 16 indicate that below a certain BED there is no benefit in going to higher Degree of Hybridisation (DoH) because the increased battery mass will cancel out any savings from the FC and TMS (Fig. 17c, d). At NPPC = 3 kW/kW, if the BED<500 Wh/kg, there is no reason for battery takeoff DoH >39%, which is also the crossover DoH above which the FC stops being sufficient to cover the cruise alone. Up to DoH<39% the battery is used only for the power peaks at take-off and climb (Fig. A.51) which results in a relative small battery mass (Fig. 17b), therefore, the energy/pax isolines are nearly horizontal when moving across the BED axis (Fig. 16). Even for battery technology close to today's (around 300 Wh/kg), a hybrid FC+Battery system with the FC being sized cruise can bring benefits compared to a FC-only aircraft of the same technology factors.

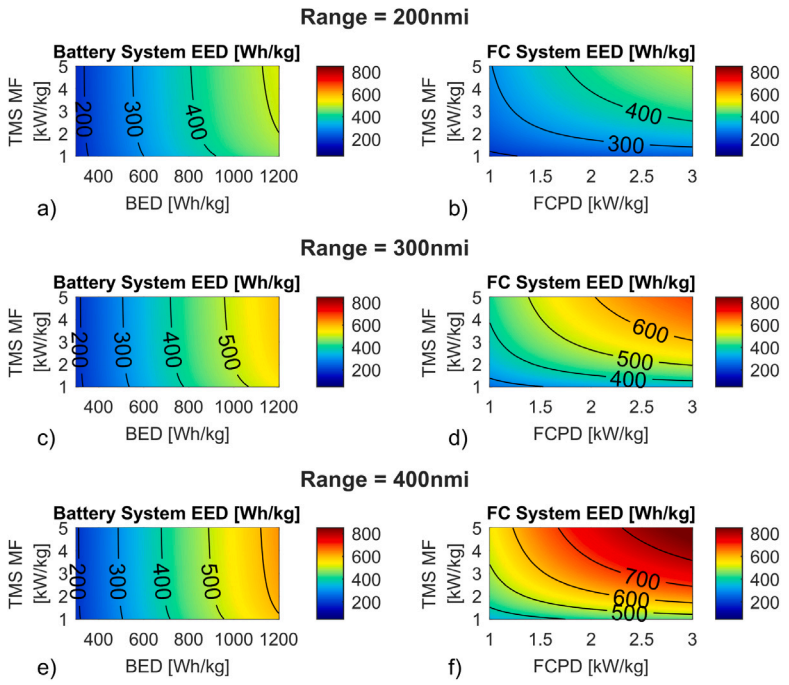

Fig. 14. Comparison of effective energy density between FC and Batteries system.

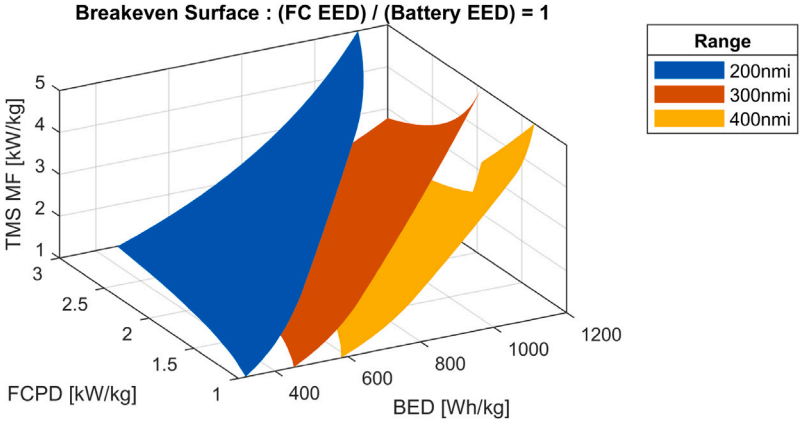

Fig. 15. Breakeven surface between FC and battery system for three ranges.

At DoH = 39% and NPPC = 3 kW/kW, the energy/pax is ~800 MJ/pax, while for a FC aircraft of the same technology factors (Table 1) and 300 nmi the energy/pax is around 1400 MJ/pax. Also, the pax capability has increased from 25 to 40.

One of the challenges with this system is that the FC is downsized so in case of a diversion mission or turnaround where the full power must be provided, the FC on its own may not be able to deliver the full power. The battery would have to be oversized. For this reason, even if the same energy/pax can be achieved with higher takeoff DoH than 39%, it is preferred to go with the lowest battery DoH that will give higher FC power capability.

4. Technology factor exploration - Lifecycle effects

4.1. Degradation

4.1.1. Fuel cell degradation rate

A target time-on-wing can be achieved with different combinations of "end of life" state of health (relative power loss in the case of fuel cells) and degradation rates (Fig. 18). To avoid severe changes and disruptions in engine availability and fleet management the time-on-wing target is set to be at least equal or greater than 8000 Engine Flight Cycles (EFC) which is the reference point for the conventional aircraft. This target can be achieved with either a fuel cell degradation rate of 0.001% power loss/flight cycle and a fuel cell oversizing factor 1.08, or a degradation rate of 0.0005% and an oversizing factor of 1.04. Ideally, the solution of the lowest degradation rate is desirable to minimise the "dead" weight of oversizing.

4.1.2. Battery degradation rate

A target time-on-wing can be achieved with different combinations of "end of life" state of health (as relative available capacity in the case of batteries) and degradation rates. A 8000FC target time on wing can be achieved with either a battery degradation rate of 0.003% capacity loss/flight cycle and an oversizing factor 1.25, or a degradation rate of 0.0006% and an oversizing factor of 1.05 (Fig. 19). Based on this oversizign decision, the technology 2D maps can be used to identify the effective BED accounting for oversizing.

The equations for the production of Fig. 18 and Fig. 19 are included in Appendix A.5.

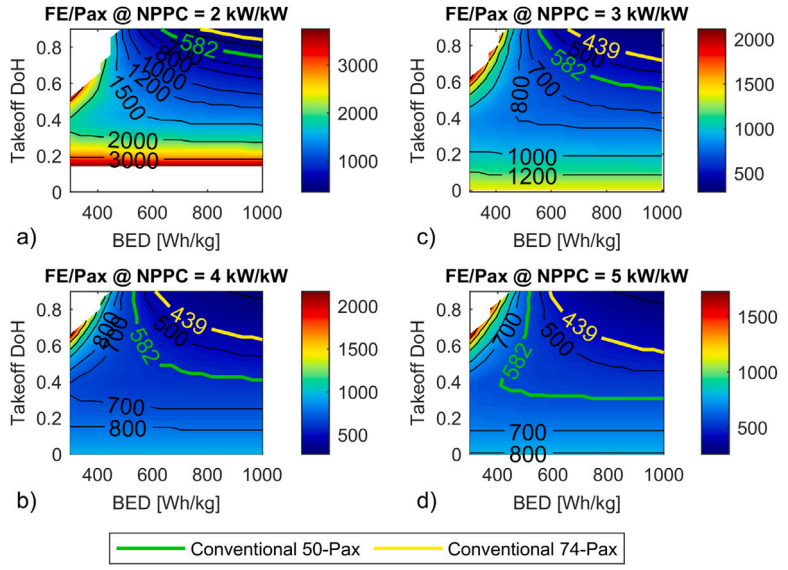

Fig. 16. Battery energy density, takeoff DoH and TMS NPPC energy/pax trade-offs for a hybrid FC+Bat system for a 300 nmi mission.

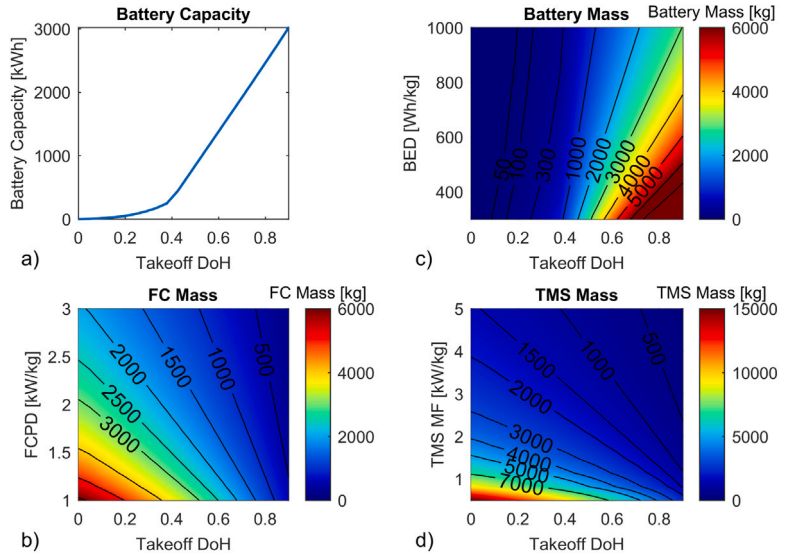

Fig. 17. Battery mass and TMS mass for variable takeoff battery DoH in a hybrid FC+Battery system.

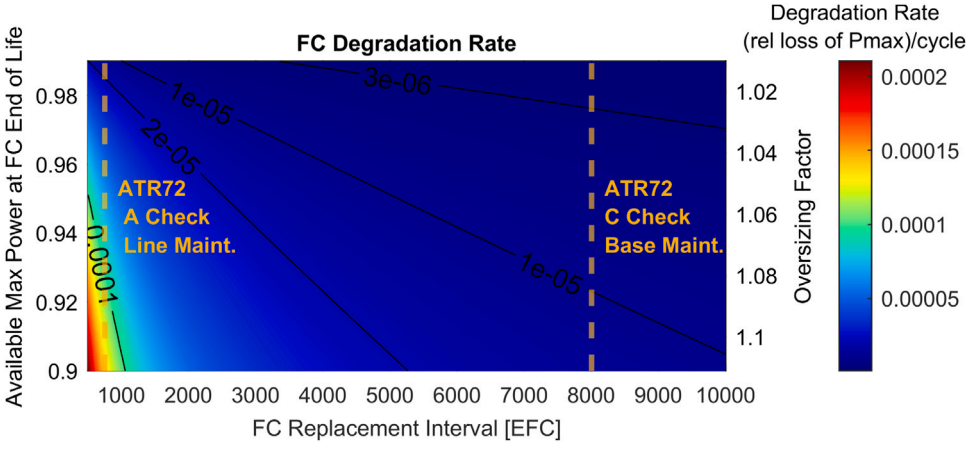

Fig. 18. Degradation rate target for the fuel cell as a function of time of intervals in relative available power at the end of life (compared to the initial).

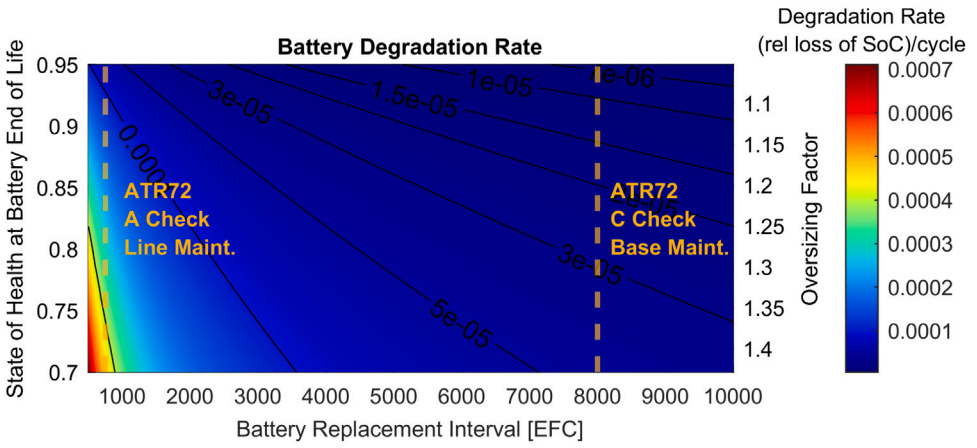

Fig. 19. Degradation rate target for the batteries as a function of time of intervals in relative available capacity at the end of life (compared to the initial).

Table 6
Energy per pax at 300 nmi for 2 selected technology scenarios.

Case	FCPD [kW/kg]	MPD [kW/kg]	CML [kg/m]	TMS MF [kW/kg]	NPPC [kW/kW]	η_{tank}	OEW/ MTOW	f_{aero}	Pax	FE/pax [MJ/pax]	FE/pax (rel)
1 (S2)	2	13	15	3.5	3.5	0.35	0.5848	0	30	1105	1.9
2 (S5)	3	13	15	4	5	0.35	0.5348	0.05	63	455	0.78

4.2. Lifecycle energy and CO_2

4.2.1. Introduction

The flight energy per pax (FE/pax) is an important figure of merit but also needs to be extended to the lifecycle CO_2 and lifecycle energy per pax. This section will investigate the interaction between aircraft-level performance and infrastructure performance. Under given infrastructure performance, a maximum FE/pax to avoid lifecycle penalties or achieve a set reduction can be identified. Then, this maximum FE/pax can be used to refer to the technology factor maps presented in the previous section and identify technology factor combinations that can deliver this FE/pax. Reversely, if the technology factors are given as constraints or targets to be achieved, their resulting FE/pax can be used to calculate the maximum infrastructure metrics needed to avoid penalties. This section will focus on lifecycle CO_2 and lifecycle energy from an energy well-to-wake perspective, ignoring the battery or fuel cell production impact. The impact of production needs to be assessed in a way that accounts for the service life on the aircraft and potential second life, and will be discussed separately in Sections 5.4.4 and 5.4.3.

4.2.2. Fuel cell aircraft

A parametric analysis for the hydrogen production energy demand and the carbon intensity of the grid is performed. In Table 6 two technology scenarios representing different horizons are selected for the FC aircraft lifecycle analysis. In the first column, the numbers in the brackets (S2) and (S5) indicate to which technology scenarios of subsequent Fig. 46 the two selected cases for the lifecycle analysis correspond. The first case refers to near-term technology with NPPC = 3.5 kW/kW that results in 30 pax and 90% in-flight energy penalty and the second case refers to a set of technology targets for an energy-efficient aircraft by 2050.

For the technology case 1 with FE/pax penalty, the lifecycle energy/pax can be 2.5–3.7 times the lifecycle energy of a conventional aircraft depending on the range, if the energy demand for LH2 is near today's value ($1.75MJ_{el}/MJ_{LH2}$) - Fig. 20. At 300 nmi, the relative lifecycle energy is 2.77.

For the technology scenario 2 that has a saving in FE/pax, today's energy demand for LH2 ($1.75MJ_{el}/MJ_{LH2}$) leads to a relative LCE/pax of 1.06 (near breakeven) for 200 nmi and 1.29 (29% LCE penalty) for the 600 nmi. If the on-board technology reaches the advanced scenario 2, a small energy improvement in the hydrogen production, transport and liquefaction from 1.75 (Fig. 21) will lead to a lifecycle energy saving.

FC aircraft will not have in-flight CO_2 emissions but lifecycle CO_2 emissions come from the CI of the hydrogen production. Using the hydrogen production methods summarized in Section 5.4.2, comparison of lifecycle CO_2 impacts, relative to conventional aircraft, is provided in Fig. 22 for technology scenario 1. For on-board technology targets to achieve 30 pax using LT-PEMFC, a CI >7.3 kg_{CO2}/kg_{H2} will create a lifecycle CO_2 penalty even for the 200 nmi mission, while a CI >5 kg_{CO2}/kg_{H2} will create a penalty at 600 nmi. The breakeven CI at 300 nmi is 6.5 kg_{CO2}/kg_{H2}.

With the further improved technology levels of scenario 2 (Table 6), even more carbon-intense hydrogen production methods (up to 17.2 kg_{CO2}/kg_{H2}) would breakeven the lifecycle CO_2, and even more countries with higher grid carbon-intensity would be able to operate and refuel the FC aircraft without a penalty in lifecycle CO_2 before green hydrogen is widely available (see Fig. 23).

There are two directions to approach the combinations of on-board and infrastructure technology targets. The first one was to start from the on-board technology and calculate the lifecycle impact for variable lifecycle figure of merits. The other way is to start from different lifecycle figures of merit and define the minimum targets needed to be set at on-board technology level. The maximum flight energy/pax needed to avoid a negative lifecycle effect for given infrastructure performance can be extracted from Fig. 24. The on-board technology combination should be able to achieve this flight energy/pax to breakeven or less to offer a saving.

If the hydrogen production infrastructure is at 10 kg_{CO2}/kg_{H2}, the flight energy per pax should be less than 1350 MJ/pax at 600 nmi and less than 500 MJ/pax at 200 nmi to breakeven the lifecycle energy per pax of the conventional. Although green hydrogen (which has a CI<5 kg_{CO2}/kg_{H2}) is already available, its high cost and land surface requirements for renewable sources may slow down its wider adoption, and different production methods are also explored and may be combined in the ecosystem. Even if green hydrogen becomes widely available and in theory can eliminate lifecycle CO_2 despite poor in-flight energy performance, there is still significant merit in reducing the flight energy per pax, as this will reduce the required green hydrogen plants size and total costs. The hydrogen production methods and how

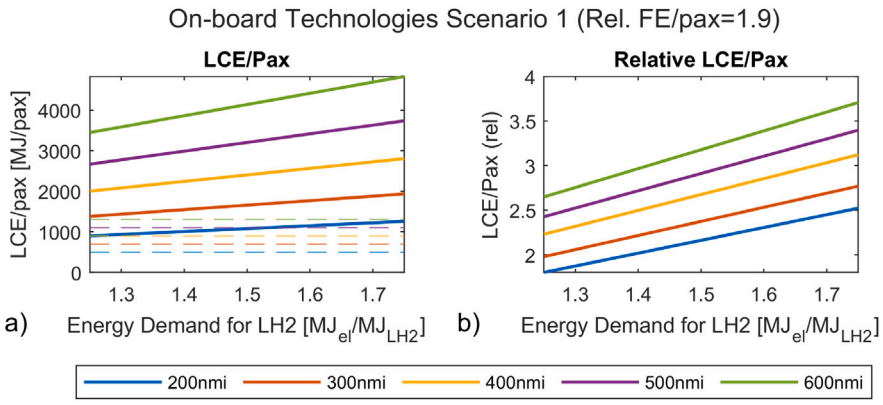

Fig. 20. Technology scenario 1 - Lifecycle energy per pax (considering flight energy, fuel production and transport) for different flight energies. The dashed lines correspond to the conventional aircraft.

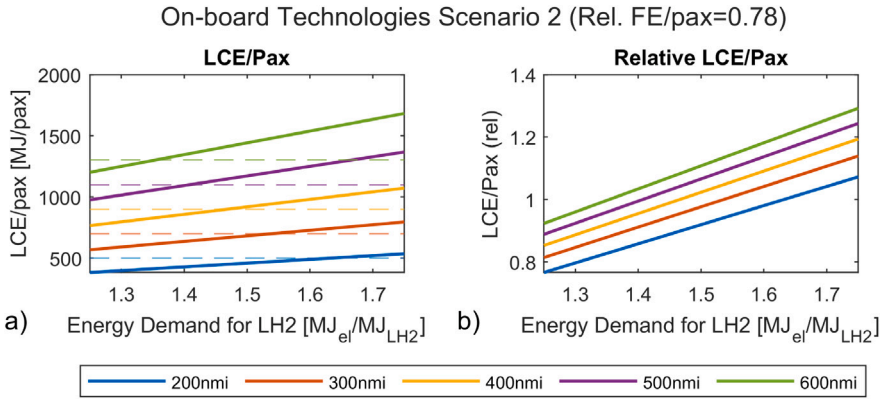

Fig. 21. FC aircraft lifecyle energy per pax for on-board technology scenario 2.

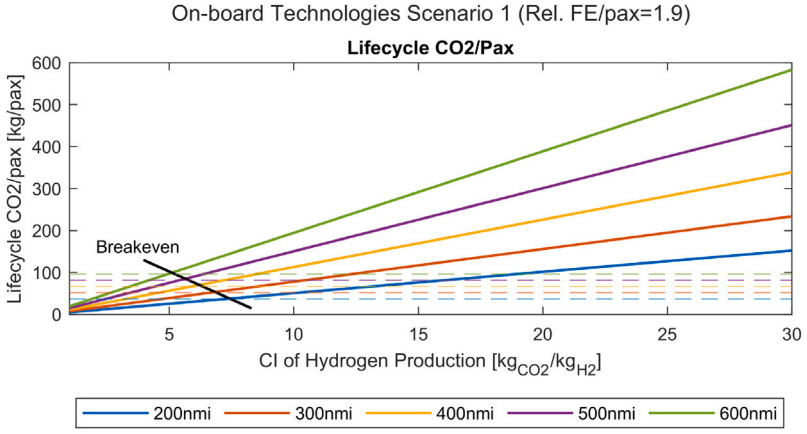

Fig. 22. FC aircraft lifecycle CO_2 per pax for different grid carbon intensity for technology scenario 1. The dashed lines correspond to the conventional aircraft.

they relate to the CI will be discussed in Section 5.4.2. Similarly, if the energy demand for the hydrogen production, liquefaction and transport reduces from today's value at 1.75 MJ_{el}/MJ_{LH2} to 1.5 MJ_{el}/MJ_{LH2}, the breakeven in-flight energy/pax, reduces by 15% (Fig. 24c).

4.2.3. Battery aircraft

The infrastructure figure of merits associated with the battery lifecycle are the efficiency and the carbon intensity of the electrical grid. The feasibility and range of a battery aircraft has less degrees of freedom and is constrained by the upper limits in battery energy density, therefore, one indicative scenario with BED = 500 Wh/kg is examined here (Table 7). In the first column, the number in the brackets (S2a) indicates to which technology scenario of subsequent Fig. 48 the selected case for the lifecycle analysis corresponds.

For this technology scenario, only the 200 nmi mission is feasible with at least 10 pax. In Fig. 25, even with 50% electricity production and transport efficiency (η_{grid}), the lifecycle energy of the conventional 50-pax can be breakeven (Fig. 25). The dashed lines represent the lifecycle energy of the jet fuel consumed by the conventional 50-pax for

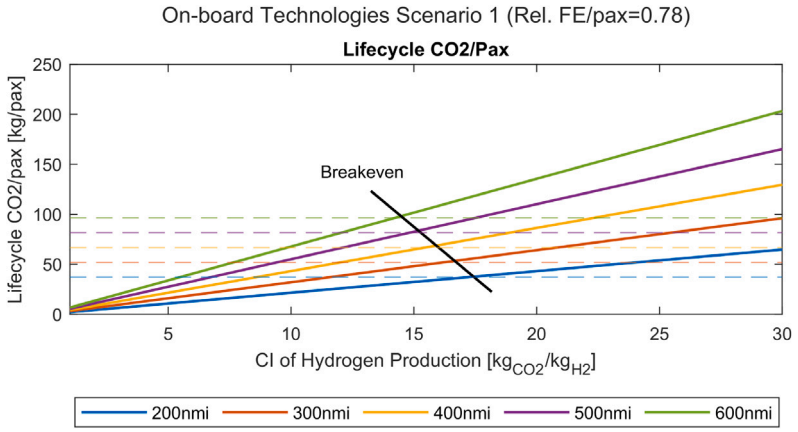

Fig. 23. FC aircraft flight and lifecycle CO_2 per pax for different grid carbon intensity for technology scenario 2. The dashed lines correspond to the conventional aircraft.

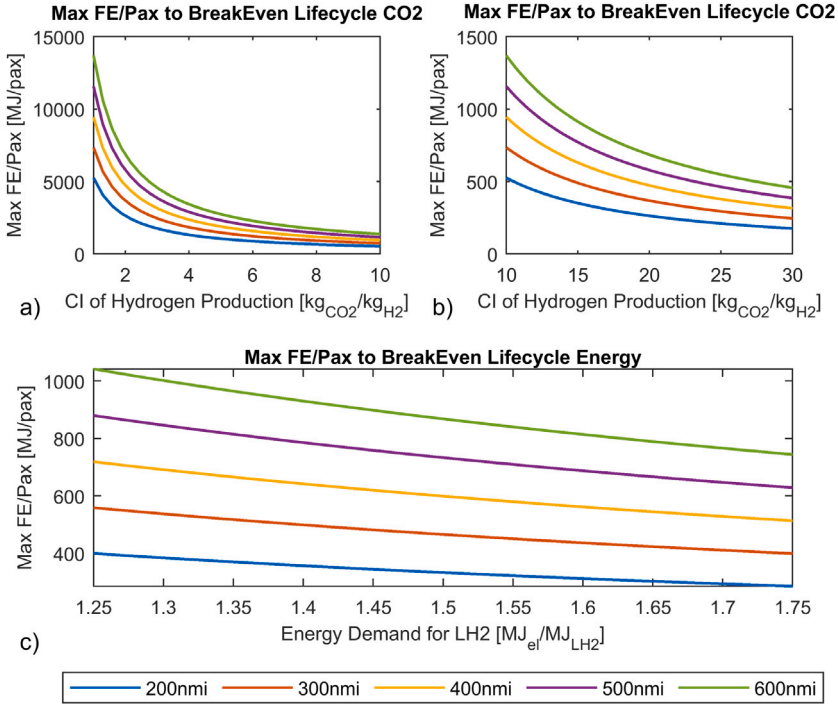

Fig. 24. Flight energy per pax target to breakeven lifecycle CO_2 and lifecycle energy of the conventional regional aircraft.

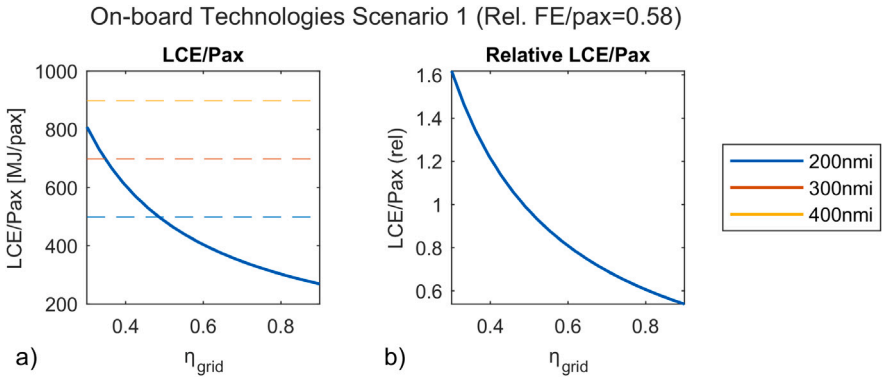

Fig. 25. Battery aircraft lifecycle energy per pax for different grid efficiencies.

Table 7
Selected on-board technology scenario for battery lifecycle analysis at 200 nmi.

Case	BED [Wh/kg]	MPD [kW/kg]	CML [kg/m]	TMS mass factor [kW/kg]	NPPC [kW/kW]	OEW/ MTOW	f_{aero}	Pax	FE/pax [MJ/pax]	FE/pax (rel)
1 (S2a)	500	13	15	3.5	3	0.5348	0.05	33	239	0.58

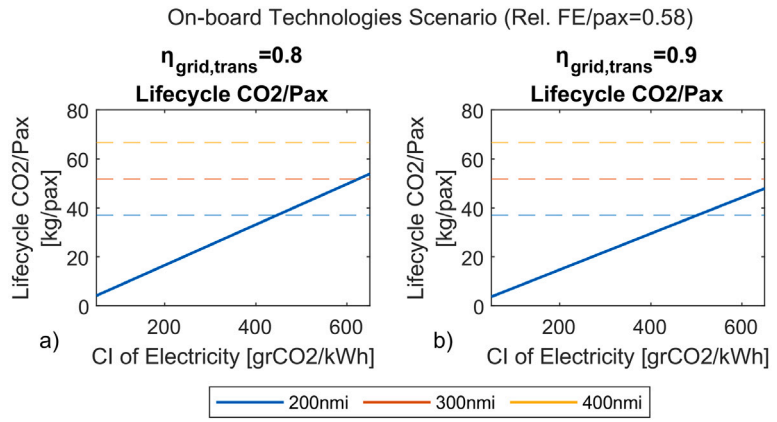

Fig. 26. Battery aircraft flight and lifecycle CO_2 per pax for different grid carbon intensity.

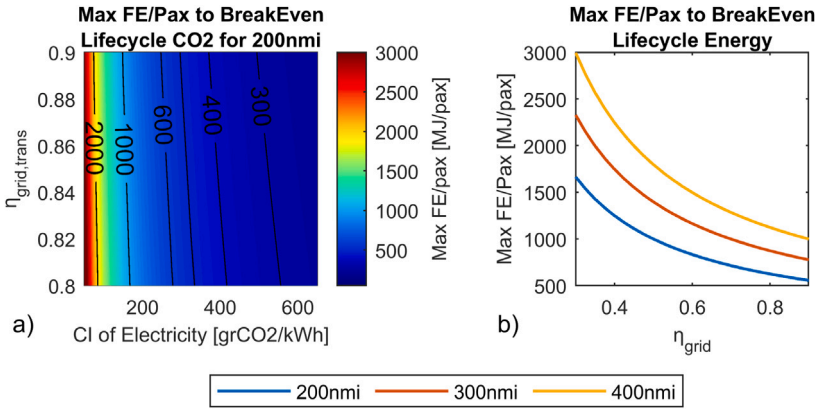

Fig. 27. In-flight energy/pax to breakeven the lifecycle energy and CO_2 of the conventional aircraft at 200 nmi.

the corresponding range of the same colour line. At 90% grid efficiency there is a ~47% lifecycle energy saving per pax.

For high electric grid transport efficiencies (0.8 and 0.9), the lifecycle CO_2 can be breakeven even with electric grid carbon intensity 400–450 gCO_2/kWh (Fig. 26).

Overall, due to the high efficiency of battery systems combined with good efficiency of the electrical grid, the lifecycle energy per pax can be breakeven at high FE/pax (Fig. 27), and, therefore, a lifecycle energy saving per passenger can be more easily obtained than FC aircraft.

5. Technology gaps and roadmaps

5.1. Enabling technologies on the aircraft

Following the design space exploration combining different technology factor levels in an agnostic way, in this section the technology levels are mapped out to specific technology gaps and developments that need to be addressed in order to achieve the selected levels. A combination of literature, analytical calculations and visualisation methods are used.

5.1.1. Batteries

State of the art Li-ion batteries for electric cars have a pack energy density between 272–296 Wh/kg [35], while current aviation batteries have a pack energy density of <200 Wh/kg [32] due to the heavier packaging to meet aviation safety requirements. The Battery2030+ roadmap report [36] evaluated the gravimetric and volumetric energy densities that can be achieved with different cell chemistries (Fig. 28) with Li-S batteries having the potential reach up to 700 Wh/kg. Tiede et al. [37] performed projections of battery specific energy per battery chemistry by fitting historical trends for different chemistries, and produced a conservative, a nominal and an aggressive scenario. The nominal scenario predicts a pack-level specific energy of 391 Wh/kg in 2030, 510 Wh/kg in 2040 and 611 Wh/kg in 2050.

Adu-Gyamfi and Good [38] reviewed enabling technologies for electric aviation and discussed Li-ion, Li-S and Li-air battery technology as well as highlighted the benefits of solid state electrolytes over liquid electrolytes. In the same direction, NASA is developing a solid-state battery (SSB) technology with targets to achieve 500 Wh/kg at pack level by 2030 [39].

The chemistry of the cell prescribes the theoretical energy density of the cell but also affects the packaging requirements. Currently, the pack mass factor for Li-ion battery for electric vehicles is 20%–25% of the cell mass which leads to a pack to cell energy density of 0.75–0.8. Considering also the capacity losses from ageing and considering state of charge safe margins (95%–5%) along with added mass for safety features, the actual battery energy density ends up being around 45% of the initial battery energy of a new cell [9]. Apart from higher

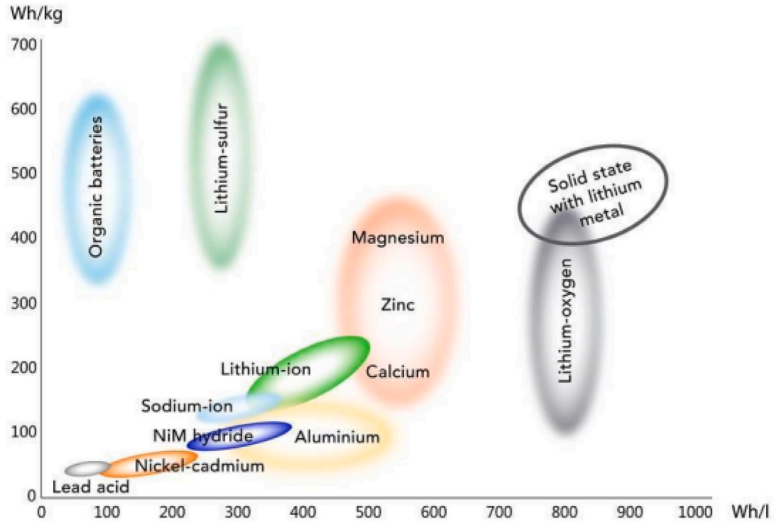

Fig. 28. Potential battery energy densities at pack-level for different cell chemistries.
Source: [36] - reprinted with permission by the authors.

theoretical cell energy densities, Li-S SSB have the potential for lighter packaging as there is a reduced risk of electrolyte leakage and reduced flammability compared to batteries with liquid electrolytes [35,40]. However, one of the challenges associated with SSBs is the low conductivity of solid electrolytes as well as chemical stability, contact issues and increased resistance at the interfaces [41,42]. Other gaps that need further research include battery thermal runaway at low pressures [41], crashworthiness [43] and certification standards. Overall, solid state batteries are considered to be safer, less flammable and have lower thermal runaway risk than liquid-electrolyte Li-ion batteries [40,43], but the limited available experimental evidence to date suggests that the thermal runway propagation rate could be higher in SSBs [40] and further research is needed in this area. Finally, it is known that charging/discharing rate affects the thermal and chemical stability as well as thermal runaway characteristics of Li-ion batteries [44], therefore the fast charging/discharging rates required for aircraft flight requirements as well as turnaround times is another factor to be considered in developing durable and safe batteries for aviation.

5.1.2. Fuel cells

Typical commercial LT-PEMFC have system power density up to 0.6 kW/kg [45,46], but the highest system-level power density has been reported for the automotive state of the art and is around 0.86 kW/kg (with stack power density at 2 kW/kg) [28,31,47] and the new Toyota Mirai version being reported at a 2.46 kW/kg stack power density [48]. PEMFC have been used for road transport and small drones, but the current power density is not sufficient for large-scale commercial aviation with 2 MW+. Regarding development efforts for aviation, ZeroAvia reports an achieved 0.88 kW/kg system power density at 150 kW power output for their SuperStack Flex with LT-PEMFC while working on a HT-PEMFC stack targetting >2 kW/kg with 500 kW power output [49]. Intelligent Energy targets a ~1.5 kW/kg for the 300 kW IE-FLIGHT FC system [50]. Other challenges of FC for aviation include the slower transient response than GTs, low tolerance to impurities, catalyst poisoning, as well as accelerated degradation under pressure imbalances between the anode and cathode, load cycling, pressure cycling and thermal stresses [51–53].

PEMFC performance is strongly influenced by the ionic conduction through the membrane. Today's LT-PEMFC membranes are perfluorosulfonic acid – based (PFSA) polymers which need to be properly humidified to have good conductivity [54], and for this reason the typical operating temperature of today's LT-PEMFC is between 60-80 °C. Above 90 °C the water starts evaporating and the membrane falls into the risk of drying out. Due to this dependence of membrane conductivity on the water content and, thus, low operating temperature where water exists in the liquid phase, the low-grade heat dissipation becomes challenging. The temperature difference between the heat source (LT-PEMFC) and the heat sink (ambient air) is small [55], therefore, large coolant mass flow rates and large heat transfer areas are required.

A breakthrough that is anticipated in FC technology for aviation is the development of HT-PEMFC with promising candidate membranes being based on Phosphoric Acid-Dopped Polybenzimidazole (PA-PBI). Alternative membrane materials for HT-PEMFC have been reviewed in [56]. PA-PBI membranes attribute their ionic conductivity to phosphoric acid and do not rely on humidification, therefore, they can have good performance at temperatures above 120 °C with potential to reach up to 180–200 °C [56,57]. However, there is ongoing research for the development of stable HT membranes with superior ionic conductivity [58] and the main challenges yet to be tackled include the premature acid loss (leaching) [59], low durability and slow oxygen reduction kinetics at the cathode side due to catalyst poisoning by the phosphoric acid [60]. Regarding the window for IT-PEM between 100 °C and 120 °C [61], pressurising the stack can provide adequate performance up to 120 °C [62]. However, the long-term durability and thermal stability of the fuel cell under intermediate temperatures and increased pressure become a concern [62]. Another way to reach 120 °C is the use of modified PFSA membranes with additives and inorganic fillers that improve water retention [63,64].

Increasing the operating temperature accelerates mass transport and reaction kinetics. Increasing the pressure increases the partial pressure of oxygen at the cathode, the Nernst Voltage, the water saturation temperature and water content in the case of PFSA membranes [62,65]. If higher temperature and higher pressure are combined with good membrane conductivity, the resulting increase in current and power density can reduce the required cell area to produce the same power, thus reducing the mass of the fuel cell. Furthermore, a higher temperature reduces the coolant mass flow and heat transfer areas, therefore there is a potential to reduce the bipolar plate size, which typically constitutes 60%–80% of the fuel cell mass [66]. Novel manufacturing techniques, optimised design of the flow fields and improved materials for bipolar plates can also offer incremental increases in the power density [67–70]. At the same time, materials for bipolar plates also need to have electrical conductivity, chemical stability and low hydrogen permeability [66].

5.1.3. Electric machines

Electrification of propulsion systems, especially for regional transport class aircraft, requires advancements in electrical machines and power electronics to achieve significant increases in power density. Today's motors and associated power electronics can achieve a specific power of around 2 kW/kg, but values above 7 kW/kg, and ideally above 12 kW/kg are necessary to retain the value of electrification [71,72]. Specific power above 7 kW/kg is attainable with available, albeit low Technology Readiness Level (TRL), technologies as summarised in a recent survey paper that compared some of the motor topologies that are popular at high power [73]. Rare-earth permanent magnet based machines, especially, do well in terms of specific power along with relatively high efficiency. These technologies can be expected to be matured through system integration and ground tests over the next few years. Attaining the higher targets for specific power will requires overcoming a series of engineering, material, thermal, and manufacturing challenges. Several ongoing programs are working to address this, including ARPA-E ASCEND, with a target of 12 kW/kg for the combined electric machine and drive sub-system. Innovation across several key areas could get us there over the next few years:

- High speed: One of the most effective ways to increase the power density is by increasing the operating speed of the motor, since electrical machines are primarily sized by torque. However, high speed comes with several challenges: the shaft speed of the propeller (or prime-mover in the case of a generator) could be constrained, requiring the use of a gearbox with its added weight, losses, and maintenance and reliability considerations [74]. The resulting high electrical frequency also leads to higher eddy current and hysteresis losses, requiring high-grade ferro-magnetics and finely stranded and transposed conductors, e.g. litz wire. The power electronic converters that drive the motor may also need to operate at significantly higher frequency, requiring wide-band-gap devices like SiC and GaN and extra care to manage electromagnetic interference. This requires better shielding and grounding strategies, which could increase system complexity. If these challenges can be overcome WBG-based power electronics combined with high-speed motors can push power density towards 13 kW/kg and above [72].

- High performance materials: Most high-performance motors being developed for electrified aircraft employ rare-earth permanent magnets (e.g., NdFeB). Higher energy density, reduced ac losses and improved tolerance to high temperature of these materials, along with lower loss soft-magnetic materials will aid in improved power density. Light-weight conductors with improved conductivity, such as carbon-nanotube composites, and emerging materials such as graphene can be used to increase electrical loading. Advanced dielectrics, materials that can withstand high thermal and electrical stress without degrading, along with high thermal conductivity to enhance heat dissipation are also enablers of high-power density. Light weight structural materials like carbon composites can also have a significant impact by reducing the weight of components that can account for about half the weight of traditional machines [75].

- Advanced cooling: Motors and power electronics generate substantial heat, and traditional cooling methods become insufficient as power density is pushed higher. Techniques like direct liquid cooling that can accommodate heat fluxes orders of magnitude higher than indirect liquid or air cooling, allowing motors to operate at higher electrical loadings without overheating, leading to high power density [76]. Cryogenic cooling that can enable higher performance at temperatures well below ambient are also a potential path to higher performance machines. Cryogenic systems reduce resistive losses and improve efficiency, pushing motor power density above 40 kW/kg [77]. However, advanced cooling systems could lead to increased weight or system reliability issues, negating some of the gains from higher power density, unless the cryogenics is already on-board as in some of the proposed hydrogen-electric aircraft concepts [78].

- Tight system integration: Integrating power electronics into motor designs also reduces weight and size, and can potentially mitigate EMI challenges at high frequency [79]. In addition to integration of the electrical components, upstream or downstream mechanical components, such as gearboxes can also be integrated, leading to weight savings by cutting cooling and structural weights.

- Superconducting technology: Superconducting motors operating at cryogenic temperatures eliminate resistive losses, offering massive power density gains, potentially 20 kW/kg or higher [80]. However, they require sophisticated cooling systems and come with higher system complexity. This is an active area of research, with potential for significant breakthroughs in the next few years.

In summary, to attain the specific power required for regional jets, advancements in motor speed, cooling, materials, power electronics, system integration, and the adoption of superconducting technologies may be necessary. In addition to the above enabling technologies, more work is needed to understand the failure modes and mechanisms associated with any new technology, and fault tolerance and safety have to be addressed at the component and system level before they are adopted. One other consideration is that all motor types exhibit similar trade-offs in terms of power density and efficiency. Given the large weight penalty for extra energy storage, high efficiency machines would be desired. In this regard, superconducting motors, in particular, represent the highest potential but come with increased engineering complexity. Recent advances made in the integration of simplified cryogenic cooling systems, to the point of eliminating the need for any cryogenic auxiliary systems [81], hold great promise. Fig. 29 shows the performance of these machines compared to the 'conventional machines' surveyed in the earlier referenced review paper. These could be enabling for the electrification of large transport class aircraft in the near future by achieving net efficiency of the electrical subsystem that approaches 99% along with significantly higher specific power than conventional technologies.

5.1.4. Cables

Recent more electric aircraft have an increasing length of cables and cable mass, and length cable is affected by the fuselage length [82]. The cross section can be analysed to the conductor area and the insulation thickness, which are the two main components to estimate the mass/length. The cross-section of the conductor is influenced by the resistivity of the conductor and increases with higher current to limit the resistance, voltage losses, heat losses and overheating, while the insulation thickness increases with higher voltage to prevent partial discharge at high altitude and low atmospheric pressure. The sizing of the insulation thickness must also consider the minimum and maximum allowed temperature and heat transfer between the conductor and the environment [83]. Overall, when targeting higher electric powers needed for aviation, an increase in voltage is desirable, despite the insulation challenges, to limit the current increase, overheating and losses, and to improve the performance of the electric system.

There are not many estimations in literature on the length of the cables for a fully electric regional aircraft. Palladino [84] assumed a range of cable length between 20–50 m for a hybrid electric regional aircraft and Vratny [85] estimated the cable length at 43 m for a regional hybrid electric aircraft, too. Palladino et al. [86] represented the impact of current on the cable/mass per length for three materials; copper, aluminum and high-temperature superconductor (Fig. 30); based on earlier work from [85].

Dever et al. [87] projected historical data of voltage and estimated that the voltage can reach 987–1620 V by 2030 and 1294–3809 V by 2050. The ranges and uncertainties are quite high and 2030 is fast approaching, so a more conservative approach is followed in Fig. 31 and the aircraft voltage evolution is considered between 500–2000 V. The technology evolution is represented by voltage increase and/or new materials. For variable voltage, the current can be calculated for a set power level, which changes with the power performance and

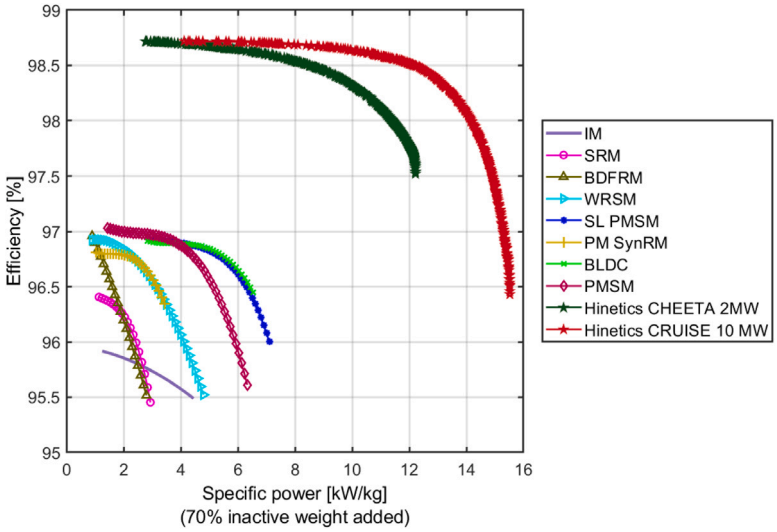

Fig. 29. Efficiency and specific power for different electric machine technologies.

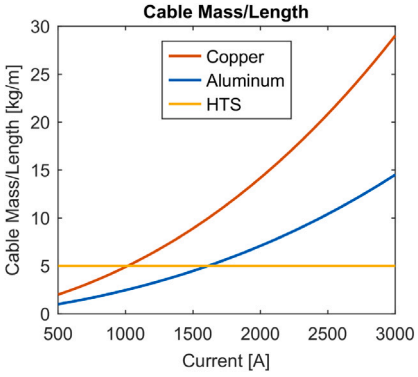

Fig. 30. Cable mass/length for 3 different material technologies and current. *Source:* Redrawn from [86].

power penalties of the TMS (Fig. 30a). Therefore, in Fig. 31b the cable mass/length is mapped out to different voltage levels by calculating the current and referring to Fig. 30. Also, the power level changes with varying TMS NPPC which is explained in more detail in the Appendix (Fig. A.50).

To achieve a target CML of ~15 kg/m with copper-based cables and NPPC = 3 kW/kW (LT-PEMFC), ~1700 V is required, but if NPPC = 5 kW/kW (HT-PEMFC), the same cable mass target can be achieved at ~1430 V. Alternatively, aluminium cables combined with NPPC = 3 kW/kW and ~1150 V, or NPPC = 5 kW/kW and ~975 V, can achieve 15 kg/m.

Although high DC voltage is available for ground applications, the low air pressure at high altitude for aircraft applications reduces the dielectric strength and the performance of the insulator, increasing the risk for partial discharge and voltage breakdown. If thicker insulator layer is used, then the weight increase may cancel out the weight reduction of the conductor [88]. In terms of conductor materials, aluminium has lower density than copper, but also higher resistivity, which means that aluminium cables need a bigger diameter than copper cables to transfer the same current with similar losses [87]. However, aluminium has lower tensile strength and is more brittle than copper therefore aluminium wiring is more prone to failures. Installation of large amount of wiring for electric aircraft also becomes more challenging in the restricted space within the fuselage, while being exposed to vibrations and varying altitude and pressure environment. Technology gaps that need to be addressed include lighter, yet durable, conductor materials and better insulators that prevent partial discharge and arcing at low pressures [88].

5.1.5. Hydrogen storage

Liquid hydrogen tanks may significantly increase the operating empty weight of an aircraft, which can further compromise the maximum payload or passenger capacity. The key figures of merit for these tanks, according to most publications, are gravimetric efficiency – the ratio of fuel mass to full tank mass including fuel – and dormancy time, which is the time it takes for a recently refuelled tank to build up enough pressure that venting is required at the airport.

The gravimetric efficiency largely depends on the diameter and architecture of the tanks (Fig. 32 based on [89]). Conventional MLI (Multi-Layer Insulation) vacuum-insulated tanks have the lowest gravimetric efficiency, around 0.3 for regional aircraft with maximum diameter tanks (fuselage diameter of 2.5 m). Using these tanks in the cargo compartment reduces the gravimetric efficiency to about 0.05. For large fuselage-inscribed tanks, using composite materials can enhance the ratio to around 0.5. Foam insulation for a tank designed for a 10-hour dormancy period offers a similar efficiency to composite materials. Reducing the insulation can increase the gravimetric efficiency to 0.65, but this comes at the cost of a significantly lower dormancy period.

The technology used also impacts the optimum operating pressure of liquid hydrogen tanks. Vacuum-insulated tanks exhibit increasing gravimetric efficiency as the operating pressure decreases, while foam-insulated tanks have an optimum operating pressure around 4 bar. It is important to note that the operating pressure cannot be lower than atmospheric pressure for safety reasons. Eliminating the dormancy time requirement at the airport offers significant advantages. A lightly insulated tank that maintains pressure during cruise when fuel extraction is significant can achieve gravimetric efficiency values around 0.8. The development of zero-boil-off tanks is ongoing and could benefit from the use of ground support equipment at airports.

Lightweight materials with low thermal conductivity are not the only properties required. The materials used for hydrogen storage and distribution need to be resistant to hydrogen permeation which promotes embrittlement and crack propagation [90] as well as resistant to thermal stresses and fatigue under pressure fluctuations and refuelling cycles [91]. Finally, safety standards for leak prevention and instrumentation requirements for leak detection in aircraft, as well as procedures for airport refuelling must be established [92,93].

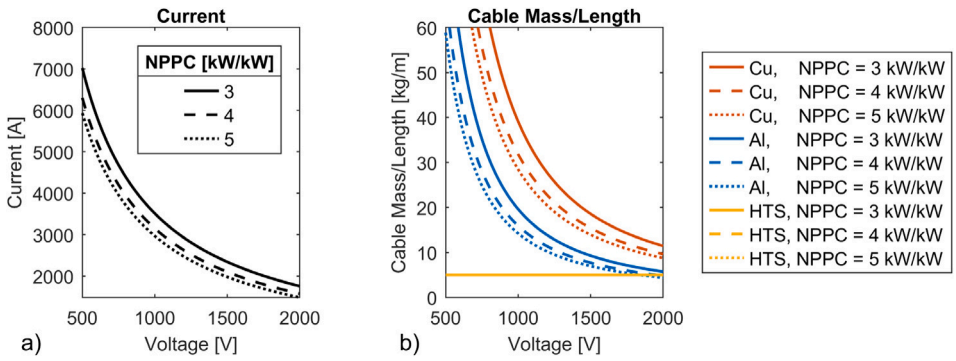

Fig. 31. (a) Current for variable voltage under different TMS NPPC scenarios resulting to different power (b) Cable mass per length for variable voltage.

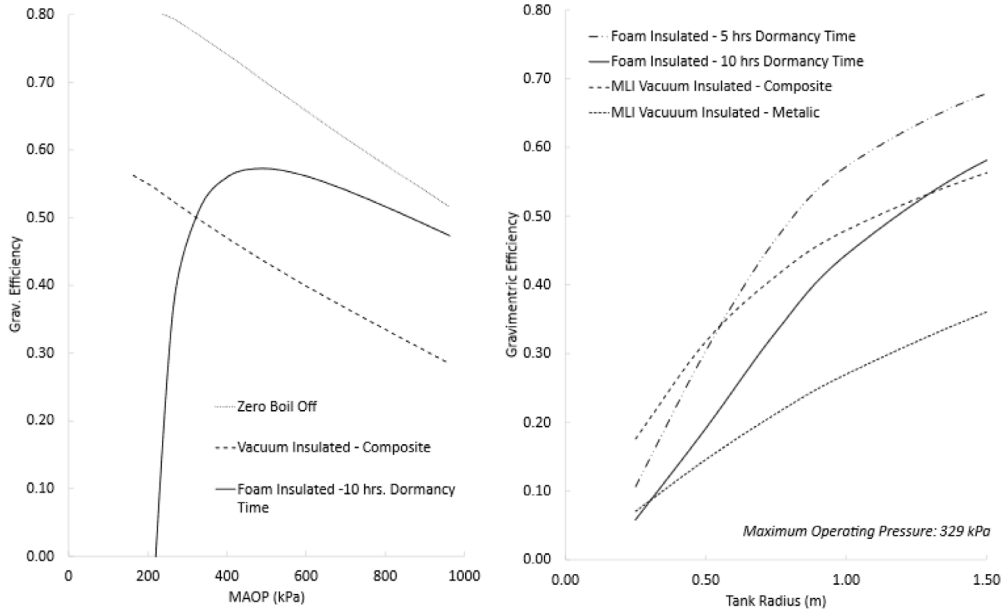

Fig. 32. Gravimetric efficiency of hydrogen tanks for variable maximum operating pressure and tank radius for different insulation methods.

5.2. Thermal management system

5.2.1. Introduction

The energy performance of the FC aircraft as well as the sizing and mass of the sized-for-power components of the propulsion system are heavily affected by the performance of the TMS. All the power-depended components have to be oversized based on the additional drag and parasitic power consumption due to the TMS. Today, one of the biggest constraints and challenges for FC propulsion is the management of the large amount of produced low-grade heat. TMS-related reviews on Hybrid-Electric Propulsion (HEP) include [94] with focus on architectures and [55] with focus at component-level. However, a very comprehensive technology mapping of the TMS metrics is not available in the literature.

Kosters [95] compared two TMS types, liquid cooling and phase-change heat pump, for their drag power and mass, and also provided the mass and power breakdown. They note that the phase-change cooling reduced the drag at the HEX by 98.7% compared to the liquid cooling. Affonso et al. [96] reviewed the literature and created plots comparing different types of TMS (air, liquid, vapour cycle etc.) using three metrics: cooling effect per electric power consumption, the cooling effect per ram air flow and the cooling effect per system mass. However, the quoted metrics were coming from different applications, operating conditions and heat loads, consequently, it is unknown if they are readily transferable to specific TMS designs for electric propulsion. Frey et al. [97] compared liquid coolants for the whole range of FC operating temperature using normalised metrics.

5.2.2. TMS power performance mapping

In terms of the TMS power performance, there are two sources of penalty:

1. the additional power consumption to drive the compressor of a VCS, the fan for air cooling, or the pump for a liquid cooling system
2. the additional drag power that needs to be overcome due to the ram air HEX momentum drag

In Fig. 33, the x axis represents the inlet temperature of the hot side of the ram air heat exchanger $T_{hot,in}$ (i.e. coolant temperature). The $T_{hot,in}$ provides a dT with the ram air which affects the required ram air mass flow through the HEX resulting in a momentum drag power which needs to be compensated by the system. The equations for the drag penalty are included in Appendix A.6. The y axis is the Energy Efficiency Ratio (EER) which represents the cooling effectiveness of the TMS per power consumption.

$$EER = \frac{Heat\ Dissipated\ by\ the\ TMS}{Power\ consumed\ to\ operate\ the\ TMS\ compressor/pump} \quad (3)$$

The combination of these two sources of additional power consumption results in a combined NPPC for the TMS (Fig. 33).

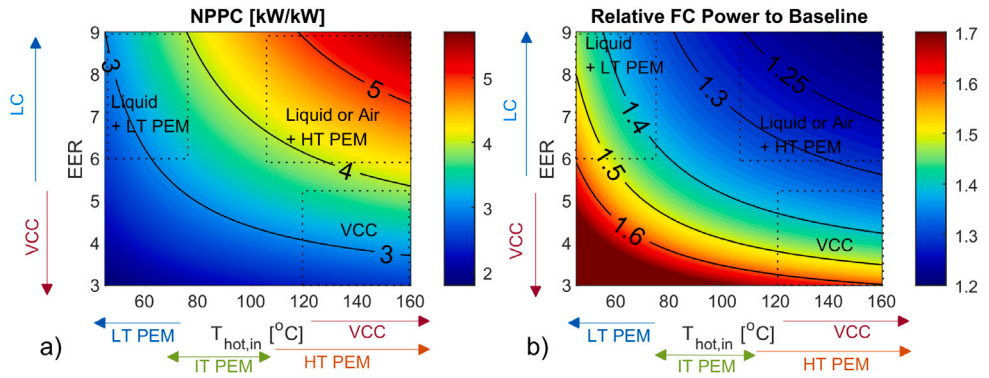

Fig. 33. FC aircraft TMS combined NPPC as a function of the EER and the heated coolant temperature (hot side of the ram air HEX).

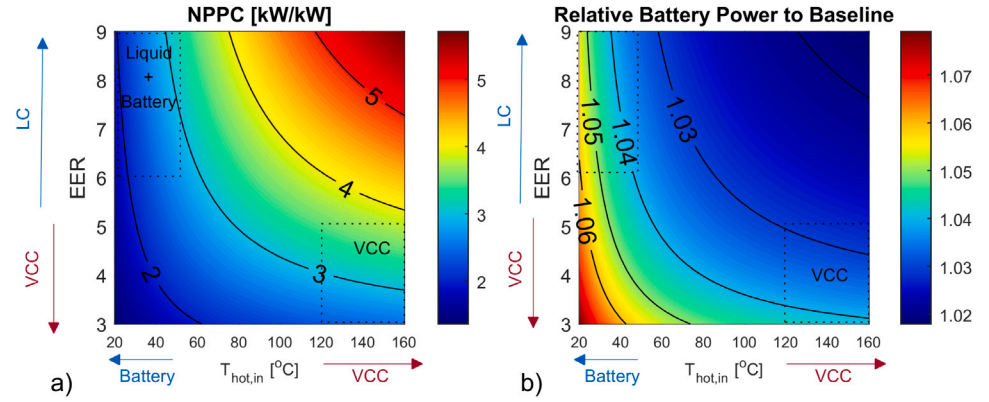

Fig. 34. Battery aircraft TMS combined NPPC as a function of the EER and the coolant temperature (hot side of the ram air HEX).

Vapour Cycle Cooling (VCC) typically has higher power requirement to compress the refrigerant gas before the condenser, therefore a lower EER, while liquid and air cooling have higher EER as there is a low pressurisation requirement to overcome a small pressure drop. However, VCC systems result in lower ram air drag due to the higher $T_{hot,in}$. Typical vapour cycle hot temperatures at the condenser/ram air HEX are between 120–160 °C, while for other systems such as liquid cooling and air cooling that do not involve high pressurisation, the coolant hot temperature is assumed to be 15 K lower than the component it cools. LT-PEMFC with either liquid cooling or VCC can result in a combined NPPC of 3 kW/kW. In the case of liquid or air cooling on LT-PEMFC more penalty comes from the low dT and high ram air mass flow, while for the VCC more penalty comes from the low EER. A transition to IT and HT-PEMFC with liquid cooling reduces the TMS penalties and can reach combined NPPC of 4 kW/kW and 5 kW/kW. Liquid/air cooling systems for HT-PEMFC benefit both from the higher dT between the coolant and ram air due to the higher component operating temperature and the higher EER. Overall, within the discussed ranges which represent the main TMS options for FC, the power penalty due to the TMS ranges between 25%–50%.

In the battery TMS metrics (Fig. 34), there are two main differences from the FC aircraft:

1. The heat generation is lower due to the higher battery efficiency, so for NPPC at 3 kW/kW, the relative power penalty to the system is lower (around 4%–5%)
2. The battery has slightly lower operating temperature, approximately 35–60 °C, therefore the $T_{hot,in}$ range is lower (20–45 °C).

5.2.3. TMS mass

The ratio of the cooling effectiveness to the mass of the TMS depends on four main factors:

- the type of the system (liquid, air, vapour cycle), which prescribes the required number of components to perform the cycle/process/loop (ducts, HEX, compressors, pumps) and system mass [98]
- the properties of the coolant (density, heat capacity, viscosity, thermal conductivity) [97]
- the materials of the components and manufacturing technologies (ex. additive manufacturing for HEX with microchannels and high surface are to volume ratio [99])
- the dT between the components to be cooled and the heat sink — which is a matter of the heat source rather the TMS itself [55]. This dT, along with the properties of the coolant, influence the coolant mass flow, the heat transfer areas and TMS component size.

Stoia et al. [100] predict that the adoption of aluminium HEX will reduce the mass of the TMS by 37% for a HT-PEMFC system. However, this estimation is dependent on the type of TMS, components to cool and design choices. Frey et al. [97] performed the mapping of the TMS mass and power in a normalised way as a function of the operating temperature for various liquid coolant types for a 1 MW fuel cell at take-off. The considered liquid coolant types including water, mixtures of water-glycol, pure glycol and various hydrocarbons. The coolant inlet temperature range was considered within the fuel cell stack operating temperature (80–200 °C) and each coolant type was only considered within a physically valid and safe operating range. They defined as reference points the mass and power for a stack (or coolant) operating temperature of 80 °C. Some of the underlying assumptions included a dT of 20–30 K at the coolant side, a pressure drop of 0.5 bar and use of aluminium pipes and radiator. A change in the coolant inlet temperature from 80 °C (using water) to 160 °C (using glycol) reduced the power by 44% and the mass by 62%.

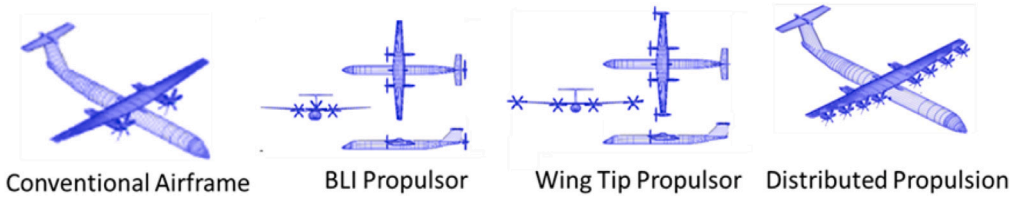

Fig. 35. Aircraft concepts with electrification synergies.

5.2.4. Summary

Incremental TMS mass improvements can be expected from advanced materials, coolants and manufacturing methods, as well as design improvements to reduce the coolant pressure losses and/or improve the performance of the TMS components (ex. compressors, pumps etc.), thus improving the Energy Efficiency Ratio or Coefficient of Performance. However, the breakthrough is not expected in the TMS itself, but most of the potential TMS mass and drag reduction will come from the HT-PEMFC development. VCC can handle low grade heat and is mature for other applications than electric propulsion but involves a lot of system complexity and additional weight due to the number of components required for its operation, along with high parasitic power consumption. If the dT increases, liquid or air cooling can offer sufficient cooling effectiveness while reducing the size of the components, system weight, complexity and produced drag.

5.3. Aircraft technologies

Aerodynamic Improvement Opportunities with Electrification

Electrification offers the opportunity to improve the aerodynamic and propulsive efficiency of the integrated aircraft through the synergistic design of the airframe and the propulsion systems and the use of distributed propulsion concepts (Fig. 35, [101]).

Distributed propulsion could encompass concepts such as Boundary Layer Ingestion (BLI), Wing Tip Propellers, Distributed Propellers as well as their combination. BLI is a concept that has been investigated for several years and considered with various aircraft configurations including blended wing bodies as well as tube and wing designs [101–104]. Examples include NASA's N3X, Starc-ABL and Pegasus concepts. A detailed review of the different concepts, potential benefits, methods and future prospects is covered in [102]. Potential savings depend heavily on the overall size, configuration and flight conditions of the aircraft and benefits can manifest through the recovery of the aerodynamic/kinetic energy left in the boundary layer and the wake of the aircraft as well as the reduction in the specific thrust of the propulsion system and the addition of a boundary layer ingesting propeller at the tail of the aircraft that could increase the total flow area of the propellers. These two elements although related to each other can be treated as separate savings and can reduce overall power requirements at typical cruise conditions by 5%–10% compared to existing regional aircraft [104–107]. Implementation of BLI would require significant modifications in the configuration of the aircraft and its structures and a number of challenges need to be resolved including impact of distorted air on propeller efficiency, noise, mechanical integrity as well as interactions with the horizontal and vertical tail. Similarly, Wing Tip Propellers can be used to reduce the lift induced drag of the aircraft and improve the propeller efficiency through the recovery of the energy in the wing tip vortex. Depending on the overall design of the propulsion system it can also enable the increase in the total area of the propulsors thus reducing specific thrust and increasing propulsive efficiency [103,108,109]. Savings depend strongly on the aspect ratio of the wing, the flight conditions and the design of the propeller and in the case of regional aircraft such as the NASA Pegasus concepts these can be in the order of 5%–10% [104]. Similar savings have been reported by [103]. Use of WTP will have a major impact on the weight and structural design of the aircraft however and this issues need to be considered in conjunction to the aerodynamic and mechanical design of the propellers. Finally, use of propellers distributed at the leading edge of the aircraft wing can also improve the overall performance of the integrated propulsion-wing system through reduced induced drag, reduced wing area and improved propulsive efficiency [101]. Taking advantage of the increased velocity of the slipstream of the propellers will increase the effective aerodynamic speed of the air over the wing reducing the induced drag. Furthermore, the wing can be re-sized to improve overall performance while once again the total flow area of the propellers can increase improving propulsive efficiency. Although there are risks and challenges associated with propeller/propeller and propeller/wing interactions in terms of turbulence, noise, mechanical integrity and fatigue as well as increase in wing form drag the concept can still offer a 5% benefit compared to conventional designs.

Despite the major challenges of the above concepts that need to be resolved and will have a detrimental impact on the potential benefits, the combined synergies of electrification and distributed propulsion should not be ignored and when coupled with advances in materials and better understanding of the flow physics still have the potential for 5%–10% benefits as documented in other studies.

Structural Efficiency

Modern aircraft have an increasing fraction of composite materials, mainly carbon fibre reinforced polymer matrix (CFRP) composites [110–112]. CFRP offer a combination of desirable properties for aircraft application such as low density, high specific strength, high specific modulus, corrosion resistance and durability [113]. Recent widebody aircraft, where fuel efficiency becomes a priority, have up to 50% composite structural weight (Fig. 36).

According to [114], replacing conventional aircraft materials (such as aluminium alloys) with composites of 18% carbon fibre (CF) volume can offer a 5% of mass reduction, while composite of 30% CF volume can offer up to 27% mass reduction. The main drawback is the expensive and energy-intensive production of CFRP [114,115]. Although the CFRP technology is mature for aircraft applications, there is significant effort in developing sustainable production and recycling methods to reduce the environmental footprint of composites, and improve the overall circularity and sustainability of composites [114,116]. Atescan-Yuksek et al. [117] performed a comparative lifecycle assessment of six CFRP composites for aircraft wings against conventional aluminium wings considering production, changes in aircraft weight, flight emissions and disposal. Despite the much higher environmental footprint (measured as CO_2e) of CFRP composites at the production phase, above a 300000 km accumulated flight distance, the CFRP composites offer a clear lifecycle CO_2e saving against aluminium wings [117].

CFRP have not been used as extensively in regional and shorter-range applications so far but in the development of zero-emission aircraft, transition to more-composite aircraft can compensate for the increase in operating empty weight due to the electric system weight. Heart Aerospace uses this opportunity and their battery-based hybrid electric aircraft protype has composite fuselage and wings [118], and by 2030 they target a fully electric range of 200 km with 30 pax [34].

5.4. Lifecycle and infrastructure

When considering the prospects of zero-emission regional aircraft, the viability of such concepts is incumbent upon developing a clean

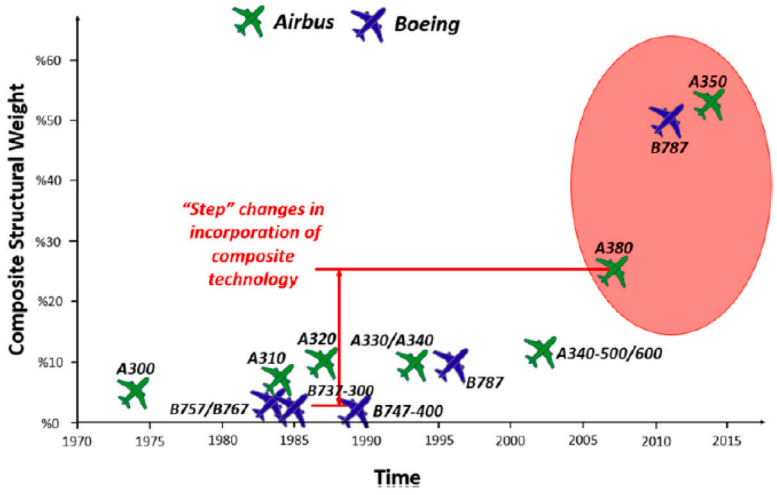

Fig. 36. Evolution of composite fraction in aircraft.
Source: Reprinted from [112] under CC BY licence.

energy infrastructure for aviation operations. Additional advancement in the efficiency, cost, and scale of renewably sourced energy will be necessary for zero-emission electricity generation and hydrogen production. Absent such developments, battery-electric and hydrogen aircraft will, at best, only be capable of partial abatement of greenhouse gas emission impacts across the full operational lifecycle. For certain energy production pathways, such as the use of coal and natural gas for electricity or hydrogen production, the emission impacts associated with energy production can be even greater than those observed for use of fossil-derived aviation kerosene fuels [119]. For this reason, the current landscape of electricity carbon intensity and hydrogen production are discussed, alongside future energy scenarios that enable a future zero-emission regional aviation lifecycle.

5.4.1. Electricity carbon intensity

The carbon intensity of electrical grids serves a pivotal role in determining the overall sustainability of the energy life cycle for battery-electric and electrolytic hydrogen systems alike. Developing a zero-emission future energy ecosystem will undoubtedly require a massive scale-up in renewable energy infrastructure, and other clean electricity generation systems. An example comparison of the CO_2 emission intensity of various electricity generation methods is shown in Fig. 37. It is broadly recognised that renewable electricity generation via methods such as solar, hydroelectric, and wind, as well as clean nuclear energy, are associated with dramatically fewer overall greenhouse gas emissions when compared to the use of natural gas, oil, and coal fossil fuels. While carbon capture and sequestration (CCS) is often envisioned as a means to further control CO_2 emission impacts of fossil sources, such systems are projected to be incapable of reducing overall greenhouse gas emissions at parity with renewable energy systems on a per-unit electricity basis [120].

An overview of the CO_2 emission intensity of electricity production across various global regions over the past decade is shown in Fig. 38. Here, it can be observed that the world average CO_2 emission intensity of electricity generation has decreased by 17.6% over the past 10 years, with reductions in this metric attributable to all five of the global regions included. However, comparing Fig. 38 with Fig. 37 evidences the limited adoption of renewable electricity pathways in certain regions of the world, where the carbon intensity of electricity generation remains above the mean value of natural gas systems.

To provide a more detailed view of the results shown in Fig. 38, the CO_2 emission intensity of electricity grids associated with select national and regional groups that are among the greatest generators of electricity are shown in Fig. 39. Here it is observed that the US

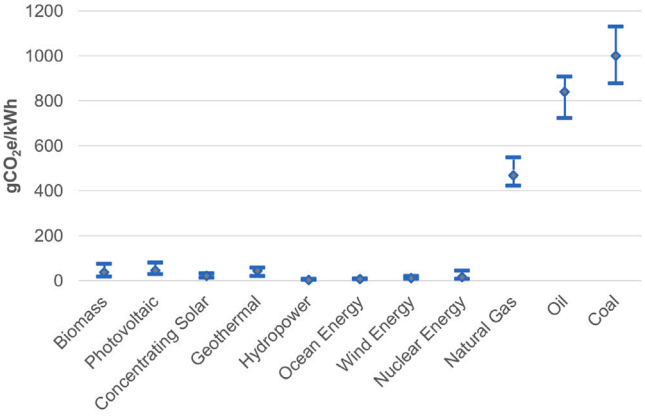

Fig. 37. CO_2 emission intensity of various methods of electricity generation, showing mean and ±25% percentile of emission impacts.
Source: IPCC [120].

and EU electricity grids are associated with fewer emissions per unit energy produced when compared to the global grids, whereas those of India, China, and Southeast Asia all demonstrate greenhouse gas emission intensities above that of the global mean. In particular, the electricity grids of India and China have historically included large use of coal-fired power plants, which have slowly been replaced in favour of natural gas or renewable electricity systems.

Under the ICAO CORSIA [122] standard, fossil-derived jet fuel produces 89 gCO_2e/MJ (320.4 gCO_2/kWh) across all production, transportation, and combustion stages. This relative carbon intensity suggests that the use of a global mix of electricity production methods currently would actually result in a more significant climate impact than simply using existing fossil fuel systems for aviation applications. However, the electricity grids of the Americas and Europe fall below this baseline threshold for fossil kerosene fuels, signalling that continued scale-up of clean energy production methods in these sectors may serve as a starting point for zero-emission regional aircraft systems in a near-term time scale.

However, it is also important to acknowledge the differences in the electricity production rates of each national or regional group, which produces disparities in the overall emission impacts of each group. The annual total emissions associated with electricity generation for the select national and regional groups is shown in Fig. 40, where it can be observed that, despite continued reductions in CO_2 intensity of

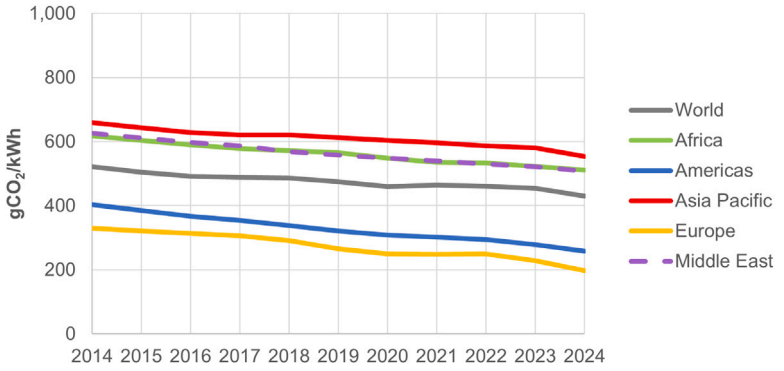

Fig. 38. CO_2 emission intensity of electricity production across global regions.
Source: IEA [121]

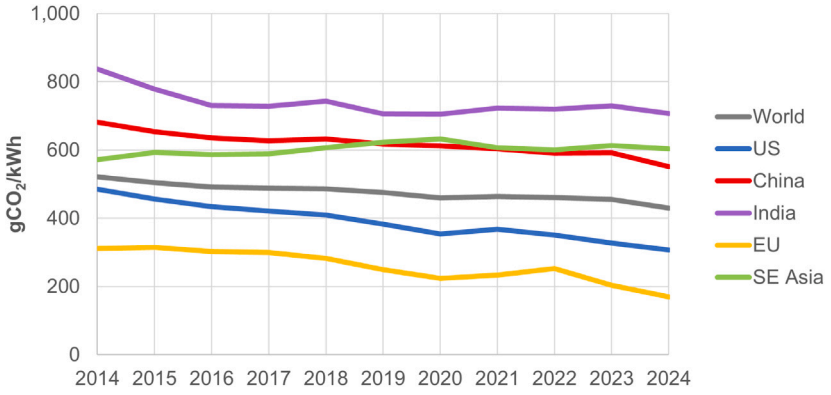

Fig. 39. CO_2 emission intensity of electricity production across national and intercontinental regions.
Source: IEA [121].

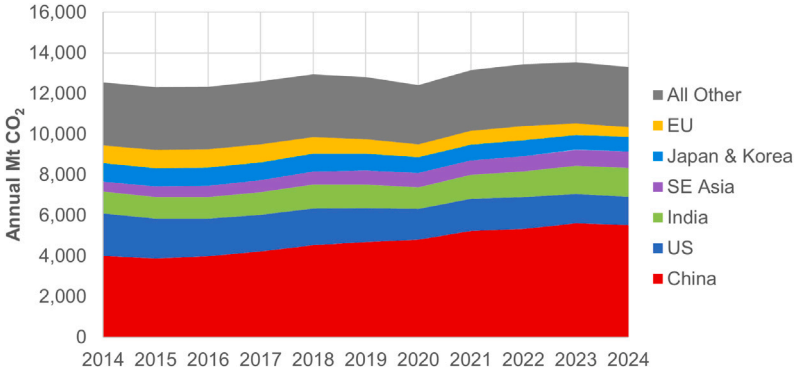

Fig. 40. Annual CO_2 emissions of electricity production across national and intercontinental regions.
Source: IEA [121].

electricity generation, the aggregate emission impacts have gradually risen over the past decade.

Working towards a net-zero emissions ecosystem, the IEA has established an energy systems roadmap that aims to reach a net-zero energy ecosystem by the year 2050 [123]. The necessary developments in the global grid mix of electricity generation methods to reach this outcome are shown in Fig. 41. In this roadmap, it can be observed that the total electricity generated monotonically increases annually, yet the final outcome is a zero-emission grid that can be utilised for the future energy needs of aviation.

5.4.2. Hydrogen production efficiency and transport

Given that hydrogen is the most abundant element in the universe, there are many ways in which it can be synthesised from other feedstocks and energy sources. A summary of the different methods for hydrogen production, colloquially referred to as the "colors" of hydrogen, is provided in Fig. 42. The accompanying greenhouse gas emission impacts of these various production pathways is shown in Fig. 43.

The large range of values provided for yellow, or grid, hydrogen is due to the many methods of sourcing electricity for electrolysis, with each grid mix being associated with different emission intensities. Considering the CORSIA baseline life cycle emission impact of fossil-derived kerosene jet fuel at 89 $grCO_2e/MJ$, on a per-energy basis this emission intensity is reached with a hydrogen production emission intensity of 10.67 kg_{CO_2e}/kg_{H_2}. As such, production pathways that utilise fossil energy resources for hydrogen production are often associated

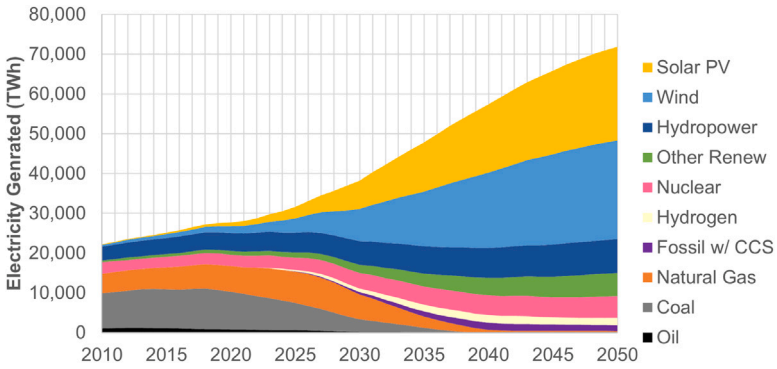

Fig. 41. Forecast development in global electrical grid under IEA net-zero emission 2050 scenario. *Source:* IEA [123].

Color	Feedstock	Production Technology
Gray	Natural gas	Steam methane reforming
Brown	Lignite	Gasification
Black	Coal	Gasification
Blue	Natural gas	Steam methane reforming with CCS
Turquoise	Natural gas	Pyrolysis
Green	Renewable electricity, water	Electrolysis
Yellow	Grid electricity, water	Electrolysis
Pink	Nuclear electricity, water	Electrolysis
Red	Nuclear heat, water	Thermolysis
Purple	Nuclear electricity and heat, water	Thermolysis and electrolysis
Orange	Solar irradiance, water	Photolysis

Fig. 42. Hydrogen production pathways.

Table 8
Energy demand for LH2 production and transport [MJ_{el}/MJ_{LH2}]. *Source:* ICAO [125].

	2020	2030	2040	2050	2060	2070
Electrolysis	1.43	1.43	1.43	1.43	1.43	1.43
Liquefaction	0.3	0.25	0.2	0.15	0.15	0.15
Transport	0.02	0.02	0.02	0.02	0.02	0.02
Total	**1.75**	**1.70**	**1.65**	**1.60**	**1.60**	**1.60**

with greater emission impacts than direct use of fossil kerosene jet fuel today. For this reason, and as with electricity generation, the development of zero-emission regional aviation is incumbent upon expansion of renewable and clean energy sources.

The emission intensity of hydrogen production can be further reduced with increased efficiency in electrolyzers, such as the systems used to produce green, yellow, pink, and purple hydrogen in Fig. 42. Furthermore, nearly all viable hydrogen aircraft concepts today assume the use of liquid hydrogen for future aviation markets, owing to the greater energy density and lighter energy storage system enabled by low-pressure cryogenic storage. As a result, additional energy requirements to liquefy gaseous hydrogen must also be considered in the overall energy and emission intensity of future hydrogen regional aircraft. A summary of the total energy required to produce and dispense a given energy content of hydrogen is summarised in Table 8 with forecasts of future electrolysis and liquefaction efficiencies provided by ICAO [125]. It is noted that this table assumes constant electrolysis efficiency of 70%, corresponding to current PEM electrolyser capabilities, though significant improvements in new technologies for next-generation electrolyzers have already been demonstrated. One example is the use of capillary-fed electrolyser systems that have resulted

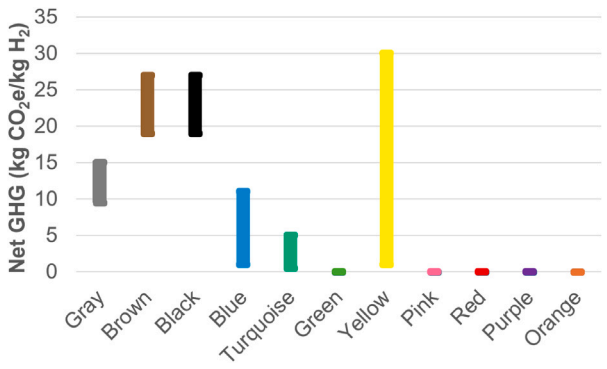

Fig. 43. CO_2e emissions associated with various pathways of hydrogen production.
Source: DNV [124].

in efficiency capabilities up to 95%, which would result in a future total energy demand factor closer to 1.25 MJ_{el}/ MJ_{LH2}.

5.4.3. Battery production

Apart from the total energy for battery charging, a lifecycle impact is also contributed by the production of the battery. The lifecycle impact of battery production can vary based on the region, supply chain, Bill of Materials (BoM), design and configuration of the battery [126,127]. Dai et al. [126] estimated that the production of 1 kWh NMC111 battery required 1126 MJ and 72.9 $kgCO_2e$. Using this Li-ion battery for reference, a battery aircraft with the technology values of Table 7 with 33 pax and 200 nmi requires a total battery capacity of 2736 kWh which corresponds to a total of 3080736 MJ and 199454 $kgCO_2e$ for the production of this battery assuming linear scaling. For a target time on wing of 8000 EFC (Fig. 19) and ignoring any battery second life, this corresponds to an additional lifecycle impact of 0.756 $kgCO_2e$/flight/pax and 11.7 MJ/flight/pax. Figures of CO_2e for the production of different cells at different locations are provided by [127] (Fig. 44).

In reality, the lifecycle impact will change based on the battery type that will be used in the future for electric propulsion. At this stage, there is no clear recommendation on the lifecycle impact of manufacturing SSB compared to current Li-ion with mixed findings in literature which rely on specific chemistries and underlying assumptions due to the limited information on the manufacturing process [128,129].

5.4.4. Fuel cell production

Usai et al. [130] estimated the CO_2e footprint of fuel cell components and reviewed the literature for similar figures. They attributed 5000 kg of CO_2e to the production of an automotive FC system, including the tank, with net power output 80 kW (Fig. 45). The 40% CO_2e was attributed to the tank, 24% to the catalyst, 17.2% to the BoP (including the air, heat, fuel, water management systems), 14.2% to the bipolar plate, 1.5% to the membrane and 2.4% to other stack components.

If the 60% impact of the FC system without the tank in Usai et al. [130] study is isolated, the equivalent carbon footprint of producing a 80 kW FC system is ~3000 kg CO_2e. The requirements and concept of hydrogen tanks for aviation will be very different from the automotive, so it cannot be used for reference. A 200 nmi, FC-only flight using the on-board technology scenario 1 (Table 6) will require ~5.8 MW net power output of the FC system and has a pax capability of 32. Assuming a linear scaling of the available values from Usai, the lifecycle impact of a 5.8 MW FC is estimated at 217500 kg CO_2e. With a target time-on-wing of 8000EFC, similar to today's time-on-wing, and 32 pax, this results in a 0.85 $kgCO_2e$/pax/flight. Although at 200 nmi this figure is ~12.4% higher than the estimated for the battery in the previous subsection, the FC production footprint is close across all the investigated ranges as the reduction in pax capability due to the hydrogen storage and fuel mass is small, while in the case of battery, the energy and size of the battery scales-up with longer range along with the battery production footprint. With transition to HT-PEMFC, some reduction in production footprint is expected to come through the reduction in the FC power requirement at NPPC = 5 kW/kW (Fig. 33) and the increase in pax capability. Membrane and catalyst materials for HT-PEMFC are expected to be different from LT-PEMFC but it is hard to make a safe estimate at this stage with limited information. Assuming similar values to LT-PEMFC production, a ~0.625 $kgCO_2e$/pax/flight is estimated for HT-PEMFC but with low confidence due to limited information on the production of future aviation-grade fuel cells. A lifecycle analysis per individual material used in PEMFC along with end of life strategies are discussed in detail in [131].

5.5. Technology pathway

5.5.1. FC aircraft

After performing energy and pax calculations, and reviewing challenges associated with the technology gaps, six technology pathways/scenarios with gradual step changes are presented (Fig. 46). Scenario 1 includes the minimum technology advancements in electrical technologies to even start talking about zero-emission aircraft of this size i.e. FCPD = 2 kW/kg, MPD = 8 kW/kg, TMS MF = 3.5 kW/kg and η_{tank} = 0.35. The FC still has an NPPC = 3 kW/kW corresponding to LT-PEM technology, and aircraft technology remains the same. The capability would be limited to 15 pax for 300 nmi and 10 pax for 500 nmi with over 3 relative energy, while longer ranges would not be available. A business case for this aircraft class cannot be created, but it could be a starting point for testing the technologies at 2 MW+ and getting experience for certification until technology progresses. For such low technology levels, a smaller 19-pax commuter class would perform better from an economic and energy perspective.

From Scenario 1 to 2, the MPD is upscaled to 13 kW/kg and the NPPC is 3.5 kW/kW potentially with a small increase in the LT-PEMFC operating temperature within the operating limits of LT-PEMFC (Fig. 33). The pax capability becomes 30 at 300 nmi and even 800 nmi becomes available with 19 pax. From Scenario 2 to 3, the NPPC has improved to 4 kW/kW potentially with transition to IT-PEMFC or design improvements and FC pressurisation, and pax > 29 is unlocked for ranges up to 500 nmi, enhancing the potential business case. The relative energy would reduce below 2 for ranges up to 500 nmi. Scenario 4a includes a further improvement in FCPD combined with an improvement in aircraft technologies for Scenario 4b. From Scenario 4b and beyond, the crossover to energy saving has been made for most mission ranges.

Scenario 5 makes the step change from NPPC 4 kW/kW to 5 kW/kW, which will correspond to HT-PEMFC technology. Scenarios 6a and b include advanced FC power density and NPPC 5 kW/kW associated with HT-PEMFC, and superconducting motors and cables. Scenario 6b also includes an ambitious advancement in aircraft technologies, too. Even without significant aircraft technology improvement, Scenario 6a offers an energy efficient aircraft (rel FE/pax < 1) with 57 pax at 300 nmi and 47 pax at 800 nmi.

If scenario 6b is reached, the maximum pax capability allowed by the hydrogen volume can be achieved for each range. Any further improvement in technology may offer only a small reduction in the total energy due to small aircraft weight reduction but the pax capability cannot be further increased unless the aircraft is resized and the fuselage is extended. In that case, further technology improvements beyond Scenario 6b, will mostly benefit larger aircraft applications, and it will be a moment for upscaling and capitalising on larger aircraft.

One of the limitations specific to hydrogen aircraft is that there is little to no flexibility to trade-off payload and range (i.e. fuel mass) as in conventional aircraft. If the design range is selected at a long range

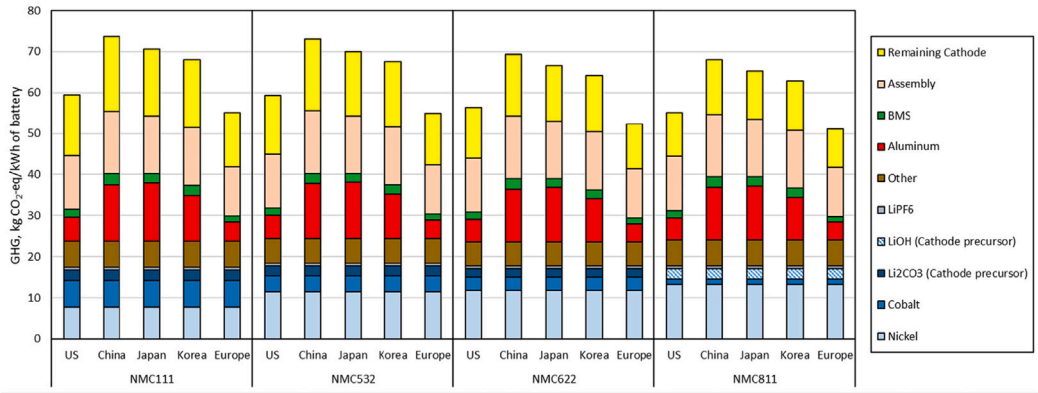

Fig. 44. Battery production CO_2e for different regions and cells.
Source: Reprinted from [127] under CC BY-NC-ND 4.0 licence.

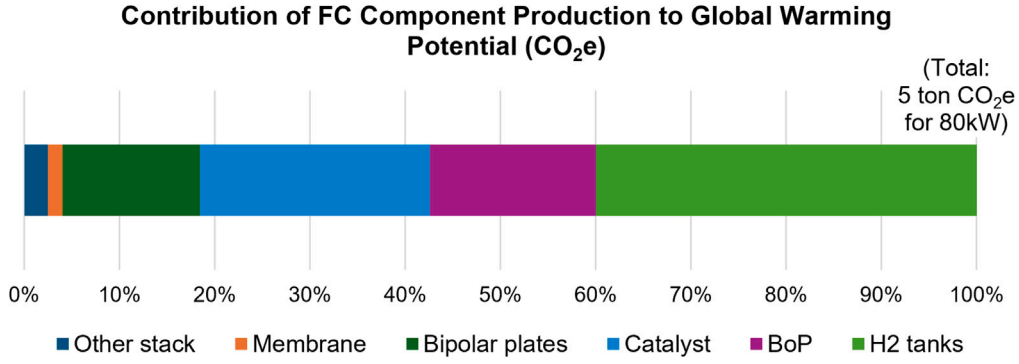

Fig. 45. Global warming potential (CO_2e) of the production of a FC system and gaseous H_2 tank with 80 kW net power output and contribution of components in automotive applications.
Source: Adapted from [130].

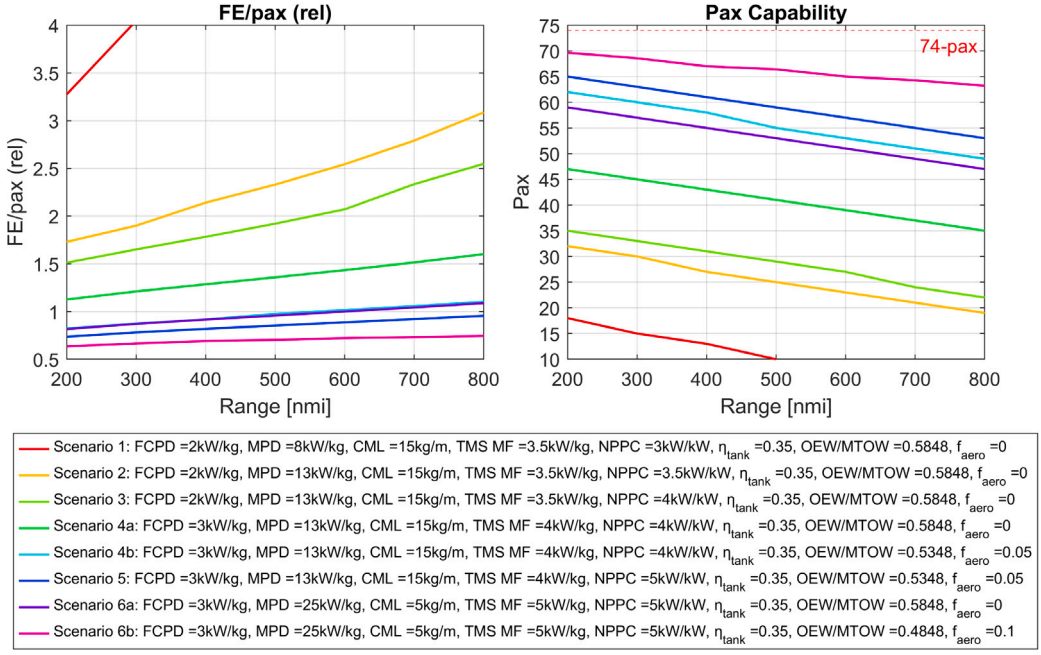

Fig. 46. Technology scenarios for FC aircraft for 200–800 nmi.

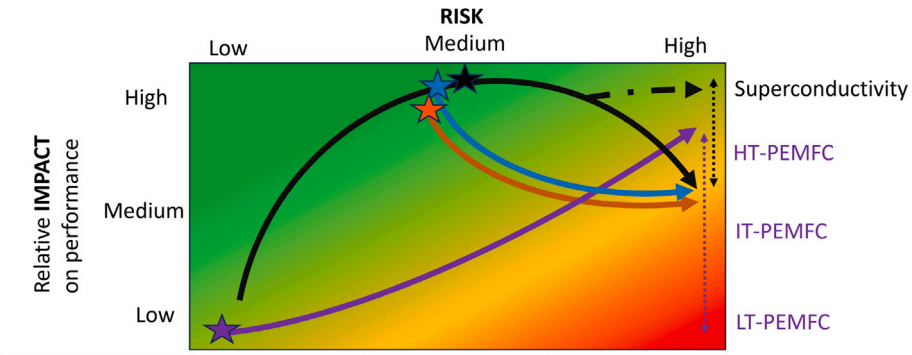

Motor & PE (kW/kg)	8	13 (2035+)	25 (2050)
FCPD (kW/kg)		2 (2035+)	3-4
TMS MF (kW/kg)		3.5 (2035+)	4-5
TMS NPPC (kW/kW)	3 (2035)	3-4 (2035+)	5

Fig. 47. Risk and impact of primary technology factors.

(Fig. 46) and the tank is sized for this range, the payload is still limited at shorter range.

Considering risks and impact in two horizons (Fig. 47) and that TRL advancement from 6 to 9 requires at least 5 years for known technologies and at least 7 years for such disruptive technologies, Scenario 4b is expected to be the absolute upper limit for entry into service (EiS) 2035 even in the most optimistic case. On the other side, Scenario 4a should be the minimum available for EiS 2050 to create a substantiated potential for decarbonising aviation.

The tank gravimetric efficiency could reach 0.4–0.5 for fuselage-inscribed tanks with MLI vacuum insulation and composite liners, but a more conservative value of 0.35 has been used in order to account for additional penalties from installation effects and the fuel distribution system because their impact is still uncertain. In the 2035 horizon, a potential transition from NPPC = 3 kW/kW to 4 kW/kW may be achieved with transition from LT to IT PEMFC or by pushing the operating temperatures and pressure to the boundaries of advanced LT-PEMFC or optimised TMS with advanced HEX. In 2050, NPPC = 4 kW/kW could be associated with more mature IT-PEMFC or with early version of HT PEMFC with lower operating temperature, while a NPPC = 5 kW/kW can be expected for mature HT-PEMFC combined with improved TMS design.

5.5.2. Battery aircraft

For the battery aircraft, targets of MPD = 13 kW/kg and CML = 15 kg/m must be considered as well, but superconducting concepts that could bring them to 25 kW/kg and 5 kg/m are more difficult to integrate due to the abscence of the cryogenic hydrogen onboard. A breakthrough in TMS is not expected due to the low operating temperature of the battery but it is not a primary enabler anyway due to the low heat generation. There is a small margin for TMS improvement coming from improved materials, the design of the system, and small increase in the operating temperature of electrical components that may be connected in the same cooling loop, but, overall, NPPC far above 3 kW/kW and MF above 3–3.5 kW/kg are not foreseen.

With medium aircraft advancements, BED ~400 is hard to create a business case with <20 pax, but ~500 Wh/kg can enable 33 pax at 200 nmi, and ~600 Wh/kg can enable 42 pax at 200 nmi. For advanced aircraft technologies, BED ~400 offers 35 pax at 200 nmi, ~500 Wh/kg offers 48 pax at 200 nmi and 24 pax at 300 nmi, and ~600 Wh/kg can enable 57 pax at 200 nmi, 37 pax at 300 nmi and, but drops below 20 pax above 380 nmi. However, in all scenarios except for Scenario 1a, there is a flight energy saving against the conventional (Fig. 48) at <250 nmi.

6. Conclusions

Today, aircraft of regional class, despite having higher capability, are mainly used for 200–300 mni flights, thus, covering 10%–20% of global flights [132]. Depending on the achieved zero-emission aircraft capability (200–800 nmi), the zero-emission regional aircraft could decarbonise up to 50% of the global flights [132] and potentially all transport needs within a country or continent if combined with multi-modal transport models and connecting flight networks. It is the initial platform to decarbonise the lower bound of flight ranges while gaining maturity and certification experience before upscaling zero-emission technologies to larger applications.

The bottleneck for fuel cell propulsion is, first, the TMS due to the low-grade heat and drag generation, and, second, the fuel cell system power density (including the BoP), while the bottleneck for batteries is the energy density of the battery. A few years ago the initial projections of battery energy density and assumption in electrification studies were more optimistic and considered values as high as 750–1000 Wh/kg but the slow evolution over the last few years and further research have brought down the most optimistic targets to 500–600 Wh/kg with Organic and Li-S batteries, and increased interest in Li-S SSBs.

A 2 kW/kg FC system-level power density can be hoped for with a combination of increase in operating temperature and pressure, design optimisation, reducing the number of BoP components and using improved materials and maufacturing for the bipolar plates. The transition to HT-PEMFC, potentially with PA-PBI membranes, is expected to be a breakthrough in FC technology by increasing the current density, saving mass through the downsizing of the cooling channels, and removing the need for humidification while alleviating the overall TMS penalties. HT-PEM can reduce the power/energy penalty by 50% (from 40% to 20%). However, it is uncertain what other technology improvements can be expected to bring the FC system power densities beyond 2–3 kW/kg. A minimum fuel cell system power density of 2 kW/kg is needed for zero-emission regional aircraft while an upscaling to 3 kW/kg and HT-PEMFC will contribute to an energy-efficient regional aircraft.

The TMS of the FC aircraft is the subsystem with the high uncertainties and dispersion of quoted values and projections in literature without clear consensus where all the technology improvements will come from. Within each TMS type (liquid, air, vapour cycle system) there can be small added benefits by changing the material of components to lighter materials, improved manufacturing techniques, geometry or system optimisation and change of coolant. However, these areas

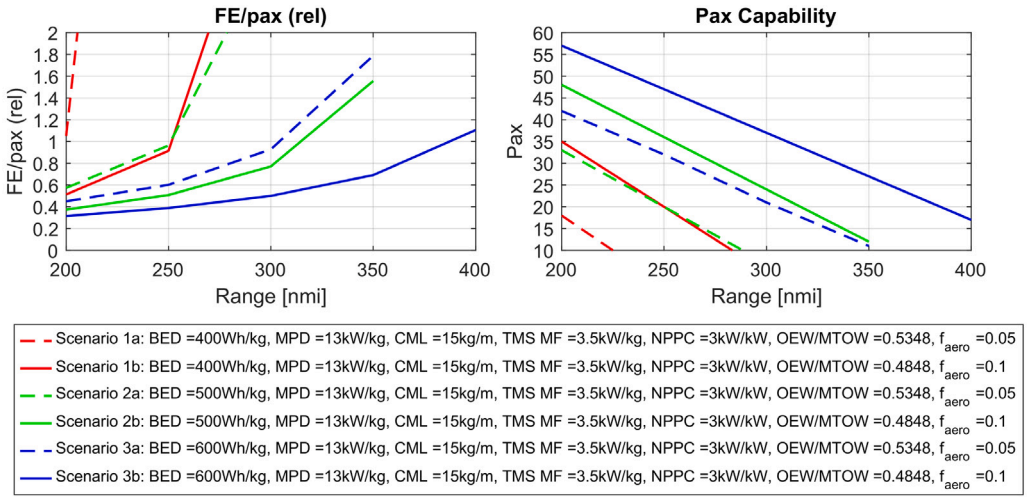

Fig. 48. Technology scenarios for battery aircraft.

seem to have limited margins for improvement and it seems more likely that the breakthrough in TMS performance will come from an increase in the operating temperature of the component to be cooled (i.e. HT-PEMFC) rather than the TMS technology itself.

Novel aerodynamic concepts (BLI, WTP, DP) that are enabled by electrification can offer solid drag reduction improvements of 5%–10%. They will not be the primary enablers such as the motors and high-temperature fuel cell technology, but at the same time the technology is more mature and lower risk. This drag reduction benefit will cascade down to the rest system and will reduce the power and energy requirement of the aircraft thus reducing the size and mass of motors, batteries, fuel cells, hydrogen storage etc.

Part of the mass penalties of electric components can be compensated by improved aircraft structures using lightweight materials. The technology for composite aircraft structures is known and used in recent long-range aircraft. A broader adoption of composites for aircraft structure could compensate for the penalties due to slow evolution of fuel cell, batteries and electric components by trading-off aircraft structural weight with electric system mass, but it would increase the cost of the aircraft. The main challenge and area for further development concerns the recyclability of composite materials as well as the manufacturing cost.

A battery aircraft or fuel cell aircraft can lead to CO_2e penalty at lifecycle due to the battery charging and the hydrogen production unless the on-board technology development is accompanied by infrastructure development. However, as the carbon intensity and infrastructure varies across the world, a zero-emission regional aircraft flying to a destination with infrastructure carbon footprint higher than the breakeven threshold can bring a lifecycle CO_2 penalty compared to the conventional. Despite the limited range of regional battery aircraft, it can offer energy savings even with a low number of passengers, while the FC aircraft is easily penalised at lifecycle level due to the energy-intense hydrogen production that is at $1.75\text{MJ}_{el}/\text{MJ}_{LH2}$ today, with the most optimistic scenario of ultra-efficient electrolysers bringing it down to $1.25\text{MJ}_{el}/\text{MJ}_{LH2}$.

Another lifecycle aspect, for which targets must be defined are the degradation rate; for different combinations of end of life state of health and target time on wings, the degradation rates have been identified. It seems that degradation rates of 0.001%–0.0005% power loss/cycle and 0.003%–0.0006% capacity loss/cycle may be required for FC and batteries respectively, but they will depend on the system oversizing factors that can be accepted.

Considering performance, risks and timeframes, technology step changes have been identified. In 2035, a FC aircraft with at least 30 pax, range of 300 nmi and a 90% flight energy penalty needs at least FCPD = 2 kW/kg, MPD = 13 kW/kg, CML = 15 kg/m, TMS MF = 3.5 kW/kg, η_{tank} = 0.35 (including the fuel distribution system) and NPPC = 3.5 kW/kW which may be achieved with advanced LT-PEMFC with high operating temperature up to 100 °C or early IT-PEMFC. In 2050, HT-PEMFC with FCPD = 3 kW/kg and NPPC = 5 kW/kW, superconducting electrical technologies with MPD = 25 kW/kg and CML = 5 kg/m and TMS MF = 5 kW/kg can enable energy-saving zero-emission flight with 57 pax over 300 nmi or 47 pax over 800 nmi. If these technologies are also combined with a 17% reduction in aircraft structural mass and 10% improvement in aerodynamic efficiency, this aircraft size can reach its maximum potential with 68 pax over 300 nmi or 63 pax over 800 nmi. These will also be technology milestones that can support the upscaling to larger aircraft. Due to the high uncertainties about technology development and future performance, the produced 2D maps can be used to trade-off technology targets among the subsystems to meet a given overall performance target.

Regarding the battery aircraft option, even with the most optimistic battery (600 Wh/kg) and aircraft technology scenarios, the threshold of >30 pax for >350 nmi cannot be crossed. For BED>400 Wh/kg combined with aircraft improvements, 33–57 pax might be feasible at 200 nmi, and for BED>500 Wh/kg 24–37 pax at 300 nmi. Despite the limited capabilities, the battery aircraft can offer significant in-flight energy savings in the order of 40% at short-range flights.

The FC and battery propulsion systems were also compared on the basis of EED. At NPPC = 3 kW/kW (LT-PEMFC), for FCPD>2 kW/kg and TMS MF>3 kW/kg the battery is hard to breakeven even at 200 nmi, and at 400 nmi BED over 600 Wh/kg would be needed to breakeven the FC EED. Considering the advantages and constraints of FC and batteries, their hybrid combination with the FC power sized for cruise and the battery sized only for the take-off and climb power peaks, can offer an increase in pax by 15 pax and reduce the energy at 300 nmi by ~600 MJ/pax (~40%) even with NPPC = 3 kW/kW (LT-PEMFC) and a BED close to today (300 Wh/kg).

7. Outlook

The development and introduction of a zero-emission regional aircraft will be a major achievement and a major milestone for the decarbonisation of the aviation system:

- Although number of passengers and flights are relatively low compared to the total numbers of global air traffic, they account for 10%–20% of emissions [132,133]. Thus, the use of

zero-emission regional aircraft can be used to develop a network of interconnected hubs that cover national and international regional transport needs while also offering connectivity to remote places and/or relieving the pressure from existing overloaded transport networks/infrastructures. The introduction of zero-emission regional aircraft will also address community impacts produced during take-off and landing cycles, where noise and non-CO_2 emissions are recognised as negatively impacting community wellbeing and air quality in regions surrounding airports. Regional aircraft have greater number take-off and landing cycles than other aircraft classes, and developing zero-emission variants will thus provide significant benefit to these communities.

- It will be a significant step towards developing the required infrastructure (including airport and energy infrastructure) that will enable the decarbonisation of the wider aviation ecosystem.
- It will have an enabling role in developing, maturing and de-risking key enabling technologies that are required for further improvements in aircraft efficiency and decarbonisation. Advancing the maturity, technical performance, and scalability of zero-emission aircraft technologies will thus allow for future applications on Short/Medium Range (SMR) and twin-aisle aircraft. Technology improvements will include those associated with safety, reliability, scalability, certification aspects of novel technologies, development of reliable and resilient supply chains and establishing appropriate operations.

There are three main options for zero emissions:

1. Full electric
2. Hydrogen electric (Fuel cell aircraft of regional class, although they produce some water/steam, their low-altitude cruise below 30000 ft combined with the absence of particulate matter and soot reduce the risk for contrail formation)
3. A hybrid solution.

These are disruptive solutions with novel technologies and aggressive targets. From a purely technical point of view, they are both feasible by 2040–2050. However, their overall feasibility for large-scale implementation needs to consider overall performance, including business viability, scalability aspects, availability of infrastructure and life cycle aspects. Overall performance and business viability need to consider payload (number of passengers) and range as well as emissions and energy consumption per passenger at a mission level. Although small electrified aircraft with limited payload and range capabilities are not that far away from a technology perspective, a large-scale implementation cannot be achieved with a business-as-usual approach as they require both enabling technology development on board the aircraft and drastic infrastructure changes. These infrastructure and life cycle aspects need to consider, among other factors, overall emissions and availability of energy sources in the form of suitable charging stations, grid capacity, the availability of low-carbon, ideally green hydrogen production and supply chain to the airports.

The full electric aircraft depends heavily on the energy density of batteries that constrain both range and payload. Development of advanced batteries with energy densities around 500 Wh/kg (double the energy density of existing batteries) could be possible by 2035–2040, and coupled with the use of advanced electric motors, could enable the introduction of a regional aircraft with ~30 passengers over 200 nmi. While such an aircraft will have superior performance in terms of energy consumption per passenger at aircraft level (~58% relative to existing conventional aircraft), its limited operational capabilities in terms of payload and range become a major disadvantage. More aggressive technology targets and synergetic benefits from improved aerodynamics, structures and advanced batteries with energy densities in the region of 600 Wh/kg could be achieved by 2050 and could enable ranges up to 400 nmi with significant reduction in energy/passenger requirements at an aircraft level. This will also be the upper limit of a fully electric battery aircraft both in terms of technological advancements and operational capabilities. Considering the energy infrastructure, even with the European Union's average carbon intensity today at ~207 gCO_2e/kWh_{el} [134], a 200 nmi, 500 Wh/kg battery aircraft will still offer a CO_2 saving and lifecycle energy saving compared to conventional aircraft. However, the infrastructure and carbon intensity of electricity production strongly vary across the world, therefore, a 200 nmi battery aircraft may offer a lifecycle CO_2 saving in countries with advanced infrastructure, and a penalty in countries with carbon intensities over 450 gCO_{2e}/kWh_{el}. And despite the improved energy performance at aircraft level, a major disadvantage and limiting factor of the full electric variant is the current limitations in scalability of key technologies, making it extremely challenging to realise further improvements.

In the case of a hydrogen-electric aircraft, longer ranges and higher number of passengers could be achieved. However, energy efficiency benefits at an aircraft level and across the life cycle of the aircraft will be difficult to achieve, even compared to existing aircraft. Increasing fuel cell system power density to 2 kW/kg (from current ~1 kW/kg) and focusing on the introduction of advanced thermal management systems and electric technologies could enable aircraft with similar operational capabilities of existing aircraft with an energy penalty at both aircraft and life cycle level by 2035–2040. The main challenge will be the available hydrogen infrastructure, availability of hydrogen and overall energy efficiency. Introduction of more aggressive technologies including high-temperature PEM fuel cells combined with hyper- or superconductive electrical distribution systems and improved aerodynamic and structural aircraft efficiency would match or even exceed the operational capabilities of existing regional aircraft, offering energy per passenger improvements at an aircraft level by 2050. A major advantage of introducing such technologies is that they have the potential to be scaled and adapted to SMR aircraft. The main challenge is the availability of green hydrogen and the challenges associated with the hydrogen and energy infrastructure. Only if an advanced superconducting FC aircraft is achieved, the lifecycle energy of the conventional regional aircraft could be nearly matched with the energy intensity of liquid hydrogen production today, and only a considerable improvement in the hydrogen production methods would start bringing lifecycle energy savings.

If the rate of research, development and adoption of sustainable technologies and infrastructure continues at the present rate, it is still possible that a small hydrogen-electric (fuel cell) aircraft and electric aircraft with batteries (potentially with hybrid GT operation as a range extender) of subregional class with limited capabilities can be certified by 2035–2040. In a scenario of modest rate of development and limited aircraft capability, there will be an energy penalty for the fuel cell aircraft, and very limited payload-range for the battery aircraft; therefore, the business case for wide adoption and economic viability will be poor. Even if other factors balance out the cost, such as political pressure to decarbonise aviation with carbon tax or other financial incentives to promote the use of green aircraft, the rate of aircraft production and delivery, following the certification, to replace existing fleets will be another limiting factor.

Regional variability in political decisions and strategies may limit the adoption within specific countries and specific airport hubs that will have the infrastructure to support such aircraft. In this case, a limited number of zero-emission, yet expensive, aircraft may be serving a network of short flights by 2050. They will not make a significant impact on reducing total emissions, but they will have greater impact on airport emissions and can serve as a demonstration of the importance of reaching this initial milestone.

To target a larger-scale transition to greener aviation, current efforts should be upscaled as soon as possible with even more coordinated and

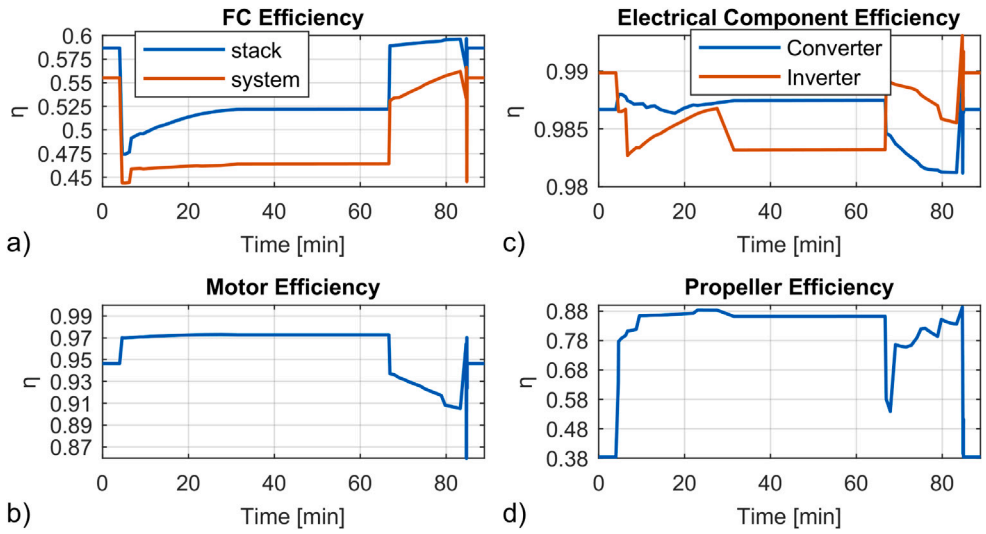

Fig. A.49. In-flight performance variation of FC system.

targeted efforts between governments and industry sectors into developing the required enabling technologies, infrastructure and production rate capacities at any cost. In an all-hands-on-deck approach, advanced technologies (superconducting electrical machines, HT-PEMFC, improved aircraft structures and aerodynamics) could lead to an optimised hydrogen electric regional aircraft with 50–68 pax over 800 nmi with potential to serve a high fraction of the total routes and upscale the technologies to larger aircraft classes.

CRediT authorship contribution statement

Evangelia Pontika: Writing – review & editing, Writing – original draft, Visualization, Software, Methodology, Investigation, Formal analysis, Data curation, Conceptualization. **Panagiotis Laskaridis:** Writing – review & editing, Writing – original draft, Supervision, Resources, Methodology, Formal analysis, Conceptualization. **Phillip J. Ansell:** Writing – original draft, Visualization, Investigation, Formal analysis, Data curation. **Kiruba Haran:** Writing – original draft, Visualization, Investigation, Formal analysis, Data curation. **Rukshan Navaratne:** Writing – original draft, Investigation, Formal analysis, Data curation. **Timoleon Kipouros:** Writing – review & editing, Visualization, Investigation.

Declaration of competing interest

The authors declare that they have no known competing financial interests or personal relationships that could have appeared to influence the work reported in this paper.

Acknowledgements

The authors acknowledge the co-authorship and valuable contribution of Dr Jon Huete Anton (Cranfield University) to this paper on hydrogen storage technologies. Sadly, our esteemed colleague and friend Dr Jon Huete Anton passed away in August 2024.

Appendix. Calculations

A.1. Performance calculations

The analysis is performed using CHARM — Cranfield Hybrid Electric Research Model. The base platform for the flight mission analysis and integrated aircraft/engine performance is described in [135] and one of the electrified version has been presented in [136,137]. Recent upgrades include the addition of the power penalty of the TMS based on the Net Power Performance Coefficient (NPPC) of the TMS and the cable mass. For each NPPC or change in the aircraft aerodynamic efficiency, the rated power of the system and components is modified, therefore the typical electric component maps and propeller map, as well as the stack modelling method from [136,137] have been used in a scaled way for this technology exploration. Representative efficiency variations during a flight are captured in Fig. A.49.

A FC system has stronger efficiency variations during the flight than a battery system, and having the lowest stack efficiency at take-off directly impacts the maximum heat generation and the sizing of the TMS, therefore it was important that this variation was captured. The battery system has less efficiency variation, and much lower heat generation, therefore the modelling was simplified assuming a typical 95% battery efficiency, 99% for inverter and converter, and 95% for the motor, and the same propeller map from [136] was used in a scaled way as propeller performance varies strongly among the flight phases.

A.1.1. Thermal management system

The components of the TMS, i.e. compressors, pumps, fans etc depending on the system type, may need to consume electric power to operate and, also, the ram air Heat Exchanger (HEX) becomes a source of drag generation due to the change in the momentum of the ram air through the HEX. This increase in drag results in an increase in thrust to maintain aircraft performance and, therefore, an increase in the power consumption by the propulsion system. The overall performance of the TMS in terms of power consumption is represented with a Net Power Performance Coefficient (NPPC) which is the ratio of the Heat Dissipated by the TMS (or often called "Cooling Effect" of the TMS) over the additional consumed power due to the TMS (which combines the electric power consumption of the TMS components and the propulsion system additional power consumption to overcome the TMS drag).

$$NPPC = \frac{Heat\ Dissipated}{P_{TMS}} = \frac{Heat\ Dissipated}{P_{drag} + P_{comp/pump}} \tag{A.1}$$

The additional power penalty of the TMS has two effects:

1. It is a direct increase in the FC power requirement
2. Due to this power requirement, there is an increase in the total heat load, which in turn increases the power consumption.

To calculate the relative FC power penalty due to TMS (drag and TMS compressor/pump power consumption) from the NPPC, Eq. (2)

has been formed by replacing the components of the Heat Dissipated in Eq. (1)

$$NPPC = \frac{1}{P_{TMS}} \cdot \left(\frac{P_{FC,prop}}{\eta_{stack}} \cdot (1-\eta_{stack}) + \eta_{BoP} \cdot P_{FC,prop} \cdot (1-\eta_{el}) + \frac{P_{TMS}}{\eta_{stack}} \cdot (1-\eta_{stack}) \right) \quad (A.2)$$

where:

$P_{FC,prop}$ is the FC power requirement for propulsion at the baseline case (before accounting the TMS penalty)

$\frac{P_{FC,prop}}{\eta_{stack}} \cdot (1-\eta_{stack})$ represents the heat produced by the FC with no TMS penalty

$\eta_{BoP} \cdot P_{FC,prop} \cdot (1-\eta_{el})$ represents the heat produced by the electric components before the TMS penalty

$\frac{P_{TMS}}{\eta_{stack}} \cdot (1-\eta_{stack})$ represents the additional heat due to the additional TMS power requirement.

Transforming Eq. (2), the power penalty due to the TMS can be calculated relative to the FC power requirement for propulsion alone (before accounting the TMS)

$$P_{TMS,rel} = P_{FC,prop} \cdot \left(\frac{1}{\eta_{stack} \cdot NPPC} \cdot (1-\eta_{stack}) + \frac{\eta_{BoP} \cdot (1-\eta_{el})}{NPPC} \right) \cdot \frac{1}{1 - \frac{1}{\eta_{stack} \cdot NPPC} \cdot (1-\eta_{stack})} \quad (A.3)$$

The split between drag power and compressor power does not play a significant role in this context. Either way it is translated to an increase in the fuel cell power requirement. There is only a small differentiation caused by different power split between drag power and compressor/pump power: If the TMS power penalty is due to compressor/pump compressor, this power is extracted right after the FC. If the power penalty is a drag power penalty, the additional FC power needs to be transferred up to the propeller to deliver more thrust to overcome the additional drag, so there is additional heat generated by the electric components, too. The heat generated at the electric components is a small fraction compared to the FC heat, so in the parametric technology sweeps, this differentiation will not be made (for different cases of power splits) as this is a generic exploration agnostic to the design. However, in Section 5.2 the technology factors and the equations that affect the split between the drag power and compressor/pump power are discussed.

Aerodynamic Efficiency Improvement

The aerodynamic efficiency improvement is considered as a drag reduction factor. This results in a proportional decrease in the power requirement at each point and total fuel/energy consumption (Eq. (A.4)).

$$c_{d,total} = (1-f_{aero}) \cdot c_{d,baseline} \quad (A.4)$$

Power, Energy and Fuel Scaling

To constrain the scope of this exploration and reduce the complexity of iterating the aircraft design and mission simulation for each step change in the combined NPPC and f_{aero}, the TMS power penalty (Eq. (A.3)) and drag reduction factors will be assumed to scale the baseline FC mission power, fuel and energy.

$$P_{new} = P_{baseline} \cdot (1 + P_{TMS,rel} - f_{aero}) \quad (A.5)$$

$$M_{f,new} = M_{f,baseline} \cdot (1 + P_{TMS,rel} - f_{aero}) \quad (A.6)$$

$$E_{new} = E_{baseline} \cdot (1 + P_{TMS,rel} - f_{aero}) \quad (A.7)$$

An improved aerodynamic efficiency can compensate for a part of the TMS power penalty (Fig. A.50b). Fig. A.50a presents the impact of fuel cell stack efficiency on the power penalty due to the TMS for a range of NPPC. An improvement in the FC efficiency either by a technology improvement or oversizing of the fuel cell can reduce the heat load and power penalty.

For the battery aircraft, a similar approach is followed by updating the battery-related efficiencies accordingly in Eqs. (A.2) and (A.3).

A.2. Mass effects

The rated power of the propulsion system is defined at the motor output and is 2 MW for the baseline aircraft before accounting for the effect of the TMS power penalty. The power output of each component of the powertrain is calculated starting from the output of the powertrain and diving by the efficiency of the component, and then the power output of each component is divided by its power density. An oversizing factor of 1.2 is applied to the motor. Using Eq. (A.8) and Eq. (A.9), payload (pax capability) is traded-off with system mass and fuel mass.

$$MTOW_{FC} = OEW_{baseline} - 2 \cdot M_{GT} + M_{FC} + M_{motor} + M_{inverter} + M_{converter} + M_{cables} + M_{tank} + M_{TMS} + M_{LH2,onboard} + Payload \quad (A.8)$$

$$MTOW_{Bat} = OEW_{baseline} - N_{GT} \cdot M_{GT} + M_{Bat} + M_{motor} + M_{inverter} + M_{converter} + M_{cables} + M_{TMS} + M_{f,reserve} + Payload \quad (A.9)$$

It should be noted that in the case of the battery aircraft, the MTOW is reduced from 23000 kg to 22350 kg to meet the maximum landing weight limit, as there is no fuel consumption or aircraft weight reduction during a battery-powered flight.

A.3. Hybrid aircraft with fuel cell and batteries

FC constraints are driven by the low power density of fuel cells combined with the demanding TMS requirements due to the heat load, which means that the system mass is affected by the maximum power of the system, while the bottleneck for batteries is the low energy density, which means that battery mass is increased with longer operating time and energy consumption. An attractive solution that has been proposed in literature is to combine fuel cells as the main power source with batteries to cover the power peaks (Eq. (A.10)), but there have not been more specific performance and technological explorations about the optimum topology. Fuel cell energy/power is replaced by battery energy/power which reduces the thermal management demands.

$$MTOW_{FC+Bat} = OEW_{baseline} - 2 \cdot M_{GT} + M_{FC} + M_{Bat} + M_{motor} + M_{inverter} + M_{converter} + M_{cables} + M_{tank} + M_{TMS} + M_{LH2,onboard} + Payload \quad (A.10)$$

The FC electric power output that corresponds to the quoted battery DoH at takeoff is kept constant until it equals the total power demand of the propeller, and the battery provides only the power peaks, as illustrated in Fig. A.51. It should be noted that the total shaft power requirement scales down when there is contribution from the battery as the power penalties due to the FC TMS start reducing.

A.4. Lifecycle aspects – total energy and CO_2

Lifecycle effects associated with the operation are discussed in this section. Energy and emissions related to the production of FC and batteries will be discussed separately in Sections 5.4.4 and 5.4.3. The lifecycle energy and CO_2 are benchmarked against today's conventional jet fuel aircraft. The jet fuel lifecycle energy and CO_2 are assumed at the typical values of 1.2 $MJ/MJ_{JetFuel}$ and 89 $grCO_2e/MJ_{Jet\ Fuel}$ [138].

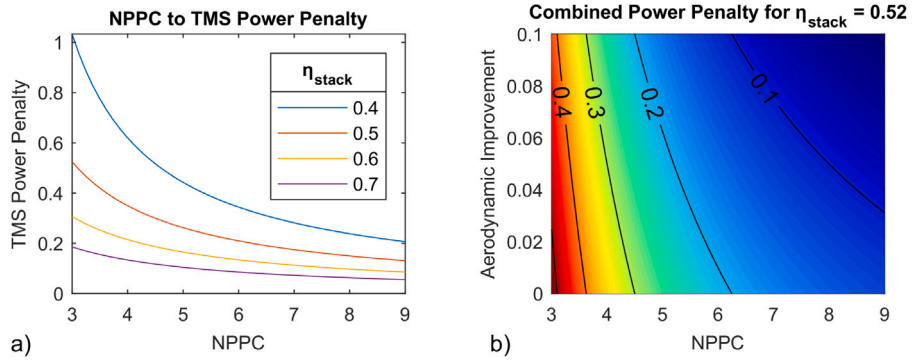

Fig. A.50. (a) Relative TMS power penalty as a function of the NPPC and stack efficiency (b) combined power penalty for combinations of NPPC and aerodynamic improvement.

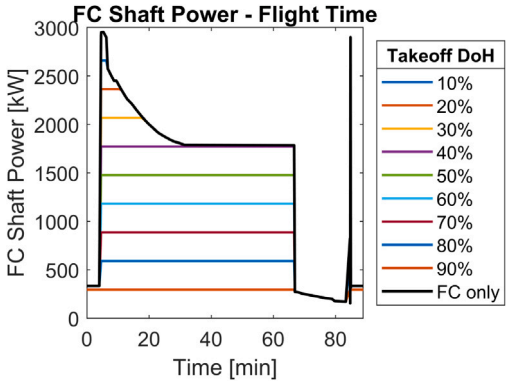

Fig. A.51. Electric power provided by the FC in a hybrid FC+battery system for different take-off DoH at NPPC = 3 kW/kW.

A.4.1. Fuel cell

The consumed hydrogen energy calculated for the flight mission is multiplied with a factor for the consumed electric energy for the electrolysis, liquefaction and transport of the hydrogen per produced hydrogen energy.

$$LCE_{FC} = M_f \cdot LHV_{H2} \cdot f_{PLT} \tag{A.11}$$

And then using the carbon intensity of the electric grid the produces the required electricity for the hydrogen production, transport and liquefaction, the lifecycle CO_2 emissions of the fuel cell mission is calculated:

$$LCCO2_{FC} = M_f \cdot CI \tag{A.12}$$

A.4.2. Batteries

The battery is sized to have a 20% State of Charge (SoC) at the end of the flight, but since the remaining 20% SoC is unconsumed energy, the lifecycle energy is based on the consumed flight energy (Eq. (A.13)) divided by the overall electric grid efficiency η_{grid} which includes the electricity production efficiency and transmission efficiency.

$$LCE_{Bat} = FE_{Bat} \cdot \frac{1}{\eta_{grid}} \tag{A.13}$$

The calculation of the lifecycle CO_2 due to the battery charging based on the electricity carbon intensity uses the consumed flight energy but divided by the grid transport efficiency $\eta_{grid,trans}$ as the carbon intensity is typically defined per generated electricity and not input energy.

$$LCCO2_{Bat} = \frac{FE_{Bat}}{\eta_{grid,trans}} \cdot CI \tag{A.14}$$

A.5. Lifecycle aspects – degradation

A.5.1. Fuel cell degradation rate

The PEMFC degradation is often driven by loss of effective catalyst area and results in voltage loss, efficiency loss and a reduction in available maximum power [139]. Therefore, the FC degradation is defined as a relative loss of maximum power and the degradation rate is defined as a relative loss of power per flight cycle:

$$RP_{end} = \frac{FCPD_{final}}{FCPD_{initial}} = (1 - degRate)^{Target\ maintenance\ interval} \tag{A.15}$$

The target maintenance intervals are benchmarked against typical Type A and Type C maintenance intervals for today's turboprop engine for regional aircraft [140–142]. The maintenance intervals can be defined either in engine flight cycles (EFC) or engine flight hours (EFH). For regional aircraft, the average hour to flight ratio is around 0.8-1 [140,141] and this ratio can be used to convert the results to the degradation rate per flight hour for a given reference mission.

The combination of target maintenance interval and acceptable state at the end of life gives the target degradation rate. The reverse of a chosen end of life relative state of health represents an oversizing factor. When a design mission is defined and the rated power of the FC propulsion system or the required battery capacity to perform this mission have been selected to meet the performance requirements, the system should be oversized according to this oversizing factor so that the degraded fuel cell or faded battery can still perform the design mission during the maintenance intervals (Fig. A.52).

This oversizing factor due to degradation has not been considered in existing studies. In Chyla project [143], an oversizing factor of 0.8 was assumed for the fuel cells and it was defined as P/Pmax. The motivation for this oversizing factor was to improve the FC efficiency by 10%. Degradation effects were not discussed.

A.5.2. Battery degradation rate

The battery degradation usually demonstrates as capacity fading [144–146], and Spinelli et al. [146] demonstrated the impact of the battery capacity degradation on the energy management strategy and resulting emissions of a hybrid electric regional aircraft with GT and batteries over one year of operations. Therefore, the battery degradation is defined here as a loss of capacity relative to the initial capacity of a clean battery.

$$SoH_{end} = \frac{BED_{final}}{BED_{initial}} = (1 - degRate)^{Target\ maintenance\ interval} \tag{A.16}$$

A.6. Thermal management metrics calculation

Heat Exchanger Effectiveness:

$$e = \frac{absorbed\ \Delta H}{ideal\ \Delta H} \tag{A.17}$$

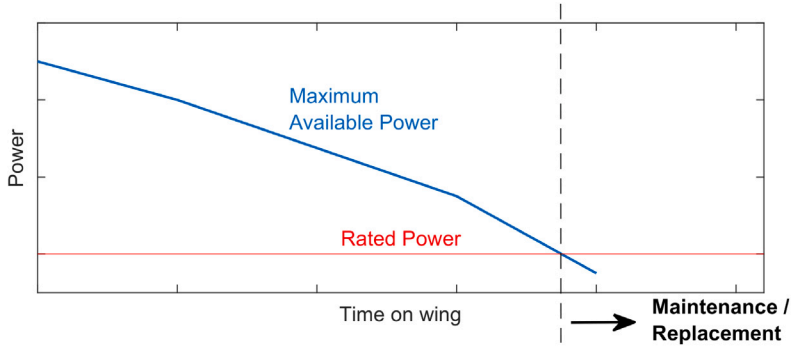

Fig. A.52. Available power of FC over time and time on wing.
Source: Adapted from [139].

Ram air ideal absorbed heat:

$$\Delta H_{HEX,ideal} = \dot{m}_{ram\ air} \cdot C_p \cdot (T_{hot,in} - T_{cold,in}) \tag{A.18}$$

Ram air absorbed heat:

$$\Delta H_{HEX} = e \cdot \dot{m}_{ram\ air} \cdot C_p \cdot (T_{hot,in} - T_{cold,in}) \tag{A.19}$$

Outlet temperature of the ram air:

$$T_2 = T_{cold,out} = T_\infty + \frac{\Delta H_{HEX}}{\dot{m}_{ram\ air} \cdot C_p} \tag{A.20}$$

Ram air velocity at the HEX exit:

$$P_2 = p_{amb} \cdot \left(1 + \frac{\gamma - 1}{2} M_2^2\right)^{\frac{\gamma}{\gamma - 1}} \rightarrow V_2 = \alpha \cdot \sqrt{\left[\left(\frac{P_2}{p_{amb}}\right)^{\frac{\gamma-1}{\gamma}} - 1\right] \cdot \frac{2}{\gamma - 1}} \tag{A.21}$$

where the outlet pressure P_2 depends on the velocity drop at the HEX and the speed of sound α which is a function of the outlet temperature T_2:

$$P_2 = (1 - dP_{rel}) \cdot P_\infty = (1 - dP_{rel}) \cdot P_{amb} \cdot \left(1 + \frac{\gamma - 1}{2} M_\infty^2\right)^{\frac{\gamma-1}{\gamma}} \tag{A.22}$$

For the values demonstrated in Figs. 33, 34, the relative pressure drop dPrel was assumed 10% and the HEX effectiveness e was assumed 80%. For different designs and HEX technologies, these values can be slightly different, but since this exploration is agnostic to the design, these typical values have been assumed.

The momentum drag due to the velocity drop through the ram air HEX can be calculated:

$$D_{TMS} = \dot{m}_{ram\ air} \cdot (V_\infty - V_2) \tag{A.23}$$

and the drag power:

$$Drag\ Power = D_{TMS} \cdot V_\infty \tag{A.24}$$

This additional drag power needs to be compensated by additional propeller thrust power. Therefore, this translates to an increase in the power consumption of the power source (battery/fuel cell). The additional power of the FC due to ram air HEX drag can be calculated:

$$P_{drag@FC} = \frac{D_{TMS} \cdot V_\infty}{\eta_{prop} \cdot \eta_{motor} \cdot \eta_{inverter} \cdot \eta_{converter}} \tag{A.25}$$

Data availability

The main datasets of the technology exploration can be accessed here on the institutional repository: https://doi.org/10.57996/cran.ceres-2809. Additional data can also be made available upon request.

References

[1] Clean Aviation, Towards Disruptive Technologies for new Generation Aircraft by 2035, Tech. rep., 2024.
[2] Jet Zero Strategy: Delivery Net Zero Aviation by 2050, Tech. rep., Department of Transport, UK, 2022, URL www.gov.uk/government/organisations/.
[3] D.E. Van Zante, R. Wahls, NASA aeronautics sustainable flight national partnership (SFNP), in: ICAO CAEP WG1 & WG3, NASA, 2023, URL https://ntrs.nasa.gov/api/citations/20230006282/downloads/SFNP_HighLevel_4ICAO_CAEP-2023may9-wahls_vanzante.pdf.
[4] P. Wheeler, Technology for the more and all electric aircraft of the future, in: 2016 IEEE International Conference on Automatica, ICA-ACCA, IEEE, 2016, pp. 1–5, http://dx.doi.org/10.1109/ICA-ACCA.2016.7778519, URL http://ieeexplore.ieee.org/document/7778519/.
[5] D.K. Hall, E.M. Greitzer, A.P. Dowdle, J.J. Gonzalez, W.W. Hoburg, J.H. Lang, J.S. Sabnis, Z.S. Spakovszky, B. Yutko, C. Courtin, W. Thalheimer, L. Trollinger, J. Tylko, N. Varney, A. Uranga, S. Byahut, M. Kruger, Feasibility of Electrified Propulsion for Ultra-Efficient Commercial Aircraft Final Report, Tech. rep., 2019, URL http://www.sti.nasa.gov.
[6] Argonne National Laboratory, The U.S. Department of Energy Vehicle Technologies Office and National Aeronautics and Space Administration Joint Assessment of the R&D Needs for Electric Aviation, Tech. rep., US Department of Energy, 2021.
[7] S. Byahut, A. Pundarika, A. Uranga, Modeling well-to-wake life-cycle CO2 emissions for electrified aircraft, in: AIAA Aviation and Aeronautics Forum and Exposition, AIAA AVIATION Forum 2021, American Institute of Aeronautics and Astronautics Inc, AIAA, 2021, http://dx.doi.org/10.2514/6.2021-2410.
[8] S. Karpuk, A. Elham, Influence of novel airframe technologies on the feasibility of fully-electric regional aviation, Aerospace 8 (6) (2021) http://dx.doi.org/10.3390/aerospace8060163.
[9] V. Viswanathan, A.H. Epstein, Y.M. Chiang, E. Takeuchi, M. Bradley, J. Langford, M. Winter, The challenges and opportunities of battery-powered flight, Nature 601 (7894) (2022) 519–525, http://dx.doi.org/10.1038/s41586-021-04139-1.
[10] J. Mukhopadhaya, D. Rutherford, Performance Analysis of Evolutionary Hydrogen-Powered Aircraft, Tech. rep., 2022, URL www.theicct.orgcommunications@theicct.org.
[11] D. Hyde, B. Barker, P. Hodgson, R. Miller, M. Rapeanu, Target True Zero: Unlocking Sustainable Battery and Hydrogen-Powered Flight, Tech. rep., World Economic Forum, 2022.
[12] A. Misley, A. Sergent, M. D'Arpino, P. Ramesh, M. Canova, Design space exploration of lithium-ion battery packs for hybrid-electric regional aircraft applications, J. Propuls. Power 39 (3) (2023) 390–403, http://dx.doi.org/10.2514/1.B38658, URL https://arc.aiaa.org/doi/10.2514/1.B38658.
[13] G. Palaia, K. Abu Salem, A.A. Quarta, Parametric analysis for hybrid–electric regional aircraft conceptual design and development, Appl. Sci. (Switz.) 13 (19) (2023) http://dx.doi.org/10.3390/app131911113.
[14] M. Staggat, J. Ludowicy, V. Bahrs, A. Link, S. Kazula, Modelling of a battery supported fuel cell electric power train topology for a regional aircraft, in: Journal of Physics: Conference Series, Vol. 2526, Institute of Physics, 2023, http://dx.doi.org/10.1088/1742-6596/2526/1/012061.
[15] J.T. Kirk, Z.J. Frederick, M.D. Guynn, B.D. Phillips, K.L. Fisher, S.J. Schneider, P. Frederic, Continued exploration of the electrified aircraft propulsion design space, in: AIAA SciTech Forum and Exposition, 2023, American Institute of Aeronautics and Astronautics Inc, AIAA, 2023, http://dx.doi.org/10.2514/6.2023-1354.
[16] M.O. Hales, N.J. Wood, S. Harrison, M. Husband, J. Stonham, C. Zhao, D. Ettridge, D. Westmore, S. Taylor, H2GEAR hydrogen electric powertrain – system architecture, in: AIAA Aviation and Aeronautics Forum and Exposition, AIAA AVIATION Forum 2023, American Institute of Aeronautics and Astronautics Inc, AIAA, 2023, http://dx.doi.org/10.2514/6.2023-3874.

[17] N.J. Wood, M.O. Hales, M. Joynt, S. Devendran, S. Taylor, Scalability of hydrogen fuel cell aircraft, in: AIAA Aviation Forum and ASCEND, 2024, American Institute of Aeronautics and Astronautics Inc, AIAA, 2024, http://dx.doi.org/10.2514/6.2024-3659.

[18] S.S. Jagtap, P.R. Childs, M.E. Stettler, Performance sensitivity of subsonic liquid hydrogen long-range tube-wing aircraft to technology developments, Int. J. Hydrog. Energy 50 (2024) 820–833, http://dx.doi.org/10.1016/j.ijhydene.2023.07.297.

[19] S. Tiwari, M.J. Pekris, J.J. Doherty, A review of liquid hydrogen aircraft and propulsion technologies, Int. J. Hydrog. Energy 57 (2024) 1174–1196, http://dx.doi.org/10.1016/j.ijhydene.2023.12.263.

[20] ZeroAvia, Scaling Hydrogen-Electric Propulsion for Large Aircraft, Tech. rep., URL https://www.energy.gov/eere/fuelcells/hydrogen-storage.

[21] E.J. Adler, J.R. Martins, Energy demand comparison for carbon-neutral flight, Prog. Aerosp. Sci. 152 (2025) http://dx.doi.org/10.1016/j.paerosci.2024.101051.

[22] S. Delbecq, J. Fontane, N. Gourdain, T. Planès, F. Simatos, Sustainable aviation in the context of the Paris Agreement: A review of prospective scenarios and their technological mitigation levers, Prog. Aerosp. Sci. 141 (2023) http://dx.doi.org/10.1016/j.paerosci.2023.100920.

[23] A.R. Gnadt, R.L. Speth, J.S. Sabnis, S.R. Barrett, Technical and environmental assessment of all-electric 180-passenger commercial aircraft, Prog. Aerosp. Sci. 105 (2019) 1–30, http://dx.doi.org/10.1016/j.paerosci.2018.11.002.

[24] P. Barros Pintos, C. Ulloa Sande, Ó. Castro Álvarez, Sustainable propulsion alternatives in regional aviation: The case of the Canary Islands, Transp. Res. D 120 (2023) http://dx.doi.org/10.1016/j.trd.2023.103779.

[25] L.M. Dray, A.W. Schäfer, K. Al Zayat, The global potential for CO2 emissions reduction from jet engine passenger aircraft, Transp. Res. Rec. 2672 (23) (2018) 40–51, http://dx.doi.org/10.1177/0361198118787361.

[26] A.W. Schäfer, A.D. Evans, T.G. Reynolds, L. Dray, Costs of mitigating CO2 emissions from passenger aircraft, Nat. Clim. Chang. 6 (4) (2016) 412–417, http://dx.doi.org/10.1038/nclimate2865.

[27] J.R. Smith, E. Mastorakos, An energy systems model of large commercial liquid hydrogen aircraft in a low-carbon future, Int. J. Hydrog. Energy 52 (2024) 633–654, http://dx.doi.org/10.1016/j.ijhydene.2023.04.039.

[28] A. Cybulsky, F. Allroggen, Y. Shao-Horn, D.S. Mallapragada, Challenges of decarbonizing aviation via hydrogen propulsion: Technology performance targets and energy system trade-offs, ACS Sustain. Chem. Eng. 12 (40) (2024) 14615–14628, http://dx.doi.org/10.1021/acssuschemeng.4c02868, URL https://pubs.acs.org/doi/10.1021/acssuschemeng.4c02868.

[29] Aerospace Technology Institute, Fuel Cells Roadmap Report - FlyZero, Tech. rep., 2022.

[30] Clean Sky 2 JU, FCH 2 JU, Hydrogen-Powered Aviation, Tech. rep., 2020, http://dx.doi.org/10.2843/766989.

[31] E. Padgett, G. Kleen, Automotive Fuel Cell Targets and Status, Tech. Rep. 1, U.S. Department of Energy, Hydrogen and Fuel Cells Program Record, 2020, http://dx.doi.org/10.4271/2015-01-1175.

[32] IATA, Aircraft Technology Net Zero Roadmap, Tech. rep., URL https://www.iata.org/contentassets/8d19e716636a47c184e7221c77563c93/aircraft-technology-net-zero-roadmap.pdf.

[33] IMOTHEP Project, D4.8: Synthesis of ASS-LA Battery Technology Evaluation, Tech. rep., 2023, URL www.imothep-project.eu.

[34] Heart Aerospace, ES-30™. URL https://heartaerospace.com/es-30/.

[35] J.T. Kim, H. Su, Y. Zhong, C. Wang, H. Wu, D. Zhao, C. Wang, X. Sun, Y. Li, All-solid-state lithium–sulfur batteries through a reaction engineering lens, Nat. Chem. Eng. 1 (6) (2024) 400–410, http://dx.doi.org/10.1038/s44286-024-00079-5.

[36] Battery 2030+ Roadmap, Inventing the Sustainable Batteries of the Future - Research Needs and Future Actions, Tech. rep., 2023.

[37] B. Tiede, C. O'Meara, R. Jansen, Battery key performance projections based on historical trends and chemistries, in: 2022 IEEE Transportation Electrification Conference and Expo, ITEC 2022, Institute of Electrical and Electronics Engineers Inc., 2022, pp. 754–759, http://dx.doi.org/10.1109/ITEC53557.2022.9814008.

[38] B.A. Adu-Gyamfi, C. Good, Electric aviation: A review of concepts and enabling technologies, Transp. Eng. 9 (2022) http://dx.doi.org/10.1016/j.treng.2022.100134.

[39] NASA, SABERS: Solid-state Architecture Batteries for Enhanced Rechargeability and Safety, Tech. rep., URL https://www.nasa.gov/wp-content/uploads/2021/04/sabers_cas_fact_sheet_508.pdf.

[40] N. Darmet, J. Charbonnel, M. Reytier, L. Broche, R. Vincent, First experimental assessment of all-solid-state battery thermal runaway propagation in a battery pack, ACS Appl. Energy Mater. 7 (10) (2024) 4365–4375, http://dx.doi.org/10.1021/acsaem.4c00248.

[41] J. Janek, W.G. Zeier, Challenges in speeding up solid-state battery development, Nat. Energy 8 (3) (2023) 230–240, http://dx.doi.org/10.1038/s41560-023-01208-9, URL https://www.nature.com/articles/s41560-023-01208-9.

[42] X. Miao, S. Guan, C. Ma, L. Li, C.W. Nan, Role of interfaces in solid-state batteries, Adv. Mater. 35 (50) (2023) http://dx.doi.org/10.1002/adma.202206402.

[43] L. Lobitz, A. Hahn, D. Vogt, T. Luplow, P. Michalowski, S. Heimbs, G. Garnweitner, Conceptual challenges for crashworthy battery-electric commercial aircraft – A review, in: AIAA SciTech Forum and Exposition, 2024, American Institute of Aeronautics and Astronautics Inc, AIAA, 2024, http://dx.doi.org/10.2514/6.2024-2156.

[44] S. Xie, L. Ren, Y. Gong, M. Li, X. Chen, Effect of charging/discharging rate on the thermal runaway characteristics of lithium-ion batteries in low pressure, J. Electrochem. Soc. 167 (14) (2020) 140503, http://dx.doi.org/10.1149/1945-7111/abbfd8.

[45] Nautilus EU Project Report, The Comparison of Different Technologies for On-Board Power Supply of Cruise Ships, Tech. rep..

[46] Ballard, FCgen®–HPS Durable heavy duty fuel cell stack. URL https://www.ballard.com/wp-content/uploads/2024/08/Ballard_FCgen_HPS_specs.pdf.

[47] T. Yoshida, K. Kojima, Toyota MIRAI fuel cell vehicle and progress toward a future hydrogen society, Electrochem. Soc. Interface 24 (2015) 45–49, http://dx.doi.org/10.1149/2.F03152if, URL https://iopscience.iop.org/article/10.1149/2.F03152if.

[48] Toyota, The all-new Toyota Mirai, 2022, URL https://media.toyota.co.uk/wp-content/uploads/sites/5/pdf/220203M-Mirai-Press-Pack.pdf.

[49] ZeroAvia, Electric and Hydrogen Aerospace Propulsion Components. URL https://zeroavia.com/wp-content/uploads/2024/04/Zero_Avia_A4_Components-Brochure_DIGITAL-V2.3-US-LETTER-SIZE.pdf.

[50] Intelligent Energy, IE-FLIGHT White Paper. URL https://www.intelligent-energy.com/wp-content/uploads/2024/07/FLIGHT-Whitepaper.pdf.

[51] E. Wallnöfer-Ogris, F. Poimer, R. Köll, M.G. Macherhammer, A. Trattner, Main degradation mechanisms of polymer electrolyte membrane fuel cell stacks – mechanisms, influencing factors, consequences, and mitigation strategies, Int. J. Hydrog. Energy 50 (2024) 1159–1182, http://dx.doi.org/10.1016/j.ijhydene.2023.06.215.

[52] D. Madhav, J. Wang, R. Keloth, J. Mus, F. Buysschaert, V. Vandeginste, A review of proton exchange membrane degradation pathways, mechanisms, and mitigation strategies in a fuel cell, Energies 17 (5) (2024) http://dx.doi.org/10.3390/en17050998.

[53] M. Chandran, K. Palaniswamy, N.B. Karthik Babu, O. Das, A study of the influence of current ramp rate on the performance of polymer electrolyte membrane fuel cell, Sci. Rep. 12 (1) (2022) http://dx.doi.org/10.1038/s41598-022-25037-0.

[54] L. Carrette, K.A. Friedrich, U. Stimming, Fuel cells - Fundamentals and applications, Fuel Cells 1 (1) (2001) 5–39, http://dx.doi.org/10.1002/1615-6854(200105)1:1<5::AID-FUCE5>3.0.CO;2-G, URL https://onlinelibrary.wiley.com/doi/10.1002/1615-6854(200105)1:1<5::AID-FUCE5>3.0.CO;2-G.

[55] M. Asli, P. König, D. Sharma, E. Pontika, J. Huete, K.R. Konda, A. Mathiazhagan, T. Xie, K. Höschler, P. Laskaridis, Thermal management challenges in hybrid-electric propulsion aircraft, Prog. Aerosp. Sci. 144 (2024) http://dx.doi.org/10.1016/j.paerosci.2023.100967.

[56] E. Qu, X. Hao, M. Xiao, D. Han, S. Huang, Z. Huang, S. Wang, Y. Meng, Proton exchange membranes for high temperature proton exchange membrane fuel cells: Challenges and perspectives, J. Power Sources 533 (2022) http://dx.doi.org/10.1016/j.jpowsour.2022.231386.

[57] R.E. Rosli, A.B. Sulong, W.R. Daud, M.A. Zulkifley, T. Husaini, M.I. Rosli, E.H. Majlan, M.A. Haque, A review of high-temperature proton exchange membrane fuel cell (HT-PEMFC) system, Int. J. Hydrog. Energy 42 (14) (2017) 9293–9314, http://dx.doi.org/10.1016/j.ijhydene.2016.06.211.

[58] J. Chen, J. Cao, R. Zhang, J. Zhou, S. Wang, X. Liu, T. Zhang, X. Tao, Y. Zhang, Modifications on promoting the proton conductivity of polybenzimidazole-based polymer electrolyte membranes in fuel cells, Membranes 11 (11) (2021) http://dx.doi.org/10.3390/membranes11110826.

[59] L.K. Seng, M.S. Masdar, L.K. Shyuan, Ionic liquid in phosphoric acid-doped polybenzimidazole (Pa-pbi) as electrolyte membranes for pem fuel cells: A review, Membranes 11 (10) (2021) http://dx.doi.org/10.3390/membranes11100728.

[60] Q. Meyer, C. Yang, Y. Cheng, C. Zhao, Overcoming the electrode challenges of high-temperature proton exchange membrane fuel cells, Electrochem. Energy Rev. 6 (1) (2023) http://dx.doi.org/10.1007/s41918-023-00180-y.

[61] A. Chandan, M. Hattenberger, A. El-Kharouf, S. Du, A. Dhir, V. Self, B.G. Pollet, A. Ingram, W. Bujalski, High temperature (HT) polymer electrolyte membrane fuel cells (PEMFC)-A review, J. Power Sources 231 (2013) 264–278, http://dx.doi.org/10.1016/j.jpowsour.2012.11.126.

[62] M. Butori, B. Eriksson, N. Nikolić, C. Lagergren, G. Lindbergh, R.W. Lindström, The effect of oxygen partial pressure and humidification in proton exchange membrane fuel cells at intermediate temperature (80–120 °C), J. Power Sources 563 (2023) http://dx.doi.org/10.1016/j.jpowsour.2023.232803.

[63] A. Zucconi, J. Hack, R. Stocker, T.A. Suter, A.J. Rettie, D.J. Brett, Challenges and opportunities for characterisation of high-temperature polymer electrolyte membrane fuel cells: a review, J. Mater. Chem. A 12 (14) (2024) 8014–8064, http://dx.doi.org/10.1039/d3ta06895a.

[64] O. Fernihough, M.S. Ismail, A. El-kharouf, Intermediate temperature PEFC's with Nafion® 211 membrane electrolytes: An experimental and numerical study, Membranes 12 (4) (2022) http://dx.doi.org/10.3390/membranes12040430.

[65] J.B. Lu, G.H. Wei, F.J. Zhu, X.H. Yan, J.L. Zhang, Pressure effect on the PEMFC performance, Fuel Cells 19 (3) (2019) 211–220, http://dx.doi.org/10.1002/fuce.201800135.

[66] M. Hala, J. Mališ, M. Paidar, K. Bouzek, Characterization of commercial polymer–carbon composite bipolar plates used in PEM fuel cells, Membranes 12 (11) (2022) http://dx.doi.org/10.3390/membranes12111050.

[67] F.B. Weng, M.M. Dlamini, J.J. Hwang, Evaluation of flow field design effects on proton exchange membrane fuel cell performance, Int. J. Hydrog. Energy 48 (39) (2023) 14866–14884, http://dx.doi.org/10.1016/j.ijhydene.2023.01.005.

[68] T. Wilberforce, Z. El Hassan, E. Ogungbemi, O. Ijaodola, F.N. Khatib, A. Durrant, J. Thompson, A. Baroutaji, A.G. Olabi, A comprehensive study of the effect of bipolar plate (BP) geometry design on the performance of proton exchange membrane (PEM) fuel cells, Renew. Sustain. Energy Rev. 111 (2019) 236–260, http://dx.doi.org/10.1016/j.rser.2019.04.081.

[69] M.T. Tran, D.H. Lee, H.W. Lee, D.K. Kim, Formability improvement in multi-stage stamping of ultra-thin metallic bipolar plate for proton exchange membrane fuel cell, Int. J. Hydrog. Energy 47 (94) (2022) 40008–40025, http://dx.doi.org/10.1016/j.ijhydene.2022.09.163.

[70] S. Khosravi H, Q. Abbas, K. Reichmann, Electrochemical aspects of interconnect materials in PEMFCs, Int. J. Hydrog. Energy 46 (71) (2021) 35420–35447, http://dx.doi.org/10.1016/j.ijhydene.2021.08.105.

[71] K.P. Duffy, Turboelectric and Hybrid Electric Aircraft Drive Key Perfomance Parameters, Tech. rep., 2018.

[72] K. Haran, N. Nadavan, T.C. O'Connell (Eds.), Electrified Aircraft Propulsion - Powering the Future Air Transport, no. 2, Cambridge University Press, 2022, http://dx.doi.org/10.1017/9781108297684.

[73] S. Sirimanna, B. Thanatheepan, D. Lee, S. Agrawal, Y. Yu, Y. Wang, A. Anderson, A. Banerjee, K. Haran, Comparison of electrified aircraft propulsion drive systems with different electric motor topologies, J. Propuls. Power 37 (5) (2021) 733–747, http://dx.doi.org/10.2514/1.B38195.

[74] A. Trentin, Z. Xu, T. Yang, C. Gerada, Deliverable 8.27 Propulsion Motor and Inverter Trade Summary, Tech. rep., NEWBORN - NExt generation high poWer fuel cells for airBORNe applications, 2023.

[75] A. Woodworth, T. Williams, M. Kelly, W. Sixel, E.E. Shin, B.N. Nguyen, Potential of materials to impact megawatt-scale electric machines, in: AIAA/IEEE Electric Aircraft Technologies Symposium, NASA, 2021, URL www.nasa.gov.

[76] D.C. Deisenroth, M. Ohadi, Thermal management of high-power density electric motors for electrification of aviation and beyond, Energies 12 (19) (2019) http://dx.doi.org/10.3390/en12193594.

[77] M.D. Sumption, J. Murphy, M. Susner, T. Haugan, Performance metrics of electrical conductors for aerospace cryogenic motors, generators, and transmission cables, Cryogenics 111 (2020) http://dx.doi.org/10.1016/j.cryogenics.2020.103171.

[78] W. Stautner, P.J. Ansell, K.S. Haran, CHEETA: An all-electric aircraft takes cryogenics and superconductivity on board: Combatting climate change, IEEE Electrification Mag. 10 (2) (2022) 34–42, http://dx.doi.org/10.1109/MELE.2022.3165948.

[79] J. Wang, T. Jahns, P. McCluskey, J. Kizito, B. Sarlioglu, R. Borjas, J. Swanke, Y. Cong, Z. Yao, H. Zeng, P. Fu, A. Schnabel, 2-kV 1-MW 20,000-RPM integrated modular motor drive for electrified aircraft propulsion, IEEE J. Emerg. Sel. Top. Power Electron. (2023) http://dx.doi.org/10.1109/JESTPE.2023.3283538.

[80] T. Balachandran, D. Lee, N. Salk, K.S. Haran, A fully superconducting air-core machine for aircraft propulsion, in: IOP Conference Series: Materials Science and Engineering, Vol. 756, IOP Publishing Ltd, 2020, http://dx.doi.org/10.1088/1757-899X/756/1/012030.

[81] S. Sirimanna, T. Balachandran, N. Salk, J. Xiao, D. Lee, K. Haran, Electric propulsors for zero-emission aircraft: Partially superconducting machines, IEEE Electrification Mag. 10 (2) (2022) 43–56, http://dx.doi.org/10.1109/MELE.2022.3165952.

[82] F. Tomasella, M. Fioriti, L. Boggero, S. Corpino, Method for estimation of electrical wiring interconnection systems in preliminary aircraft design, J. Aircr. 56 (3) (2019) 1259–1263, http://dx.doi.org/10.2514/1.C034943.

[83] E. Aretskin-Hariton, M. Bell, S. Schnulo, J. Gray, Power cable mass estimation for electric aircraft propulsion, in: AIAA Aviation and Aeronautics Forum and Exposition, AIAA AVIATION Forum 2021, American Institute of Aeronautics and Astronautics Inc, AIAA, 2021, http://dx.doi.org/10.2514/6.2021-3021.

[84] V. Palladino, Méthode de Conception Pluridisciplinaire Appliquée à un Avion Régional à Faibles Émissions (Ph.D. thesis), Institut Supérieur de l'Aéronautique et de l'Espace, 2023.

[85] P.C. Vratny, Conceptual Design Methods of Electric Power Architectures for Hybrid Energy Aircraft, Tech. rep..

[86] V. Palladino, A. Jordan, N. Bartoli, P. Schmollgruber, V. Pommier-Budinger, E. Benard, Preliminary studies of a regional aircraft with hydrogen-based hybrid propulsion, 2021, pp. 1–29, http://dx.doi.org/10.2514/6.2021-2411.

[87] T.P. Dever, T.J. Lantz, R.H. Jansen, Cable key performance parameter projections for megawatt electrified aircraft propulsion models, in: AIAA SciTech Forum and Exposition, 2024, American Institute of Aeronautics and Astronautics Inc, AIAA, 2024, http://dx.doi.org/10.2514/6.2024-1328.

[88] J. Jiang, Z. Li, W. Li, P. Ranjan, X. Wei, X. Zhang, C. Zhang, A review on insulation challenges towards electrification of aircraft, High Volt. 8 (2) (2023) 209–230, http://dx.doi.org/10.1049/hve2.12304.

[89] J. Huete, D. Nalianda, P. Pilidis, Impact of tank gravimetric efficiency on propulsion system integration for a first-generation hydrogen civil airliner, Aeronaut. J. 126 (1302) (2022) 1324–1332, http://dx.doi.org/10.1017/aer.2022.60.

[90] P.C. Okonkwo, E.M. Barhoumi, I. Ben Belgacem, I.B. Mansir, M. Aliyu, W. Emori, P.C. Uzoma, W.H. Beitelmal, E. Akyüz, A.B. Radwan, R.A. Shakoor, A focused review of the hydrogen storage tank embrittlement mechanism process, Int. J. Hydrog. Energy 48 (35) (2023) 12935–12948, http://dx.doi.org/10.1016/j.ijhydene.2022.12.252.

[91] I.K. Giannopoulos, E.E. Theotokoglou, Liquid hydrogen storage tank loading generation for civil aircraft damage tolerance analysis, in: Journal of Physics: Conference Series, Vol. 2692, Institute of Physics, 2024, http://dx.doi.org/10.1088/1742-6596/2692/1/012048.

[92] M.W. Qanbar, Z. Hong, A review of hydrogen leak detection regulations and technologies, Energies 17 (16) (2024) http://dx.doi.org/10.3390/en17164059.

[93] C.M. Benson, P.G. Holborn, A.M. Rolt, J.M. Ingram, E. Alexander, Combined hazard analyses to explore the impact of liquid hydrogen fuel on the civil aviation industry, in: Volume 3: Ceramics; Coal, Biomass, Hydrogen, and Alternative Fuels, American Society of Mechanical Engineers, 2020, http://dx.doi.org/10.1115/GT2020-14977, URL https://asmedigitalcollection.asme.org/GT/proceedings/GT2020/84119/Virtual,%20Online/1094644.

[94] M. Coutinho, D. Bento, A. Souza, R. Cruz, F. Afonso, F. Lau, A. Suleman, F.R. Barbosa, R. Gandolfi, W. Affonso, F.I. Odaguil, M.F. Westin, R.J. dos Reis, C.R. da Silva, A review on the recent developments in thermal management systems for hybrid-electric aircraft, Appl. Therm. Eng. 227 (2023) http://dx.doi.org/10.1016/j.applthermaleng.2023.120427.

[95] T.L. Kösters, X. Liu, D. Kožulović, S. Wang, J. Friedrichs, X. Gao, Comparison of phase-change-heat-pump cooling and liquid cooling for PEM fuel cells for MW-level aviation propulsion, Int. J. Hydrog. Energy 47 (68) (2022) 29399–29412, http://dx.doi.org/10.1016/j.ijhydene.2022.06.235.

[96] W. Affonso, R. Tavares, F.R. Barbosa, R. Gandolfi, R.J.N. dos Reis, C.R.I. da Silva, T. Kipouros, P. Laskaridis, H.B. Enalou, A. Chekin, A. Kukovinets, K. Gubernatorov, Y. Ravikovich, N. Ivanov, L. Ponyaev, D. Holobtsev, System architectures for thermal management of hybrid-electric aircraft - FutPrInt50, IOP Conf. Ser.: Mater. Sci. Eng. 1226 (1) (2022) 012062, http://dx.doi.org/10.1088/1757-899x/1226/1/012062.

[97] A.C. Frey, D. Bosak, J. Stonham, C.M. Sangan, O.J. Pountney, Liquid cooling fuel cell powered aircraft: The effect of coolants on thermal management, in: ASME Turbo Expo, American Society of Mechanical Engineers, London, UK, 2024, http://dx.doi.org/10.1115/GT2024-FM1, URL https://asmedigitalcollection.asme.org/GT/proceedings/GT2024/87929/V001T00A001/1203727.

[98] W. Affonso, R. Gandolfi, R.J. Nunes dos Reis, C.R. Ilário da Silva, N. Rodio, T. Kipouros, P. Laskaridis, A. Chekin, Y. Ravikovich, N. Ivanov, L. Ponyaev, D. Holobtsev, Thermal management challenges for HEA – FUTPRINT 50, in: IOP Conference Series: Materials Science and Engineering, Vol. 1024, IOP Publishing Ltd, 2021, http://dx.doi.org/10.1088/1757-899X/1024/1/012075.

[99] J. Liu, D. Cheng, K. Oo, T.-L. McCrimmon, S. Bai, Design and additive manufacturing of TPMS heat exchangers, Appl. Sci. 14 (10) (2024) 3970, http://dx.doi.org/10.3390/app14103970, URL https://www.mdpi.com/2076-3417/14/10/3970.

[100] M.F. Stoia, M. Shi, Thermal challenges and solutions for hydrogen fuel cell aircraft, in: AIAA AVIATION 2023 Forum, American Institute of Aeronautics and Astronautics, Reston, Virginia, 2023, http://dx.doi.org/10.2514/6.2023-4475, URL https://arc.aiaa.org/doi/10.2514/6.2023-4475.

[101] P. Laskaridis, V. Pachidis, P. Pilidis, Opportunities and challenges for distributed propulsion and boundary layer ingestion, Aircr. Eng. Aerosp. Technol. 86 (6) (2014) 451–458, http://dx.doi.org/10.1108/AEAT-05-2014-0067.

[102] N.G. Moirou, D.S. Sanders, P. Laskaridis, Advancements and prospects of boundary layer ingestion propulsion concepts, Prog. Aerosp. Sci. 138 (2023) http://dx.doi.org/10.1016/j.paerosci.2023.100897.

[103] T. Sinnige, N. Van Arnhem, T.C. Stokkermans, G. Eitelberg, L.L. Veldhuis, Wingtip-mounted propellers: Aerodynamic analysis of interaction effects and comparison with conventional layout, J. Aircr. 56 (1) (2019) 295–312, http://dx.doi.org/10.2514/1.C034978.

[104] N.J. Blaesser, Z.J. Frederick, I. Ordaz, F. Valdez, Mission and Vehicle-Level Updates for the Parallel Electric-Gas Architecture with Synergistic Utilization Scheme (PEGASUS) Concept Aircraft, Tech. rep., URL http://www.sti.nasa.gov.

[105] D.S. Sanders, P. Laskaridis, Full-aircraft energy-based force decomposition applied to boundary-layer ingestion, AIAA J. 58 (10) (2020) 4357–4373, http://dx.doi.org/10.2514/1.J058695.

[106] I. Lamprakis, D.S. Sanders, P. Laskaridis, Energy-based aerodynamic loss and recovery characteristics of adiabatic and heated fuselages, J. Aircr. 60 (6) (2023) 1947–1964, http://dx.doi.org/10.2514/1.C037246.

[107] C. Goldberg, D. Nalianda, P. Laskaridis, P. Pilidis, Performance assessment of a boundary layer ingesting distributed propulsion system at off-design, in: 53rd AIAA/SAE/ASEE Joint Propulsion Conference, 2017, American Institute of Aeronautics and Astronautics Inc, AIAA, 2017, http://dx.doi.org/10.2514/6.2017-5055.

[108] T. Sinnige, B.D. Corte, Aerodynamic performance of a tip-mounted propeller-wing system at positive and negative thrust, in: AIAA Aviation Forum and ASCEND, 2024, American Institute of Aeronautics and Astronautics Inc, AIAA, 2024, http://dx.doi.org/10.2514/6.2024-3520.

[109] Q. van der Leer, M.F. Hoogreef, Aero-propulsive and aero-structural design integration of turboprop aircraft with electric wingtip-mounted propellers, in: AIAA Science and Technology Forum and Exposition, AIAA SciTech Forum 2022, American Institute of Aeronautics and Astronautics Inc, AIAA, 2022, http://dx.doi.org/10.2514/6.2022-0167.

[110] J. Zhang, G. Lin, U. Vaidya, H. Wang, Past, present and future prospective of global carbon fibre composite developments and applications, Composites B 250 (2023) http://dx.doi.org/10.1016/j.compositesb.2022.110463.

[111] R.M.A. Sapuan, in: N. Mazlan, S. Sapuan, R. Ilyas (Eds.), Advanced Composites in Aerospace Engineering Applications, Springer International Publishing, Cham, 2022, http://dx.doi.org/10.1007/978-3-030-88192-4, URL https://link.springer.com/10.1007/978-3-030-88192-4.

[112] S.D. Müzel, E.P. Bonhin, N.M. Guimarães, E.S. Guidi, Application of the finite element method in the analysis of composite materials: A review, Polymers 12 (4) (2020) http://dx.doi.org/10.3390/POLYM12040818.

[113] B. Parveez, M.I. Kittur, I.A. Badruddin, S. Kamangar, M. Hussien, M.A. Umarfarooq, Scientific advancements in composite materials for aircraft applications: A review, Polymers 14 (22) (2022) http://dx.doi.org/10.3390/polym14225007.

[114] F. Meng, Y. Cui, S. Pickering, J. McKechnie, From aviation to aviation: Environmental and financial viability of closed-loop recycling of carbon fibre composite, Composites B 200 (2020) http://dx.doi.org/10.1016/j.compositesb.2020.108362.

[115] T. Groetsch, M. Maghe, C. Creighton, R.J. Varley, Environmental, property and cost impact analysis of carbon fibre at increasing rates of production, J. Clean. Prod. 382 (2023) 135292, http://dx.doi.org/10.1016/j.jclepro.2022.135292, URL https://linkinghub.elsevier.com/retrieve/pii/S0959652622048661.

[116] A. Filippatos, D. Markatos, G. Tzortzinis, K. Abhyankar, S. Malefaki, M. Gude, S. Pantelakis, Sustainability-driven design of aircraft composite components, Aerospace 11 (1) (2024) http://dx.doi.org/10.3390/aerospace11010086.

[117] Y. Atescan-Yuksek, A. Mills, D. Ayre, K. Koziol, K. Salonitis, Comparative life cycle assessment of aluminium and CFRP composites: the case of aerospace manufacturing, Int. J. Adv. Manuf. Technol. 131 (7–8) (2024) 4345–4357, http://dx.doi.org/10.1007/s00170-024-13241-3.

[118] CompositesWorld, Heart Aerospace reveals hybrid-electric aircraft demonstrator. URL https://www.compositesworld.com/news/heart-aerospace-reveals-hybrid-electric-aircraft-demonstrator.

[119] P. Ansell, Review of sustainable energy carriers for aviation: Benefits, challenges, and future viability, Prog. Aerosp. Sci. 141 (2023) 100919.

[120] O. Edenhofer, R. Madruga, Y. Sokona, Renewable Energy Sources and Climate Change Mitigation: Special Report of the Intergovernmental Panel on Climate Change, Cambridge University Press, 2012.

[121] E. Çam, Z. Hungerford, N. Schoch, F. Miranda, C. de León, Electricity 2024: Analysis and Forecast to 2026, International Energy Agency, 2024.

[122] M. Prussi, U. Lee, M. Wang, R. Malina, H. Valin, F. Taheripour, C. Velarde, M. Staples, L. Lonza, J. Hileman, CORSIA: The first internationally adopted approach to calculate life-cycle GHG emissions for aviation fuels, Renew. Sustain. Energy Rev. 150 (2021) 111398.

[123] S. Bouckaert, A. Pales, C. McGlade, U. Remme, B. Wanner, Net Zero by 2050: A Roadmap for the Global Energy Sector, International Energy Agency, 2021.

[124] S. Alvik, O. Ozgun, Hydrogen Forecast to 2050: Energy Transition Outlook 2022, DNV, 2012.

[125] ICAO, Report on the Feasibility of a Long-Term Aspirational Goal (LTAG) for International Civil Aviation CO2 Emission Reduction - Appendix M5 Fuels Sub Group Report, Tech. rep., 2022.

[126] Q. Dai, J.C. Kelly, L. Gaines, M. Wang, Life cycle analysis of lithium-ion batteries for automotive applications, Batteries 5 (2) (2019) http://dx.doi.org/10.3390/batteries5020048.

[127] O. Winjobi, J.C. Kelly, Q. Dai, Life-cycle analysis, by global region, of automotive lithium-ion nickel manganese cobalt batteries of varying nickel content, Sustain. Mater. Technol. 32 (2022) http://dx.doi.org/10.1016/j.susmat.2022.e00415.

[128] C. Rietdorf, C. De la Rúa, S. Kiemel, R. Miehe, Cradle-to-gate life cycle assessment of cylindrical sulfide-based solid-state batteries, Int. J. Life Cycle Assess. (2024) http://dx.doi.org/10.1007/s11367-024-02355-1.

[129] P. Mandade, M. Weil, M. Baumann, Z. Wei, Environmental life cycle assessment of emerging solid-state batteries: A review, Chem. Eng. J. Adv. 13 (2023) http://dx.doi.org/10.1016/j.ceja.2022.100439.

[130] L. Usai, C.R. Hung, F. Vásquez, M. Windsheimer, O.S. Burheim, A.H. Strømman, Life cycle assessment of fuel cell systems for light duty vehicles, current state-of-the-art and future impacts, J. Clean. Prod. 280 (2021) http://dx.doi.org/10.1016/j.jclepro.2020.125086.

[131] R. Stropnik, A. Lotrič, A. Bernad Montenegro, M. Sekavčnik, M. Mori, Critical materials in PEMFC systems and a LCA analysis for the potential reduction of environmental impacts with EoL strategies, Energy Sci. Eng. 7 (6) (2019) 2519–2539, http://dx.doi.org/10.1002/ese3.441, URL https://onlinelibrary.wiley.com/doi/10.1002/ese3.441.

[132] A.W. Schäfer, S.R. Barrett, K. Doyme, L.M. Dray, A.R. Gnadt, R. Self, A. O'Sullivan, A.P. Synodinos, A.J. Torija, Technological, economic and environmental prospects of all-electric aircraft, Nat. Energy 4 (2) (2019) 160–166, http://dx.doi.org/10.1038/s41560-018-0294-x.

[133] N. Thonemann, E. Pierrat, K.M. Dudka, K. Saavedra-Rubio, A.L.S. Tromer Dragsdahl, A. Laurent, Towards sustainable regional aviation: Environmental potential of hybrid-electric aircraft and alternative fuels, Sustain. Prod. Consum. 45 (2024) 371–385, http://dx.doi.org/10.1016/j.spc.2024.01.013.

[134] European Environment Agency, Greenhouse gas emission intensity of electricity generation in Europe. URL https://www.eea.europa.eu/en/analysis/indicators/greenhouse-gas-emission-intensity-of-1?activeAccordion=546a7c35-9188-4d23-94ee-005d97c26f2b.

[135] P. Laskaridis, P. Pilidis, P. Kotsiopoulos, An integrated engine-aircraft performance platform for assessing new technologies in aeronautics, in: ISABE 2005, Munich, 2005, pp. 1–13.

[136] E. Pontika, B. Zaghari, T. Zhou, H.B. Enalou, P. Laskaridis, Integrated Mission Performance Analysis of Novel Propulsion Systems: Analysis of a Fuel Cell Regional Aircraft Retrofit, American Institute of Aeronautics and Astronautics (AIAA), 2023, http://dx.doi.org/10.2514/6.2023-0840.

[137] T. Zhou, H.B. Enalou, E. Pontika, B. Zaghari, P. Laskaridis, Minimising the effect of degradation of fuel cell stacks on an integrated propulsion architecture for an electrified aircraft, in: 2022 IEEE Transportation Electrification Conference and Expo, ITEC 2022, Institute of Electrical and Electronics Engineers Inc., 2022, pp. 1064–1069, http://dx.doi.org/10.1109/ITEC53557.2022.9813899.

[138] ICAO, ICAO Report on the Feasibility of a Long-Term Aspirational Goal (LTAG) for International Civil Aviation CO2 Emission Reductions, Tech. rep..

[139] M. Bressel, M. Hilairet, D. Hissel, B. Ould Bouamama, Model-based aging tolerant control with power loss prediction of Proton Exchange Membrane Fuel Cell, Int. J. Hydrog. Energy 45 (19) (2020) 11242–11254, http://dx.doi.org/10.1016/j.ijhydene.2018.11.219.

[140] Aircraft Commerce, ATR 42 & 73 Maintenance Analysis & Budget, Aircraft Commerce, 2007, (49).

[141] Aircraft Commerce, Regional Aircraft Engine Maintenance, Aircraft Commerce, 2016, (108).

[142] A. Derber, Maintenance at heart of PW127 engine upgrade | aviation week network, 2022, URL https://aviationweek.com/mro/aircraft-propulsion/maintenance-heart-pw127-engine-upgrade.

[143] N. Wahler, L. Radomsky, L.V. Hanisch, J. Göing, P. Meyer, R. Mallwitz, J. Friedrichs, M. Henke, A. Elham, An integrated framework for energy network modeling in hybrid-electric aircraft conceptual design, in: AIAA AVIATION 2022 Forum, American Institute of Aeronautics and Astronautics Inc, AIAA, 2022, http://dx.doi.org/10.2514/6.2022-3741.

[144] O. Erdinc, B. Vural, M. Uzunoglu, A dynamic lithium-ion battery model considering the effects of temperature and capacity fading, in: 2009 International Conference on Clean Electrical Power, IEEE, 2009, pp. 383–386, http://dx.doi.org/10.1109/ICCEP.2009.5212025, URL http://ieeexplore.ieee.org/document/5212025/.

[145] J. Schmalstieg, S. Käbitz, M. Ecker, D.U. Sauer, A holistic aging model for Li(NiMnCo)O2 based 18650 lithium-ion batteries, J. Power Sources 257 (2014) 325–334, http://dx.doi.org/10.1016/j.jpowsour.2014.02.012.

[146] A. Spinelli, G.P. Krupa, T. Kipouros, Set-based design space exploration to investigate the effect of energy storage durability on the energy management strategy of a hybrid-electric aircraft, in: AIAA SciTech Forum and Exposition, 2023, American Institute of Aeronautics and Astronautics Inc, AIAA, 2023, http://dx.doi.org/10.2514/6.2023-0837.